A dissertation entitled

SOLVENT EFFECTS ON THE DECARBOXYLATIVE-DECHLORINATION OF N-CHLORO-α-AMINO ACIDS IN BINARY AQUEOUS-ORGANIC COSOLVENT SYSTEMS: THE PHENOMENOLOGICAL MODEL APPLIED TO CHEMICAL REACTION KINETICS

submitted to the Graduate School of the
University of Wisconsin-Madison
in partial fulfillment of the requirements for the
degree of Doctor of Philosophy

by

Jason M. LePree

Degree to be awarded: December 19___ May 1995 August 19___

Approved by Dissertation Readers:

Kenneth G. Conn
Major Professor

5/8/95
Date of Examination

C Rayn

George Zografi

Dean, Graduate School

SOLVENT EFFECTS ON THE DECARBOXYLATIVE-DECHLORINATION OF N-CHLORO-α-AMINO ACIDS IN BINARY AQUEOUS-ORGANIC COSOLVENT SYSTEMS: THE PHENOMENOLOGICAL MODEL APPLIED TO CHEMICAL REACTION KINETICS

by

Jason M. LePree

A dissertation submitted in partial fulfillment of the requirements for the degree of

Doctor of Philosophy

(Pharmacy)

at the

UNIVERSITY OF WISCONSIN - MADISON

1995

Acknowledgments

This work and my academic activities over the past four years would not have been possible without the support, encouragement, and guidance of Dr. Kenneth A. Connors. He is a great mentor, and I thank him for all his assistance. I would also like to thank Dr. George Zografi for his unfailing moral support and advice throughout my stay in the graduate program.

I wish the best to all my friends, too numerous to mention here, and thank them for their company, good humor, and kindness.

I extend all the health, happiness, and success to group members Michael Brown, Ashwini Gadre, and Rachel Leiterman.

I thank my father and mother, John and Carol LePree, and my fiancée Nancy Chang, for their support and understanding; this thesis is your work as much as it is mine.

Lastly, I thank Syntex and Pharmaceutical Research and Manufactures of America Foundation for funding my years of graduate study.

Table of Contents

Acknowledgments ii

Abstract iv

Chapter 1 Review of the Phenomenological Model 1

1.1 General Concepts 1
1.1.1 The Solvation Effect 2
1.1.2 The General Medium Effect 6

1.2 Application to Solubility 9
1.2.1 Theory 9
1.2.2 Results 14

1.3 Application to Surface Tension 33
1.3.1 Theory 33
1.3.2 Results 33

1.4 Application to Solvatochromatic Effects 38
1.4.1 Solvatochromic Behavior 38
1.4.2 Theory 40
1.4.3 Results 43

1.5 Application to Complexation 47
1.5.1 Theory 47
1.5.2 Results 57

1.6 Theory for Application to Chemical Kinetics 62
1.6.1 Theory 62

1.7 Statement of the Problem 67

1.8 Chapter 1 References 69

Chapter 2 Decarboxylative-Dechlorination of N-chloro-α-amino Acids 71

2.1 Chemistry of the reaction 71

2.2 Chapter 2 References 93

Chapter 3 Pressure Effects 95

3.1 Activation Volumes 95

3.2 Concentration Units 97

3.3 Data Treatment and Calculation of $\Delta V^{\ddagger}$ 102

3.4 Interpretation of Activation Volumes 108

3.5 Chapter 3 References 114

Chapter 4 Experimental 116

4.1 Materials 116

4.2 Apparatus 117

4.3 Procedures 118

4.3.1 Preliminary Studies 118

4.3.2 Solvent Effect Studies 119

4.3.3 Blank Studies 120

4.3.4 Effect of UV-Radiation on the Decomposition of N-Chloroalanine 121

4.3.5 Pressure Effect Studies 122

4.4 Calculations 123

4.4.1 Rate Constant Calculations 123

4.4.2 Calculation of Mole Fraction of Organic Cosolvent in the Reaction Solution 124

4.4.3 Calculation of $\delta_m \Delta G^{\ddagger}$ 125

4.4.4 Calculation of the Volume of Activation, $\Delta V^{\ddagger}$ 125

4.5 Chapter 4 References 126

Chapter 5. Results 127

5.1 Preliminary Studies 127

5.2 Solvent Effect Studies 132

5.3 Parameter Estimates 145

5.4 Curve Fits 149

5.5 Pressure Effect Studies 174
5.5.1 Rate Constants 174
5.5.2 Volume of Activation 179

5.6 Chapter 5 References 181

Chapter 6 Discussion

6.1 Other Approaches to the Description of Solvent Effects on Chemical Reaction Kinetics 182
6.1.1 Models Based on Physical Theory 182
6.1.2 Empirically Based Models 191

6.2 Solvent and Pressure Effects on the Reaction Rate 194

6.3 The Curve-Fits 195

6.4 The Solvation Exchange Constants 205

6.5 The $\Delta gA^{\ddagger}$ Parameter 210
6.5.1 Average $\Delta gA^{\ddagger}$ Values and Their Implications for the Curvature Correction Factor 210
6.5.2 The $\Delta gA^{\ddagger}$ Parameter Sign, Magnitude, and Variation 214

6.6 Conclusions 218

6.7 Chapter 6 References 220

Abstract

SOLVENT EFFECTS ON THE DECARBOXYLATIVE-DECHLORINATION OF N-CHLORO-α-AMINO ACIDS IN BINARY AQUEOUS-ORGANIC COSOLVENT SYSTEMS: THE PHENOMENOLOGICAL MODEL APPLIED TO CHEMICAL REACTION KINETICS

Jason M. LePree

Under the supervision of Professor Kenneth A. Connors

at the University of Wisconsin-Madison

A theory of solvent effects developed in this laboratory, referred to as the phenomenological model, had previously been used to successfully describe solvent effects, in binary aqueous-organic cosolvent systems, on solubility, surface tension, complexation, and absorption spectra. The model separates the observed solvent effect into contributions from solvent-solute interactions (expressed by a one or two-step solvation scheme), solvent-solvent interactions (expressed by a cavity model), and solute-solute interactions (which are eliminated from the model via the Leffler-Grunwald delta operator). The goal of this study was to test the applicability of the phenomenological model to solvent effect data on chemical reaction rates. To this end, the decarboxylative-dechlorination of N-chloroalanine was studied in eight

aqueous-organic cosolvent systems, and the decarboxylative-dechlorination of N-chloroleucine was studied in 4 aqueous-organic cosolvent systems. This reaction possesses several features that made it well suited for a solvent effect study, among them being its pH independence (in the pH range from 5 to 13), its insensitivity to ionic strength in this pH range, its sensitivity to solvent effects, its unimolecularity, and its first-order decomposition kinetics. These properties simplified the interpretation of the solvent effects.

The curve-fits to the data were very good. The model parameters include solvation exchange constants, K_1 and K_2, and a curvature-corrected molecular surface area of activation term, $\Delta gA^{\ddagger}$. The exchange constants are correlated with log P (P is the 1-octanol-water partition coefficient) of the organic cosolvents used in the studies. The curvature-corrected molecular surface area of activation term, $\Delta gA^{\ddagger}$, agrees with the direction and magnitude of the volume of activation, $\Delta V^{\ddagger}$, for the reaction.

Chapter 1 The Phenomenological Model

A theory of solvent effects developed in this laboratory, and referred to as the phenomenological model has been used to successfully describe solvent effects, in binary solvent systems, on solubility (1-3), surface tension (4), complexation (5-7), and absorption spectra (8). The theory of this model, and its application to the chemical processes listed above will be discussed in this chapter. This review will provide the framework to understand the theory, and to appreciate its extension to the description of solvent effects on chemical kinetics.

1.1 General Concepts

The phenomenological model of solvent effects, as developed in this laboratory, separates the observed solvent effect on a chemical process into contributions from solvent-solute interactions, solvent-solvent interactions, and solute-solute interactions. In our model, solvent-solute interactions are described by the Solvation Effect, $\Delta G_{solv.}$; solvent-solvent interactions are described by the General Medium Effect, $\Delta G_{gen.\,med.}$, and solute-solute interactions are described by the Intersolute Effect, $\Delta G_{intersolute}$. Explicit mathematical expressions for the solvation and general medium effects will be presented in the ensuing two sections. The solute-solute interactions are assumed to be independent of solvent composition, and

through application of the Leffler-Grunwald delta operator (9), which will be discussed later, the Intersolute Effect will be eliminated, therefore negating the need to develop an expression for it.

1.1.1 *The Solvation Effect*

The Solvation Effect, which describes solute-solvent interactions, is modeled as a stepwise, competitive, exchange equilibrium between water, W, and organic cosolvent, M, for a solute, R. We denote the equilibrium exchange constant as K_n, where n refers to the n^{th} step in the process. This is illustrated in Scheme 1.1 for a two-step equilibrium process. The number of steps may be generalized if desired, but this discussion will be restricted to the two-step process.

$$RW_2 + M \underset{}{\overset{K_1}{\rightleftharpoons}} RWM + W \qquad (1.1)$$

$$RWM + M \underset{}{\overset{K_2}{\rightleftharpoons}} RM_2 + W \qquad (1.2)$$

Scheme 1.1

Though the equilibria are depicted on an individual molecular exchange basis for mathematical convenience, a chemically more defensible view is that the solute can exist in a fully hydrated state, a partially solvated state, or a

fully solvated state; the preceding chemical equations convert this concept to a quantifiable form.

By expressing the total free energy change of solvation as the weighted average of the three species we write, for a single solute,

$$\Delta G_{solv.} = \Delta G_{RW_2} F_{RW_2} + \Delta G_{RWM} F_{RWM} + \Delta G_{RM_2} F_{RM_2} \quad (1.3)$$

where F_{RW_2}, F_{RWM}, and F_{RM_2} are the fractions of solute in the fully hydrated, partially solvated, and fully solvated forms. Because the sum of these fractions is equal to one, equation (1.3) is rewritten as

$$\Delta G_{solv.} = \Delta G_{RW_2} + (S_1)F_{RWM} + (S_2)F_{RM_2} \quad (1.4)$$

where

$$S_1 = \Delta G_{RWM} - \Delta G_{RW_2} \quad (1.5)$$

and

$$S_2 = \Delta G_{RM_2} - \Delta G_{RW_2} \quad (1.6)$$

The equilibrium constants, K_1 and K_2, depicted in Scheme 1.1 may be used in conjunction with the bulk mole fractions of water, x_1, and organic cosolvent, x_2, to obtain explicit expressions for F_{RWM} and F_{RM_2}.

$$F_{RWM} = \frac{K_1 x_1 x_2}{(x_1)^2 + K_1 x_1 x_2 + K_1 K_2 (x_2)^2} \quad (1.7)$$

$$F_{RM_2} = \frac{K_1 K_2 (x_2)^2}{(x_1)^2 + K_1 x_1 x_2 + K_1 K_2 (x_2)^2} \quad (1.8)$$

Combining equations (1.4, 1.7, and 1.8) gives

$$\Delta G_{solv.} = \frac{S_1 K_1 x_1 x_2 + S_2 K_1 K_2 (x_2)^2}{(x_1)^2 + K_1 x_1 x_2 + K_1 K_2 (x_2)^2} + \Delta G_{RW_2} \quad (1.9)$$

Using the thermodynamic cycles given in Schemes 1.2 and 1.3 expressions for S_1 and S_2 in terms of the solvation exchange constants are obtained, and we write

$$S_1 = \Delta G_{RWM} - \Delta G_{RW_2} = -k_B T \ln K_1 = \Delta G_1 \quad (1.10)$$

and

$$S_2 = \Delta G_{RM_2} - \Delta G_{RW_2} = -k_B T \ln K_1 K_2 = \Delta G_2 \quad (1.11)$$

where k_B is the Boltzmann constant, and T is the absolute temperature.

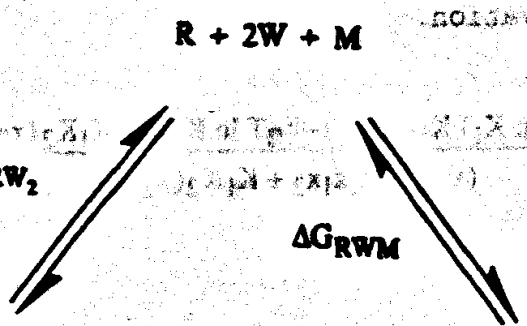

Scheme 1.2. The thermodynamic cycle that gives the relations for equation (1.10).

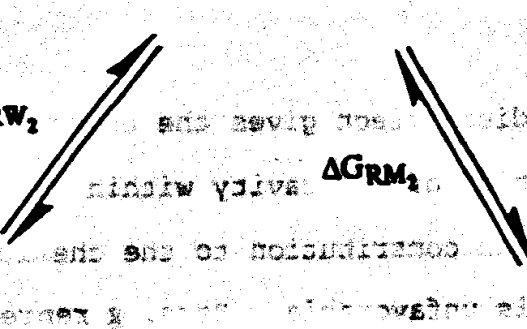

Scheme 1.3. The thermodynamic cycle that gives the relations for equation (1.11).

Substituting equations (1.10) and (1.11) into equation (1.9), we arrive at the expression for the free energy change of solvation.

$$\Delta G_{solv.} = \frac{(-k_B T \ln K_1)\, K_1 x_1 x_2 + (-k_B T \ln K_1 K_2)\, K_1 K_2 (x_2)^2}{(x_1)^2 + K_1 x_1 x_2 + K_1 K_2 (x_2)^2} + \Delta G_{RW_2} \qquad (1.12)$$

1.1.2 The General Medium Effect

The General Medium Effect describes solvent-solvent interactions. Using a modified version of Uhlig's gas solubility model (10), the General Medium Effect on taking a single solute into solution (i.e., for the equilibrium dissolution process) is expressed as

$$\Delta G_{gen.\ med.} = gA\gamma \qquad (1.13)$$

The General Medium Effect gives the energy change associated with the formation of the cavity within the bulk solvent, and its energetic contribution to the chemical process under investigation is unfavorable. Here, g represents an empirical curvature correction factor which corrects for deviations in the effective surface tension caused by curvature on the molecular level. The van der Waals surface contact area of the solute is given by A. This area is

defined as the locus of all exterior points of the van der Waals surface of the solute molecule that could be in contact with the van der Waals surface of a solvent molecule. The area is treated as a composition independent term (though this must be an approximation).

The surface tension, γ is that for a cavity of surface phase composition f_2, which is defined as the mean fractional composition of the solvation shell with respect to the organic cosolvent. An expression for f_2 is derived through use of the following summation.

$$f_2 = \frac{1}{k}\sum j F_{RW_i M_j} \qquad (1.14)$$

The solvation stoichiometry is denoted by RW_iM_j, and $k = i + j$ (k is also equal to the number of solvation steps). Analogous to the definition and derivation of f_2, we define f_1 as the mean fractional composition of the solvation shell with respect to water, given by

$$f_1 = \frac{1}{k}\sum i F_{RW_iM_j} \qquad (1.15)$$

For a two-step solvation process f_2 is given by equation (1.16)

$$f_2 = \frac{F_{RWM} + 2F_{RM_2}}{2} \qquad (1.16)$$

The surface tension of the solvation shell is defined by equation (1.17),

$$\gamma = \gamma_1 f_1 + \gamma_2 f_2 = \gamma_1 + (\gamma_2 - \gamma_1) f_2 \qquad (1.17)$$

where γ_1 and γ_2 are the bulk surface tensions of pure water and organic cosolvent, respectively. Substituting equations (1.7), (1.8), and (1.16) into (1.17), we express the surface tension of the solvation shell as

$$\gamma = \gamma_1 + \gamma' \left(\frac{K_1 x_1 x_2 + 2K_1 K_2 (x_2)^2}{(x_1)^2 + K_1 x_1 x_2 + K_1 K_2 (x_2)^2} \right) \qquad (1.18)$$

where $\gamma' = \left(\frac{\gamma_1 - \gamma_2}{2} \right)$. (In general, $\gamma' = \left(\frac{\gamma_1 - \gamma_2}{k} \right)$).

Thus, the general medium effect is given by substitution of (1.18) into (1.13) to give

$$\Delta G_{\text{gen. med.}} = gA\gamma_1 + gA\gamma' \left(\frac{K_1 x_1 x_2 + 2K_1 K_2 (x_2)^2}{(x_1)^2 + K_1 x_1 x_2 + K_1 K_2 (x_2)^2} \right) \qquad (1.19)$$

1.2 Application of the Phenomenological Model to Solubility

1.2.1 Theory

The phenomenological model envisions solubility as the four-step process depicted in Scheme 1.4. The first step involves removal of a molecule from the crystal lattice and subsequent transformation to a liquid phase. The second step involves formation of a cavity, of surface phase composition f_2, within the bulk solvent. Here f_2 is the mean fractional organic composition of the solution immediately surrounding the cavity; in general its composition differs from that of the bulk solution. In the third step, the liquid solute molecule is inserted into the cavity (of surface phase composition f_2) resulting in an unsolvated solute within the cavity. The fourth step involves transformation of the unsolvated solute into a solvated solute.

Step 1.	Crystalline Solute	⟷	Liquid Solute
Step 2.	Bulk Solvent	⟷	Solvent with molecular cavity (surface phase composition f_2)
Step 3.	Solvent with molecular cavity (surface phase composition f_2) + liquid solute	⟷	Unsolvated solute in the cavity (surface phase composition f_2)
Step 4.	Unsolvated solute in cavity (surface phase composition f_2)	⟷	Solvated cavity (Surface phase composition f_2)
Sum	Crystalline Solute + Bulk Solvent	⟷	Solvated solute

Scheme 1.4. The four-step dissolution process.

Using Scheme 1.4, we write the total free energy change of dissolution as

$$\Delta G^{*}_{soln} = \Delta G_{intersolute} + \Delta G_{gen.\ med.} + \Delta G_{insertion} + \Delta G_{solv.} \qquad (1.20)$$

where $\Delta G_{intersolute}$, the Intersolute Effect, is the free energy contribution from solute-solute interactions in both the solution and solid phases. The solute-solute interactions in the solution phase are considered negligible in dilute solutions, or in solutions in which non-ideality effects are minimal. Solid phase solute-solute interactions are controlled by the crystal lattice energy of the solute molecule. $\Delta G_{gen.\ med.}$, the General Medium Effect, accounts for all solvent-solvent interactions within the system; an expression for this quantity was given on page 8. $\Delta G_{insertion}$ is the free energy change ascribed to the insertion of a solute molecule into a cavity of surface phase composition f_2. Since the solvation term, $\Delta G_{solv.}$, accounts for interaction of the solute with the cavity surface phase, the insertion energy is included within the Solvation Effect.

We now rewrite equation (1.20) as

$$\Delta G^{*}_{soln} = \Delta G_{intersolute} + \Delta G_{gen.\ med.} + \Delta G_{solv.} \qquad (1.21)$$

The total energy of dissolution is given by substituting equations (1.12) and (1.19) into equation (1.21)

$$\Delta G^{*}_{soln} = gA\gamma_l + \left(\frac{(-k_B T \ln (K_1) + gA\gamma') K_1 x_1 x_2 + (-k_B T \ln (K_1 K_2) + 2gA\gamma') K_1 K_2 (x_2)^2}{(x_1)^2 + K_1 x_1 x_2 + K_1 K_2 (x_2)^2} \right) + \Delta G_{RW_2} + \Delta G_{intersolute} \quad (1.22)$$

In a pure aqueous medium ($x_2 = 0$), this equation reduces to

$$\Delta G^{*}_{soln\,(x_2=0)} = gA\gamma_l + \Delta G_{RW_2} + \Delta G_{intersolute} \quad (1.23)$$

Using the Leffler-Grunwald operator (9), the solvent effect is defined as

$$\delta_m \Delta G^{*}_{soln} = \Delta G^{*}_{soln\,(x_2)} - \Delta G^{*}_{soln\,(x_2=0)} \quad (1.24)$$

Application of this operator to equation (1.22) eliminates the solvent independent terms, and allows equation (1.22) to be expressed as

$$\delta_m \Delta G^*_{soln} = \left(\frac{(-k_B T \ln (K_1) + gA\gamma') K_1 x_1 x_2 + (-k_B T \ln (K_1 K_2) + 2gA\gamma') K_1 K_2 (x_2)^2}{(x_1)^2 + K_1 x_1 x_2 + K_1 K_2 (x_2)^2} \right) \quad (1.25)$$

Equation (1.25) is the phenomenological model for solvent effects on solubility in binary mixed solvents. Because the equation was derived from a two-step solvation scheme, it will be called a two-step solubility model.

Experimentally we measure the equilibrium mole fraction solubility of the solute, x_3, as a function of the mole fraction of organic cosolvent, x_2, in the binary solvent mixture. The free energy of solution per molecule is calculated with equation (1.26)

$$\Delta G^*_{soln} = -k_B T \ln x_3 \quad (1.26)$$

Thermodynamically the standard free energy of solution is related to the solute activity, a_3, by equation (1.27).

$$\Delta G^0_{soln} = -k_B T \ln a_3 \quad (1.27)$$

It follows that ΔG^*_{soln} and ΔG^0_{soln} are related by equation (1.28),

$$\Delta G^{*}_{soln} = \Delta G^{0}_{soln} + k_B T \ln \gamma_3 \qquad (1.28)$$

where γ_3 is the solute activity coefficient.

Equation (1.25) is used for fitting $\delta_m \Delta G^{*}_{soln}$, calculated from equations (1.24) and (1.26), to x_1 and x_2 by means of nonlinear regression analysis. This analysis yields estimates for the model's three adjustable parameters, namely, the solvation exchange constants K_1 and K_2, and the product, gA, of the curvature correction factor and the cavity's surface area.

1.2.2 Results

Three papers have appeared describing the application of the phenomenological model to solubility data (1-3). Owing to the precision of the data, and the ability to extend such studies to the full range of mixed cosolvent composition, the solubility work has contributed greatly to our understanding of the model, and in this sense was more important than any other studies. I have chosen to present the findings of these papers in chronological order, so the reader can witness the growth of our laboratory's understanding of the model, and the motivation for each study. Prior to delving into these topics, however, I would like report that equation (1.25) has been applied to 62 systems comprised of combinations of 40 solutes in 12

different organic cosolvent systems (1-3,11). These solutes included both nonpolar [4-bromobiphenyl, biphenyl(2), and naphthalene(1,3)] and polar [sucrose(3)] examples. Despite the chemical differences among these solutes, the curve fits to all the solubility data were excellent; two characteristic plots of these fits are shown in Figure 1.1 (3).

A simplified, one-step model can be derived from a one-step solvation scheme (See Scheme 1.5); this model given by equation (1.29), has only two adjustable parameters, namely gA and K_1.

$$\delta_M \Delta G^*_{soln} = \frac{\left(gA\gamma' - k_B T \ln K_1\right) K_1 x_2}{x_1 + K_1 x_2} \qquad (1.29)$$

Here $\gamma' = \gamma_2 - \gamma_1$.

$$RW + M \underset{}{\overset{K_1}{\rightleftharpoons}} RM + W$$

Scheme 1.5

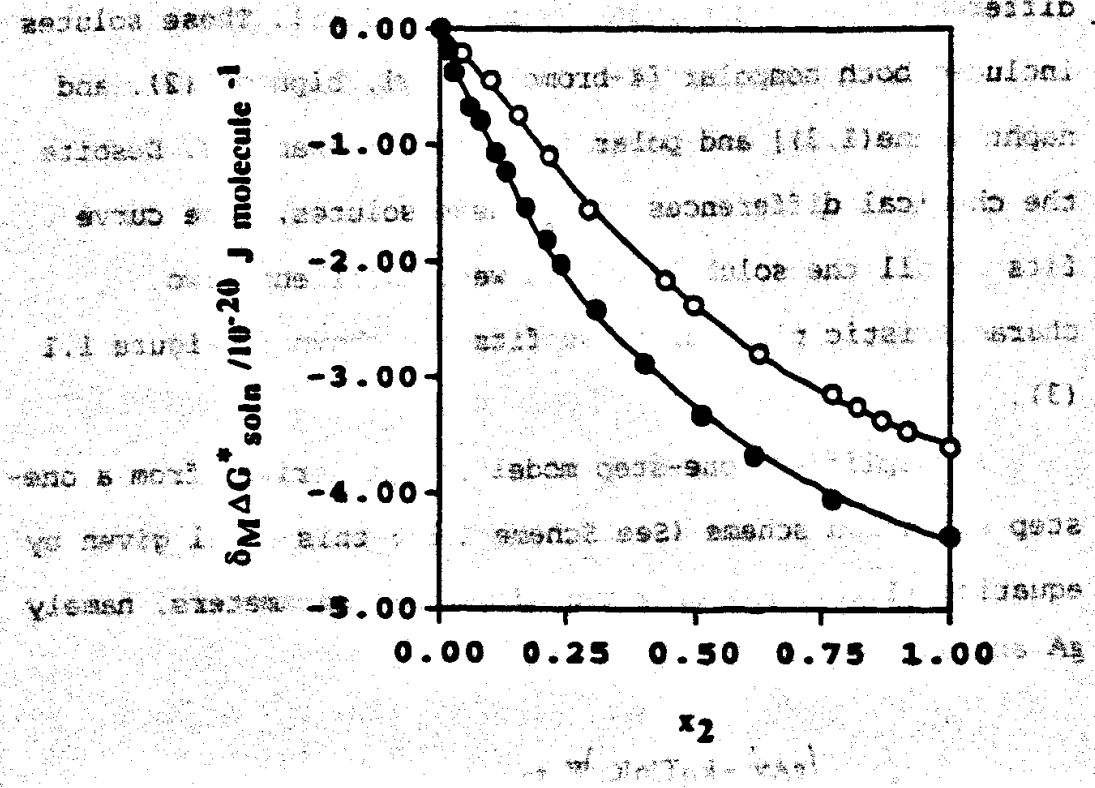

Figure 1.1 Solubility curves for naphthalene in water-methanol (open circles) and water-DMSO (closed circles). The points are experimental, and the line is the fit of the data to equation (1.25). Data are from reference (3).

The curve-fits with this one-step model are excellent for many systems; however, for some systems they are poor. Owing to the ability of equation (1.25), the two-step model, to fit all the data, it has been used in favor of the one-step model, equation (1.29).

The first study of equation (1.25) was conducted by Khossravi and Connors (1) on 44 systems comprised of a combination of 31 solutes in 8 different organic cosolvents.

Several observations, relating to the parameter estimates, were made. These workers noticed that the parameter estimates for the solvation exchange constants K_1 and K_2 were usually between 1 and 10. The physical significance of these values was justified as follows; the constants describe solvation of uncharged, organic compounds by organic cosolvents in the binary solvent mixtures, therefore values larger than 1 were expected; however, all the organic cosolvents were water miscible, and in this sense water-like, so the constants were not expected to be very large. It was also noted that the values depended on the identity of the solute and cosolvent used in the study, but precise correlations could not be established.

The gA term, which represented the product of the curvature correction factor and the surface area of the solvent cavity, was shown to vary for a single solute in different cosolvent systems. Separation of the gA term into the g and A term was done by dividing gA by the solvent accessible surface area of the solute molecule. In reference (1) it was suggested that the gA term varied in a way that depended on solvent polarity; however, whether the source of the variation was from the g term, the A term, or both terms could not be deduced.

This paper also introduced a simple, inexpensive, non-computational method for calculating the solvent accessible

molecular surface area of a solute (1). A Corey-Pauling-Kolton (CPK) space-filling model was tightly wrapped with aluminum foil so that it resembled a smooth shell. The foil was removed and weighed; this weight was converted to an area via a standard curve relating surface area of aluminum foil to its weight. This method gave values which were in agreement with values calculated by other methods. For example, the surface area of naphthalene was determined to be 150 $Å^2$/molecule (1), which compared favorably with Pearlman's calculated result of 156.72 $Å^2$/molecule (12).

In the second solubility paper, Khossravi and Connors (2) postulated that the area term, A, in the gA parameter estimate represented the hydrophobic portion of the solute molecule. To examine this hypothesis, they interpreted solubility data for biphenyl, 4-hydroxybiphenyl, 4,4'-hydroxybiphenyl, and 4-bromobiphenyl in water-methanol cosolvent systems. The solutes were selected to be similar in shape and to allow easy estimation of the nonpolar area of the solute, denoted by $A_{nonpolar}$. Because the solutes were of similar molecular shape, g was treated as a constant, and if A corresponded to $A_{nonpolar}$ then $gA = gA_{nonpolar}$, and $g = gA/A_{nonpolar}$. With this reasoning, a plot of the solutes' estimated gA values against their nonpolar surface areas was expected to be linear and to pass through the origin. These results were observed, for the

equation of the line from this analysis was $gA = 8(\pm 4.3) + 0.037(\pm 0.025)A_{nonpolar}$, where g=0.037, and the A term could indeed be associated with the nonpolar surface area of the solute molecule. The total area, the nonpolar area and the gA estimates of the solutes are given in Table 1.1., and the gA vs. $A_{nonpolar}$ plot is shown in Figure 1.2.

Table 1.1 Surface area and gA estimates of the biphenyl compounds[a] (2).

Compound	A_{total}	$A_{nonpolar}$	gA
Biphenyl	179 (3)	179 (3)	74.3 (0.6)
4-Hydroxybiphenyl	185 (4)	155 (7)	66.8 (0.3)
4,4'-Dihydroxybiphenyl	203 (5)	126 (7)	53.1 (0.5)
4-Bromobiphenyl	217 (7)	217 (7)	86.9 (1.4)

[a]Units are in $Å^2$/molecule. The actual estimates are in units of 10^{-17} m^2/molecule. Multiplication of these values by 10^3 gives the areas in the Table 1.1.
[b]Standard deviations are in parentheses.

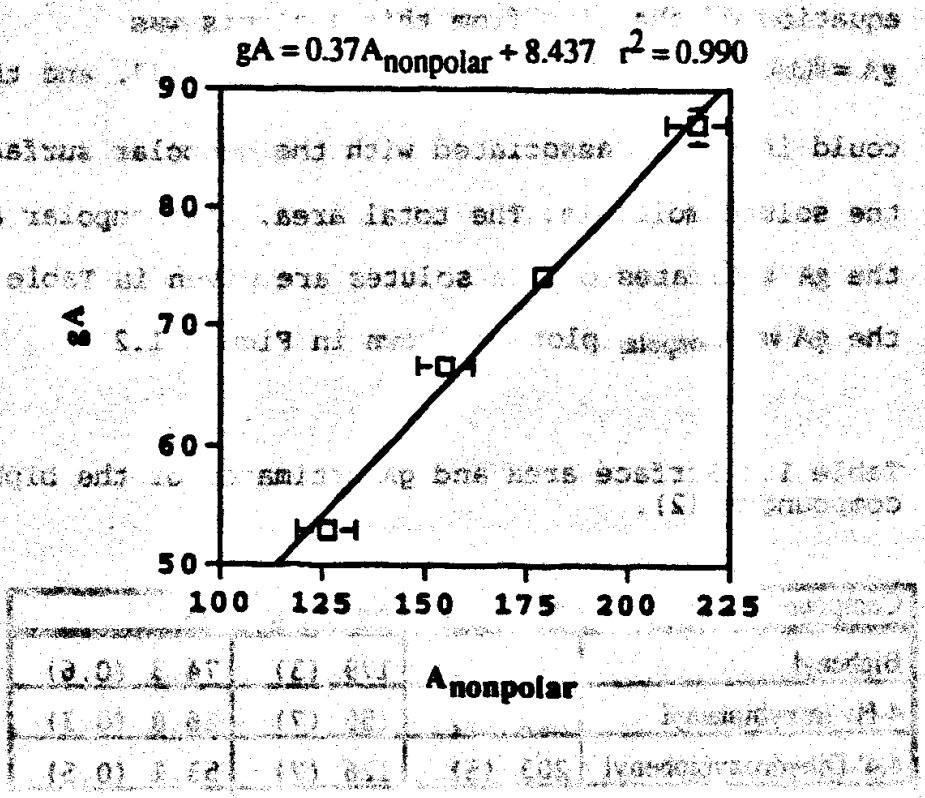

Figure 1.2 Plot of the model parameter gA vs. $A_{nonpolar}$, the estimated nonpolar surface area of the solute. Units of both axes are $Å^2$/molecule. The data are given in Table 1.1 (2).

This study showed that the A term corresponded to the nonpolar surface area of the solute molecule and hence was physically significant. The physical significance of the curvature correction factor to the surface tension is more difficult to assess; the value from these studies indicates that the surface tension of the curved solvation shell is smaller than its bulk (planar) value by a factor of 0.37.

Numerous theoretical arguments concerning this phenomenon have been made; however, they not only lack agreement on the magnitude of the change but also on its direction. Tolman (13), Vogelsberger and coworkers (14), Ahn and coworkers (15), and Goncalves and coworkers (16) have postulated the surface tension increases with the decrease in cavity size. Other workers, including Hooper and Nordholm (17) and Choi *et. al.* (18) propose that the opposite effect occurs. Schmelzer and Mahnke (19) predict that the surface tension may change in either direction, depending on certain parameter values that are used in their equation. Sinanoglu (20) states that the surface tension of polar liquids increases as the cavity is decreased, but decreases for nonpolar liquids.

Experimentally, Fischer and Israelachvili (21-23) measured adhesion forces and vapor pressures between curved mica surfaces in vapors of various liquids; their measurements indicated that the surface tension of these liquids decreased when the radius of curvature became lower than 1 to 0.5 nm for hydrocarbons and 5 nm for water. The direction of these changes is in agreement with the results of Khossravi and Connors' study (2).

Yalkowski and coworkers obtained an estimate of 0.33 to 0.57 for this curvature correction factor from analysis of solubility data with their Molecular Group Surface Area

Approach (MGSA) solubility theory (24,25). Considering the significant differences between the MGSA theory and the phenomenological model, the agreement between the curvature correction factor values is remarkable.

Clearly, the estimation of A_{total} and $A_{nonpolar}$ was of critical importance in this study, and therefore a discussion on this subject is warranted. The nonpolar surface area for a solute was determined with the foil wrapping technique described above; however, a subjective judgment was used to distinguish between the polar and nonpolar surface area of the hydroxy- and dihydroxybiphenyls, so that only the nonpolar area would be wrapped. The area of polar influence of these groups was believed to extend into the nonpolar portions of these molecules, and therefore the nonpolar surface area of the hydroxy-substituted biphenyls was less than the surface area of biphenyl. Figure 1.3 demonstrates this idea for 4-hydroxybiphenyl.

Figure 1.3 The range of polar influence of the hydroxy group is shown within the solid semicircle. The remaining area is considered hydrophobic.

In addition to the information connected with the gA term, this study furnished important information regarding the solvation exchange constants (2). The constants from this (2) and the first (1) study are presented in Table 1.2. These observations were made by Connors; the exchange constant values were between 1 and 10 as was observed from the first study. The arithmetic mean and standard deviation of the parameter values were $K_1 = 2.53 \pm 0.24$ and $K_2 = 1.77 \pm 0.36$. The small variation in these averages suggested that the solvation exchange constants were insensitive to solute structure; Khossravi and Connors speculated that this was due to the small differences in solute polarity relative to the polarity differences between the solutes and the cosolvent system.

Table 1.2 The Solvation Exchange Constant Estimates for Seven Solutes in a Water-Methanol Cosolvent System.

Solute	K_1	K_2
Biphenyl[b]	2.45 (0.07)[a]	1.28 (0.07)
4-Hydroxybiphenyl[b]	2.33 (0.04)	1.61 (0.05)
4,4'-Dihydroxybiphenyl[b]	2.52 (0.08)	2.2 (0.11)
4-Bromobiphenyl[b]	2.6 (0.13)	1.4 (0.16)
Naphthalene[c,d]	2.28 (0.04)	2.0 (0.17)
Acetanilide[c]	2.5 (0.13)	2.2 (0.19)
Diphenylhydantoin[c]	3.00 (0.07)	1.71 (0.08)

[a]Numbers in parentheses are standard deviations.
[b]Data from reference (2)
[c]Data from reference (1)
[d]Only studied solubility to organic mole fraction concentration $x_2 = 0.46$. The study was not complete.

The objective of the most recent solubility study from this laboratory was to augment our understanding of the gA and solvation exchange constant parameters and to achieve the ability to predict these quantities. In these investigations, LePree, Mulski, and Connors (3) studied the solubility of naphthalene in six aqueous-organic cosolvent systems and 4-nitroaniline in seven aqueous-organic cosolvent systems. Naphthalene was selected to represent a nonpolar solute, and 4-nitroaniline to represent a semipolar solute. All studies were conducted over the entire composition range (x_2= 0 to 1), and the data were analyzed with equation (1.25). The parameter estimates are given in Table 1.3.

As seen from the data in Table 1.3, the exchange constants were typically between 1 and 10, though a few deviations from this range are seen for the 4-nitroaniline data. The magnitude of these values was justified as in the first paper (1), namely that these solutes were less polar than water and therefore organic cosolvents are expected to displace water from the solvation shell, thus values greater than unity were expected; yet the cosolvents were infinitely miscible with water, and in this sense water-like, so the exchange constants were not expected to be very large.

Table 1.3 Model parameters for the solubility of naphthalene and 4-nitroaniline in aqueous-organic cosolvents.(3)

Cosolvent	K_1	K_2	gA /Å^2 molecule^{-1}
Naphthalene			
Methanol	2.52 (0.07)	1.19 (0.09)	63 (0.8)[a]
Ethanol	3.6 (0.4)	3.5 (0.6)	54 (1.5)
2-Propanol	7.0 (1.1)	6.0 (1.5)	43 (2.3)
Propylene glycol	4.0 (0.1)	2.2 (0.2)	71 (1.3)
Ethylene glycol[b]	3.04 (0.03)	1.21 (0.04)	102 (1.0)
Acetone	6.5 (0.5)	2.9 (0.4)	69 (1.6)
DMSO	4.8 (0.2)	1.3 (1.3)	127 (2.2)
4-Nitroaniline			
Methanol	2.7 (0.4)	1.5 (0.5)	35 (3.0)
Ethanol	4.2 (0.3)	5.1 (0.6)	21.2 (0.9)
2-Propanol	5.9 (0.5)	10.4 (1.1)	11.0 (0.5)
Ethylene glycol	3.9 (0.2)	0.65 (0.21)	84 (7.2)
Acetone	9.5 (1.8)	3.5 (1.3)	37 (4.0)
DMSO	3.9 (0.5)	3.8 (0.8)	86 (3.5)
Acetonitrile	8.1 (0.9)	5.6 (1.0)	29 (1.8)

[a]Numbers in parentheses are standard deviations.
[b]Data are from ref. (1).

The exchange constants were observed to depend on the polarity of the organic cosolvents. To study this dependence the values log K_1K_2 were plotted against log P of the pure organic cosolvents. (P is the 1-octanol-water partition coefficient; its value increases with the nonpolarity of the organic cosolvent. All log P values were taken from reference (26).) A plot of the data from Table 1.3 (3) and some of the data from Table 1.2 (2) is shown in Figure 1.4. Two classes of cosolvents appear to exist (except for the divergent propylene glycol point): those with log P less than -1 and those with log P greater than -1. Because log K_1K_2 increases with log P for cosolvents with log P greater than -1, these cosolvents are postulated to solvate through nonpolar interactions. The solvents with log P less than -1 show the opposite behavior, and thus are believed to solvate through a polar interaction. (A plot of log K_1 against log P values shows two classes also, but the data are more scattered.)

The presence of the two solvent classes is consistent with earlier analyses of surface tension data, which showed two classes of cosolvents; one class with log P values greater than -1 whose surface activity increased with hydrophobicity (where log P is used as a measure of hydrophobicity), and a second class, with log P values less than -1, that exhibited higher surface activity as

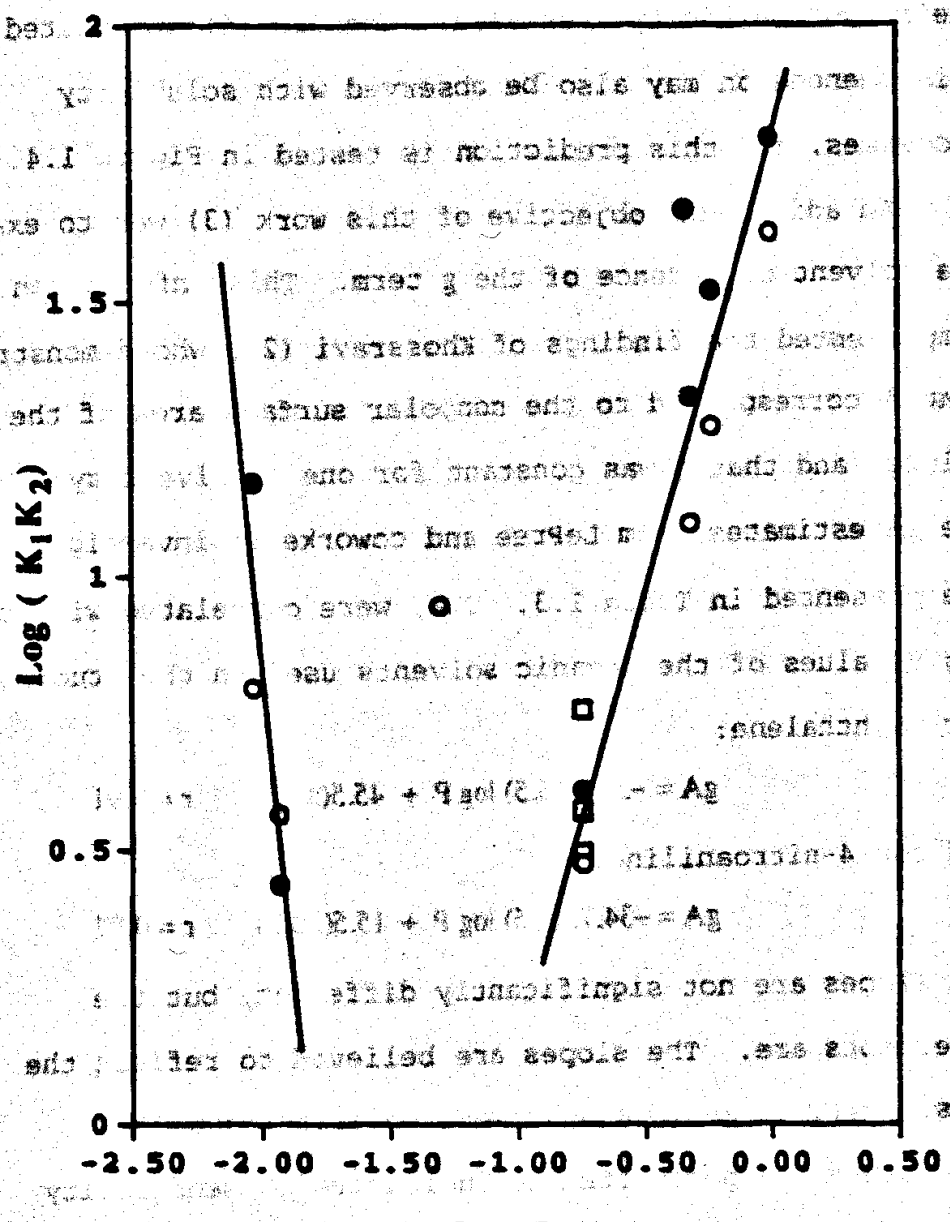

Figure 1.4 Plot of log K_1K_2 against log P of the organic cosolvents showing two solvent classes. The lines have no theoretical significance. Data are from reference (3).

their hydrophilicity increased. Connors (4) speculated that this phenomenon may also be observed with solubility processes, and this prediction is tested in Figure 1.4.

An additional objective of this work (3) was to examine the solvent dependence of the g term. This information complemented the findings of Khossravi (2), who demonstrated that A corresponded to the nonpolar surface area of the solute, and that g was constant for one cosolvent system. The gA estimates from LePree and coworkers' investigation are presented in Table 1.3. They were correlated with the log P values of the organic solvents used in the studies. For naphthalene:

$$gA = -32.1(\pm 6.5)\log P + 45.5(\pm 7.8) \qquad r = 0.91$$

and for 4-nitroaniline:

$$gA = -34.7(\pm 3.5)\log P + 15.5(\pm 3.9) \qquad r = 0.97$$

The slopes are not significantly different, but the intercepts are. The slopes are believed to reflect the sensitivity of gA toward solvent polarity, and the intercepts are postulated to indicative gA sensitivity toward solute polarity. These results led to analysis of the data by equation (1.30)

$$gA = M\log P_M + R\log P_R \qquad (1.30)$$

where P_M and P_R are the 1-octanol-water partition coefficients of the organic cosolvent and the solute respectively. From the empirical correlations given above, M was set equal to -33.4. R was then estimated from the experimental gA values and equation (1.30); for naphthalene R = 13.8 (±3.9) and for 4-nitroaniline R = 12.9 (±4.4).

Since the preceding investigation, equation (1.30) has been used to analyze data for 33 systems comprised of 18 solutes and 11 organic cosolvents (1-3). The values for R and M were obtained by multiple linear regression and are R = 11 (± 1.6), and M =-42 (± 3.9), with the correlation coefficient r^2 = 0.937. Substituting the R and M values into equation (1.30) gives equation (1.31).

$$gA = -42 \log P_M + 11 \log P_R \qquad (1.31)$$

The values for the experimental gA parameter estimates and the gA values calculated from equation (1.31) are in Table 1.4, and a plot of the experimental estimates against the calculated gA values is shown in Figure 1.5.

Table 1.4 Experimental and calculated gA values from equation (1.31)

Solute	log P_R[a]	Solvent	log P_M[a]	gA/Å^2 molecule^{-1} Obs.	Calc.	Ref.
Naphthalene	3.2	Methanol	-0.74	63	66	3
Naphthalene	3.2	Ethanol	-0.32	54	48	3
Naphthalene	3.2	2-Propanol	0	43	35	3
Naphthalene	3.2	1,2-Propanediol	-1.35	71	92	3
Naphthalene	3.2	1,2-Ethanediol	-1.93	102	116	1
Naphthalene	3.2	Acetone	-0.24	69	45	3
Naphthalene	3.2	DMSO[b]	-2.03	127	120	3
4-Nitroaniline	1.39	Methanol	-0.74	35	46	3
4-Nitroaniline	1.39	Ethanol	-0.32	21	29	3
4-Nitroaniline	1.39	2-Propanol	0	11	15	3
4-Nitroaniline	1.39	1,2-Ethanediol	-1.93	84	96	3
4-Nitroaniline	1.39	Acetone	-0.24	37	25	3
4-Nitroaniline	1.39	DMSO	-2.03	86	101	3
4-Nitroaniline	1.39	Acetonitrile	-0.34	29	30	3
Sucrose	-3.67	Ethanol	-0.32	-40	-27	3
Biphenyl	4.09	Methanol	-0.74	74	76	2
4-HBP[c]	3.42	Methanol	-0.74	67	69	2
4,4'-DHBP[d]	3.04	Methanol	-0.74	53	65	2
4-BBP[e]	4.96	Methanol	-0.74	87	86	2
Acetanilide	1.2	Methanol	-0.74	28	44	1
Acetanilide	1.2	Ethanol	-0.32	19	27	1
Sulfadiazine	-0.1	DMF[f]	-0.73	81	30	1
Phenylsalicylate	3.02	Ethanol	-0.32	55	47	1
Methylsalicylate	1.82	Ethanol	-0.32	60	33	1
Phenacetin	1.58	Ethanol	-0.32	19	31	1
Barbital	0.65	Ethanol	-0.32	10	21	1
Phenobarbital	1.42	Ethanol	-0.32	28	29	1
Diphenylhydantoin	2.06	Methanol	-0.74	52	54	1
Diphenylhydantoin	2.06	Ethanol	-0.32	37	36	1
Diphenylhydantoin	2.06	Glycerol	-2.56	172	130	1
MAP[g]	1.63	Ethanol	-0.32	18	31	1
Caffeine	-0.07	1,4-Dioxane	-0.42	3	17	1
Theobromine	-0.78	1,4-Dioxane	-0.42	10	9	1

[a] Values from reference (25)
[b] Dimethylsulfoxide
[c] 4-Hydroxybiphenyl
[d] 4,4'-Dihydroxybiphenyl
[e] 4-Bromobiphenyl
[f] Dimethylformamide
[g] Methyl *p*-aminobenzoate

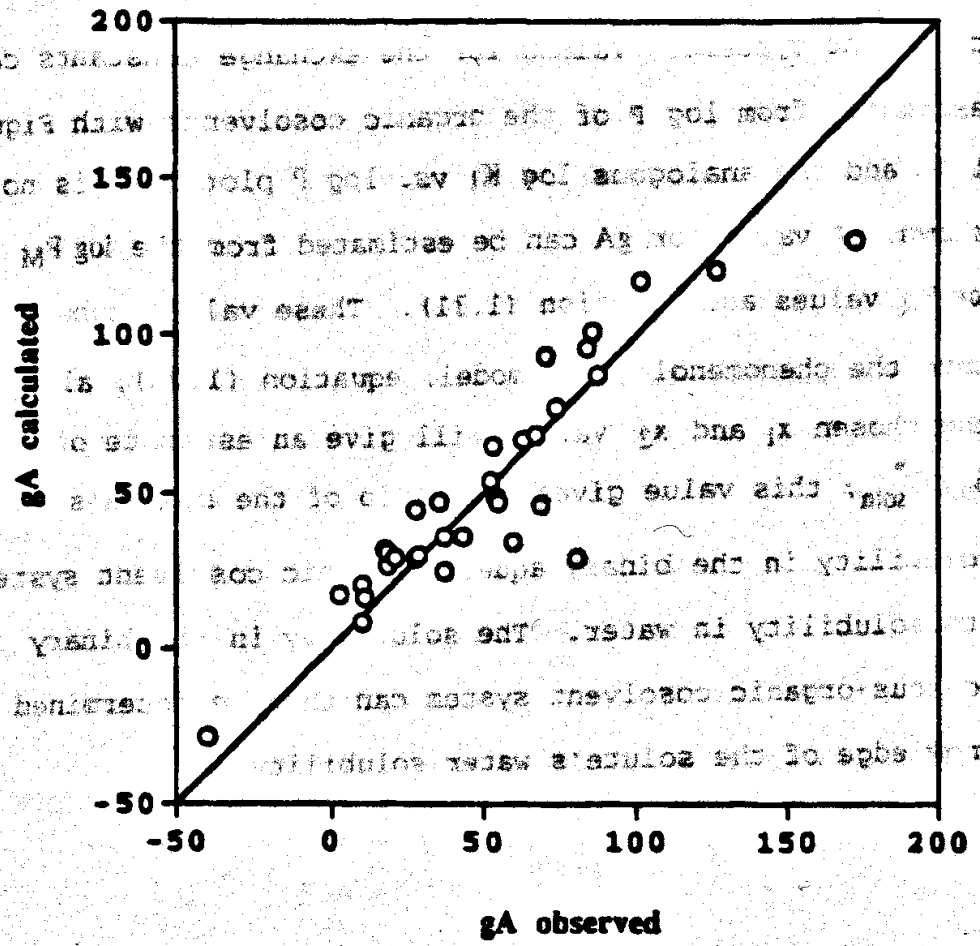

Figure 1.5 A plot of the gA values calculated from equation (1.31) against the experimental gA values, the values obtained by fitting the experimental data to equation (1.25). The slope of the line is 1.00.

The correlations in Figures 1.4 and 1.5 provide a means to predict solubility of solutes in aqueous-organic cosolvent systems. Values for the exchange constants can be estimated from log P of the organic cosolvents with Figure 1.4, and the analogous log K_I *vs.* log P plot that is not shown. A value for gA can be estimated from the log P_M and log P_R values and equation (1.31). These values substituted into the phenomenological model, equation (1.25), along with the chosen x_1 and x_2 values will give an estimate of $\delta_m \Delta G^*_{soln}$; this value gives the ratio of the solute's solubility in the binary aqueous-organic cosolvent system to its solubility in water. The solubility in the binary aqueous-organic cosolvent system can then be determined from knowledge of the solute's water solubility.

1.3 The Application of the Phenomenological Model to Surface Tension

1.3.1 Theory

The surface tension of the solvation shell was given by equation (1.18)

$$\gamma = \gamma_1 + \gamma' \left(\frac{K_1 x_1 x_2 + 2K_1 K_2 (x_2)^2}{(x_1)^2 + K_1 x_1 x_2 + K_1 K_2 (x_2)^2} \right) \qquad (1.18)$$

where all terms have been previously defined. Because it was derived from a two-step solvation scheme (Scheme 1.1), it will be called the two-step model. If a one-step solvation scheme is used, equation (1.18) reduces to equation (1.32),

$$\gamma = \gamma_1 + \gamma' \left(\frac{K_1 x_2}{x_1 + K_1 x_2} \right) \qquad (1.32)$$

where $\gamma' = \gamma_2 - \gamma_1$.

1.3.2 Results

Both equations were applied to surface tension data of thirteen aqueous-organic cosolvent systems (4). The cosolvents were methanol, 2-propanol, 1-propanol, t-butanol, acetic acid, acetone, acetonitrile, dioxane,

tetrahydrofuran, glycerol, dimethylsulfoxide, formamide, and ethylene glycol. As observed with the two-step solubility model (1), the two-step surface tension model, given by equation (1.18), fit all the data, whereas the one-step surface tension model, given by equation (1.32), fit most, but not all the data. Figure 1.6 shows a characteristic plot of the fit of equation (1.18) to the surface tension data.

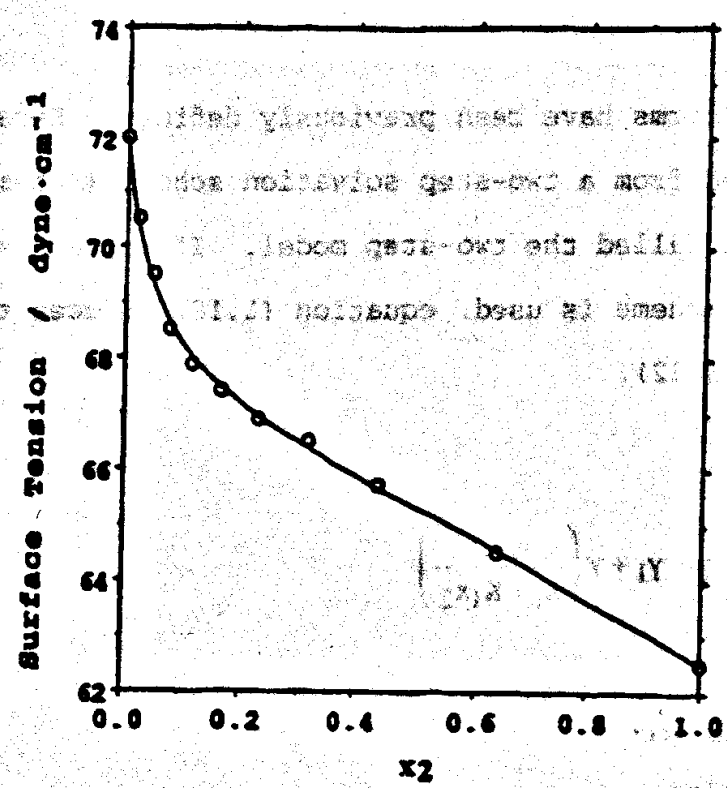

Figure 1.6 Plot of the surface tension against the mole fraction of organic cosolvent for water-glycerol mixtures showing the experimental data points and the fitted curve (equation 1.18) (4). References to the data are cited in Ref. (27).

Two pertinent conclusions can be drawn from this study. The first is that equation (1.18) can describe the surface tension of aqueous-organic cosolvent systems, which somewhat substantiates its use to describe the surface tension of a solvation shell that surrounds a solute. (If the air-water interface is assumed to represent a solvation shell where air acts as a solute.) The second is that the cosolvents fall into two classes, as was discussed in the earlier section. Plots of the ln K_1 (4) against log P and ln K_1K_2 (28) against log P demonstrate this behavior and are shown in Figures 1.7 and 1.8. Connors hypothesized that such behavior would be observed for the solvation of solutes. This hypothesis was realized when the model was applied to solubility data from naphthalene and 4-nitroaniline in various aqueous-organic cosolvent systems (3), as can be inferred from the similarity in the data patterns of Figures 1.4 and 1.8.

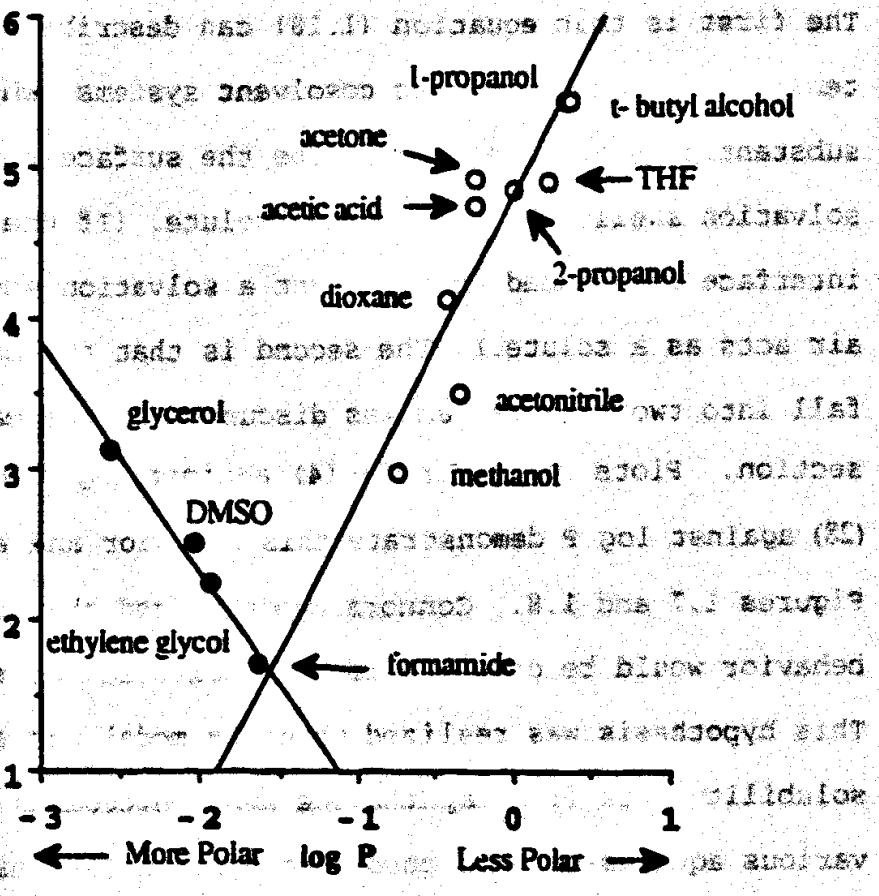

Figure 1.7 Plot of ln K_I from the surface tension analysis against log P of the cosolvents (4). The lines have no theoretical significance.

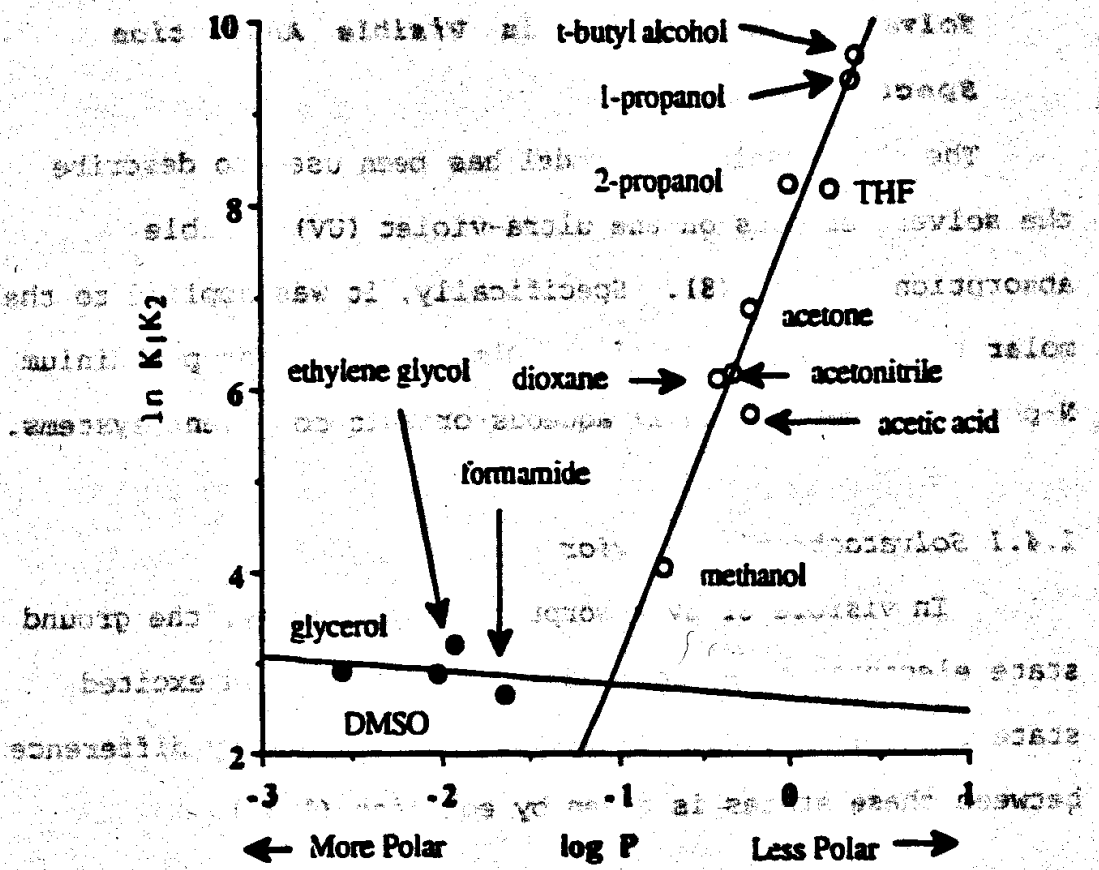

Figure 1.8 Plot of ln K_1K_2 from the surface tension analysis against log P of the cosolvents (28). The lines have no theoretical significance.

1.4 Application of the Phenomenological Model to Solvatochromic Shifts in Visible Absorption Spectra

The phenomenological model has been used to describe the solvent effects on the ultra-violet (UV)-visible absorption spectra (8). Specifically, it was applied to the molar transition energy of the Dimroth-Reichardt pyridinium N-phenoxide betaine in 17 aqueous-organic cosolvent systems.

1.4.1 Solvatochromic Behavior

In visible or UV absorption spectroscopy, the ground state electrons of a compound are promoted to an excited state by an electronic transition, and the energy difference between these states is given by equation (1.33)

$$\Delta E = h\upsilon = hc/\lambda \qquad (1.33)$$

where h is Planck's constant, υ is the frequency of light that is absorbed, c is the speed of light, and λ is the wavelength of light that is absorbed. Changes in solvent composition can change the frequency of the absorbed radiation of some solutes; this phenomenon is called solvatochromism.

It follows from equation (1.33) that if the spectrum is shifted to longer wavelengths (a red shift or bathochromic

shift) by a change in the solvent composition, then the energy difference between the ground and electronic states was decreased by the solvent change; if the shift is toward shorter wavelengths (blue shift or hypsochromic shift) then the solvent increased the energy difference between the ground and the excited states. The solvent affects the energy differences through either stabilization or destabilization of the excited state or ground state. The stabilization of these species can occur through dipole-dipole interactions, dipole-induced dipole interactions, and/or induced dipole-induced dipole interactions. The magnitude of these interactions depend upon the polarity of the solvent, which in turn controls the solvatochromic shifts.

Because solvatochromic shifts depend on the solvent polarity, the shifts of some compounds have been used as empirical measures of solvent polarity; one of them is Dimroth-Reichardt's betaine (2,6-diphenyl-4-(2,4,6-triphenylpyridino)phenolate) (29) (1) which absorbs light in the visible range and displays extremely large hypsochromic shifts as solvent polarity is increased. The phenomenological model has been used to quantitatively describe the solvent effects on the molar transition energies for Dimroth-Rieichardt's betaine.

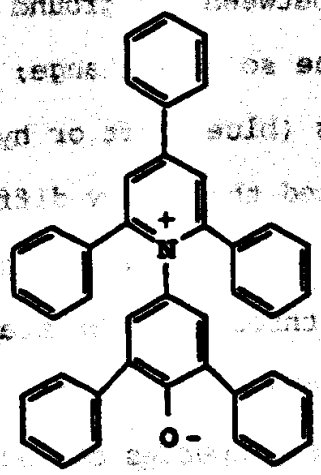

1.4.2 Theory

The molar transition energy of Dimroth-Reichardt's betaine, $E_T(30)$, was calculated from equation (1.34), which is obtained from equation (1.33).

$$E_T(30)\,/\,\text{kcal mol}^{-1} = \frac{28591.5}{\lambda_{max}\,/\,\text{nm}} \qquad (1.34)$$

To model $E_T(30)$ as a function of x_2, only solvent-solute interactions (the Solvation Effect component of the phenomenological model) were considered. It was assumed that solute-solute interactions (the Intersolute Effect) were negligible because the concentration of the dye was always low. The General Medium Effect which accounts for

the solvent-solvent interactions was set to zero because it was accepted that the solvent cavity would not change size or shape during an electronic transition. (Here, Connors and Skwierczynski (3) made use of the Franck-Condon Principle which states that atomic nuclei do not undergo significant motion on the time scale of an electronic transition.)

For the one-step solvation scheme presented in Scheme 1.5 (page 15), the fractions of fully hydrated species and fully solvated species are given by equations (1.35) and (1.36) respectively; all terms have been previously defined.

$$F_{RW} = \frac{x_1}{x_1 + K_1 x_2} \qquad (1.35)$$

$$F_{RM} = \frac{K_1 x_2}{x_1 + K_1 x_2} \qquad (1.36)$$

The molar transition energy at any organic mole fraction concentration was expressed as the weighted average of the E_T for the fully hydrated and fully solvated species. This is given by equation (1.37),

$$E_T(x_2) = F_{RW}E_T(RW) + F_{RM}E_T(RM) \qquad (1.37)$$

where $E_T(RW)$ is the value of E_T in the fully aqueous system and $E_T(RM)$ is the value for E_T in the fully organic system. A new quantity, Γ, is defined by combining equations (1.37) and (1.36) to give equation (1.38).

$$\Gamma = \frac{E_T(x_2) - E_T(RW)}{E_T(RM) - E_T(RW)} = \frac{K_1 x_2}{x_1 + K_1 x_2} \quad (1.38)$$

For a two-step solvation scheme (see Scheme 1.1) $E_T(x_2)$ is given by equation (1.39),

$$E_T(x_2) = F_{RW_2} E_T(RW_2) + F_{RWM} E_T(RWM) + F_{RM_2} E_T(RM_2) \quad (1.39)$$

where it is assumed that $E_T(RWM) = (E_T(RW_2) + E_T(RM_2))/2$, and all other terms have been previously defined. Γ is then given by equation (1.40).

$$\Gamma = \frac{E_T(x_2) - E_T(RWW)}{E_T(RMM) - E_T(RWW)} = \frac{K_1 x_1 x_2 / 2 + K_1 K_2 x_2^2}{x_1^2 + K_1 x_1 x_2 + K_1 K_2 x_2^2} \quad (1.40)$$

Γ was measured as a function of x_2 and values for the parameters K_1 and K_2 were extracted by fitting equations (1.38) and (1.40) to the data using non-linear regression.

1.4.3 Results

Equations (1.38) and (1.40) were applied to $E_T(30)$ data for 17 aqueous-organic cosolvent systems; the cosolvents were methanol, ethanol, 1-propanol, 2-propanol, ethylene glycol, propylene glycol, 1,3-propanediol, dimethylsulfoxide, acetone, acetonitrile, dioxane, tetrahydrofuran, N,N-dimethylformamide, piperidine, 2,6-lutidine, 2-picoline, and pyridine.

In the previously described solubility and surface tension studies it was seen that the organic cosolvents could be separated into two classes. Skwierczynski and Connors (8) observed that equation (1.38), which was derived from the one-step solvation scheme, could quantitatively describe solvent effect curves of hydroxylic solvents and dimethylsulfoxide, thus these solvents were classified as one-step solvents. An example of the fit to the methanol-water system is presented in Figure 1.9. Equation (1.40), which was derived from a two-step solvation scheme was needed to fit all the other solvent systems; these systems gave sigmoidal solvent effect curves and were classified as two-step solvents. Figure 1.10 shows an example for the acetone-water system.

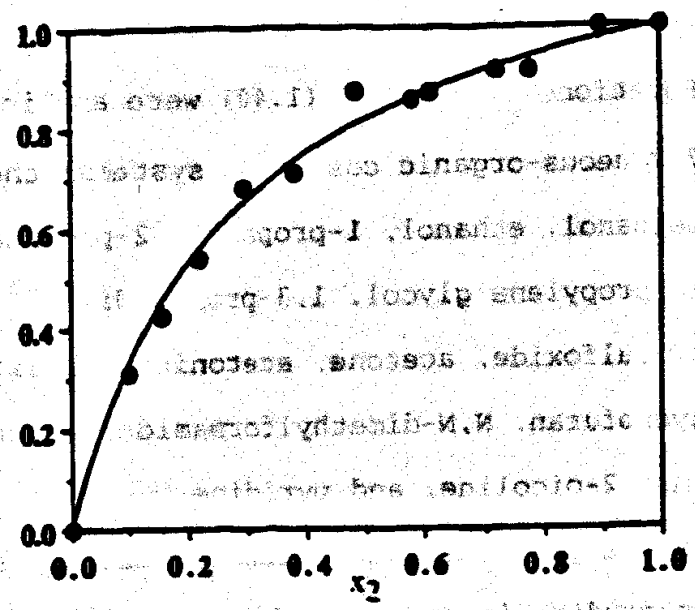

Figure 1.9 Plot of Γ against x_2, showing the experimental data points (methanol-water system) and the curve-fit to the data according to equation (1.38). This is a one-step solvent.

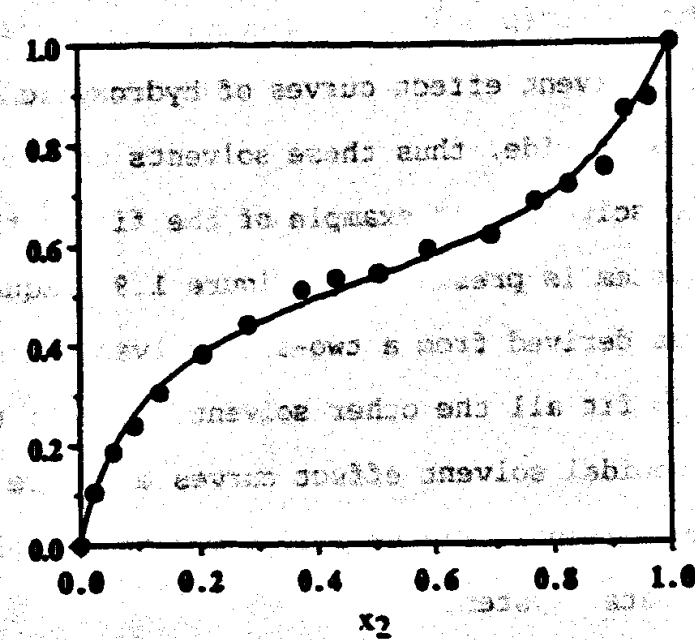

Figure 1.10 Plot of Γ against x_2, showing the experimental data points (acetone-water system) and the curve-fit to the data according to equation (1.40). This is a two-step solvent.

More importantly, the solvation exchange constants were observed to correlate with several parameters. The log K_1 values from both the one-step and two-step models were observed to correlate positively with log P values of the cosolvents that were used in these studies. The log K_1 or log K_1K_2 values were also observed to correlate positively with β, the Taft-Kamlet solvatochromic (30) measure of solvent hydrogen bond basicity, and to ΔH^0, the enthalpy change for boron trifluoride-solvent Lewis acid base complex formation in dichloromethane (31). The correlations of the solvation exchange constants with log P of the cosolvent suggests that the solvent hydrophobicity influences the exchange constant values. The positive correlations with β and ΔH^0 suggest that the ability of the solvent to donate an electron-pair also influences the solvation exchange constant parameter estimates. The correlation data are presented in Table 1.5.

Table 1.5 Correlation of exchange constants with empirical solvent characteristics

Correlation Equation	r	n[b]
$\log K_1 = 0.265 \log P + 1.06$	0.904	17
$\log K_1 = -0.032E_T + 2.44$	-0.711	17
$\log (K_1 \text{ or } K_1K_2)^a = 1.47\beta - 0.37$	0.732	11
$\log (K_1 \text{ or } K_1K_2) = 0.016\Delta H^0 - 1.06$	0.872	7
$\log K_2 = 2.30\beta - 1.82$	0.826	5
$\log K_2 = 0.0131\Delta H^0 - 1.83$	0.794	6

[a] K_1 for one-step solvents; K_1K_2 for two-step solvents
[b] No. of data points

Acree and coworkers (32) have criticized this work because the two-step solvation scheme implies that three kinds of solvated dye molecules exist in the experimental solutions; these are the fully hydrated, partially solvated, and fully solvated species. If each species acts as a distinct chromophore, having its own wavelength of maximum absorption, then each species should be observable as a distinct absorption band, yet only one absorption band was observed for each experimental solution. This indicates that the three types of solvated dye molecule may not be present in the experimental solutions on the time scale of electronic transitions. Acree postulates that the success of the model in describing the data probably arises from the mathematical form of the model, rather than its depiction of chemical reality.

1.5 Application of the Phenomenological Model to Complexation Data

1.5.1 Theory

The phenomenolcgical model has been applied to 1:1 stoichiometric complexation reactions, where a substrate and a ligand combine to form a complex (5-7). This reaction is depicted in equation (1.41) where the substrate is denoted by S, the ligand by L, and the complex by C. The equilibrium for this reaction is described by the equilibrium constant K_{11}, where the subscript indicates 1:1 stoichiometery.

$$S + L \underset{}{\overset{K_{11}}{\rightleftharpoons}} C \qquad (1.41)$$

The theory that has been developed for solubility can be used here, but the presence of three species increases the number of adjustable parameters in the equation, making it impractical to use directly; therefore much of this section will discuss assumptions that can be used to simplify the model and to reduce the number of adjustable parameters.

The thermodynamic cycles given in Figure 1.11 are helpful in analyzing this problem. As will be seen later, a portion of Figure 1.11 will be used to describe the kinetics model. The cycles describe both complexation and solubility

processes in the solid, liquid, and gas phases. This treatment was first presented by Connors and Khossravi(6).

In this cycle, the letters in parentheses denote either the solid (s), the liquid (l), or the gas (g) phase. The free energy of complexation is denoted by $\Delta G^{(j)}_{complex.}$ where j indicates the phase. The lattice energy, the General Medium Effect and the Solvation Effect, are denoted by $\Delta G_{lat.}$, $\Delta G_{gen.\ med.}$, and $\Delta G_{solv.}$ respectively. The superscripts are used to indicate the substrate, ligand, and the complex.

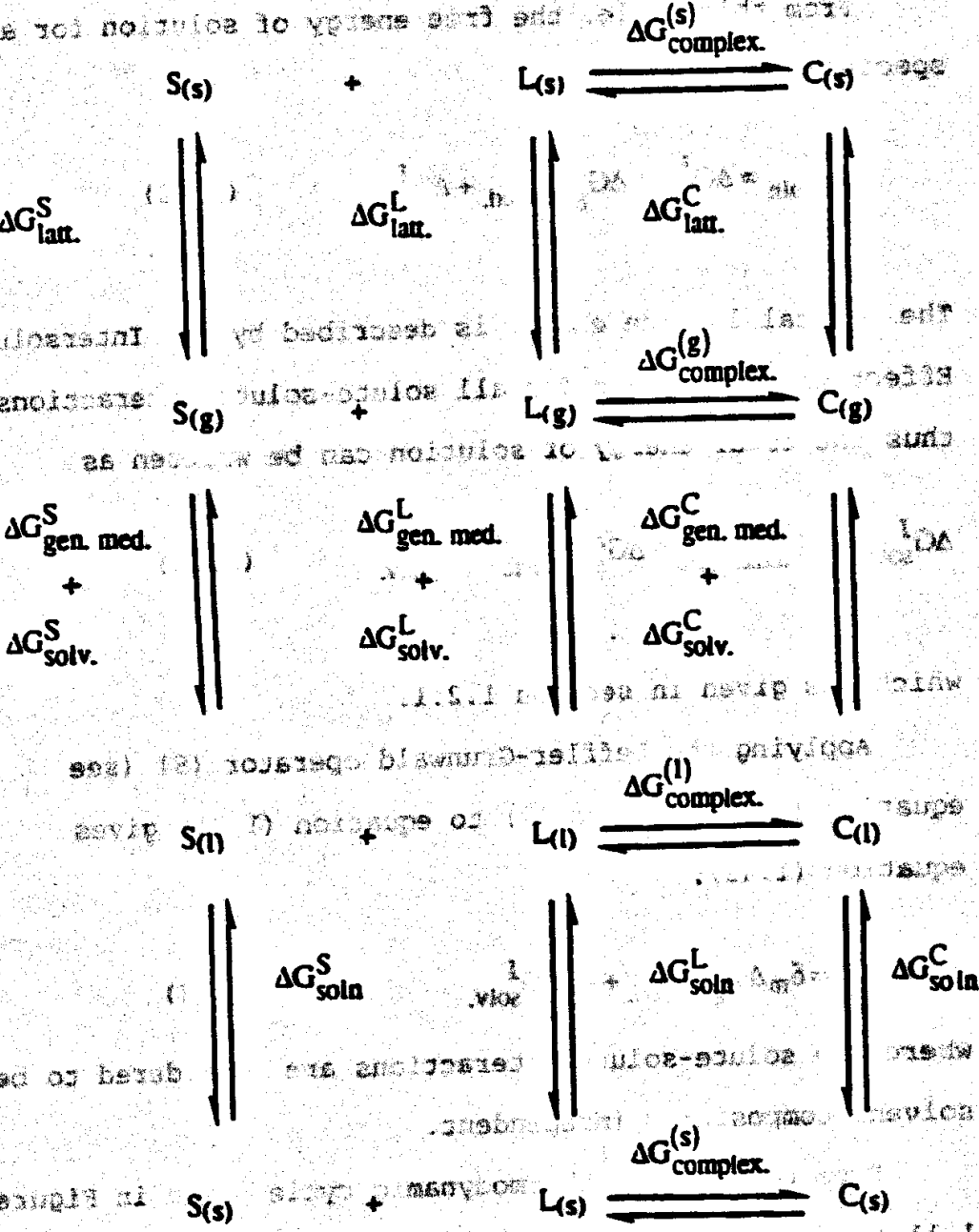

Figure 1.11 The thermodynamic cycles for complexation. The terms are defined in the text. These cycles were first presented in reference (6).

From this cycle, the free energy of solution for any species J is given by

$$\Delta G^{J}_{soln} = \Delta G^{J}_{latt} + \Delta G^{J}_{gen.\ med.} + \Delta G^{J}_{solv.} \qquad (1.42)$$

The crystal lattice energy is described by the Intersolute Effect which accounts for all solute-solute interactions and thus the total energy of solution can be written as

$$\Delta G^{J}_{soln} = \Delta G^{J}_{intersolute} + \Delta G^{J}_{gen.\ med.} + \Delta G^{J}_{solv.} \qquad (1.21)$$

which was given in section 1.2.1.

Applying the Leffler-Grunwald operator (9) (see equation (1.24) on page 12) to equation (1.21) gives equation (1.43),

$$\delta_m \Delta G^{J}_{soln} = \delta_m \Delta G^{J}_{gen.med.} + \delta_m \Delta G^{J}_{solv.} \qquad (1.43)$$

where the solute-solute interactions are considered to be solvent composition independent.

From the central thermodynamic cycle given in Figure 1.11 the expression for the free energy of complexation is given by

$$\Delta G^{(l)}_{complex.} = \Delta G^{(g)}_{complex.} + \left(\Delta G^{C}_{gen.\ med.} + \Delta G^{C}_{solv.}\right)$$

$$-\left(\Delta G^{S}_{gen.\ med.} + \Delta G^{S}_{solv.}\right) - \left(\Delta G^{L}_{gen.\ med.} + \Delta G^{L}_{solv.}\right) \quad (1.44)$$

Applying the Leffler-Grunwald delta operator (9) to this equation gives

$$\delta_m \Delta G^{(l)}_{complex.} = \left(\delta_m \Delta G^{C}_{gen.\ med.} + \delta_m \Delta G^{C}_{solv.}\right)$$

$$-\left(\delta_m \Delta G^{S}_{gen.\ med.} + \delta_m \Delta G^{S}_{solv.}\right) - \left(\delta_m \Delta G^{L}_{gen.\ med.} + \delta_m \Delta G^{L}_{solv.}\right) \quad (1.45)$$

where the free energy for complexation in the gaseous state is independent of solvent composition.

Substitution of equation (1.43) into equation (1.45) gives

$$\delta_m \Delta G^{(l)}_{complex.} = \delta_m \Delta G^{C}_{soln} - \delta_m \Delta G^{S}_{soln} - \delta_m \Delta G^{L}_{soln} \quad (1.46)$$

where $\delta_m \Delta G^{C}_{soln}$, $\delta_m \Delta G^{S}_{soln}$, and $\delta_m \Delta G^{L}_{soln}$ are the solubility solvent effect expressions for the complex, substrate, and ligand. Equation (1.46) relates the solvent effects on complexation to the solvent effects on solubility of the several species involved; this was a significant finding of this paper (6). Substitution of the one-step model expression for solubility, which is given by equation (1.29)

(see page 15), into equation (1.46) leads to equation (1.47),

$$\delta_m \Delta G^{(1)}_{complex} = \frac{\left(gA^C\dot{\gamma} - k_B T \ln K_1^C\right) K_1^C x_2}{x_1 + K_1^C x_2} - \frac{\left(gA^S\dot{\gamma} - k_B T \ln K_1^S\right) K_1^S x_2}{x_1 + K_1^S x_2} - \frac{\left(gA^L\dot{\gamma} - k_B T \ln K_1^L\right) K_1^L x_2}{x_1 + K_1^L x_2} \quad (1.47)$$

which has six adjustable parameters. Substitution of the two-step model for solubility, given by equation (1.25), for each species in solution gives equation (1.48)

$$\delta_m \Delta G^{(1)}_{complex} \quad (1.48)$$

$$= \left(\frac{(-k_B T \ln (K_1^C) + gA^C\dot{\gamma})\, K_1^C x_1 x_2 + (-k_B T \ln (K_1^C K_2^C) + 2gA^C\dot{\gamma})\, K_1^C K_2^C (x_2)^2}{(x_1)^2 + K_1^C x_1 x_2 + K_1^C K_2^C (x_2)^2} \right)$$

$$- \left(\frac{(-k_B T \ln (K_1^S) + gA^S\dot{\gamma})\, K_1^S x_1 x_2 + (-k_B T \ln (K_1^S K_2^S) + 2gA^S\dot{\gamma})\, K_1^S K_2^S (x_2)^2}{(x_1)^2 + K_1^S x_1 x_2 + K_1^S K_2^S (x_2)^2} \right)$$

$$- \left(\frac{(-k_B T \ln (K_1^L) + gA^L\dot{\gamma})\, K_1^L x_1 x_2 + (-k_B T \ln (K_1^L K_2^L) + 2gA^L\dot{\gamma})\, K_1^L K_2^L (x_2)^2}{(x_1)^2 + K_1^L x_1 x_2 + K_1^L K_2^L (x_2)^2} \right)$$

which has nine adjustable parameters.

In principle, equations (1.47) and (1.48) can describe the solvent effects on the complexation process, but they

are not practically useful, owing to the large number of adjustable parameters. In previous papers, three approximation methods were examined as means to reduce the number of adjustable parameters; these were called the *semi-empirical approximation* (6), the *full cancellation approximation* (5,6,7), and the *partial cancellation approximation* (7).

The *semi-empirical approximation* invoives rearranging equation (1.46) to give equation (1.49)

$$\delta_m\Delta G^{(I)}_{complex.} + \delta_m\Delta G^{S}_{soln} + \delta_m\Delta G^{L}_{soln} = \delta_m\Delta G^{C}_{soln} \qquad (1.49)$$

On substituting the two-step solubility equation, (1.25), equation (1.49) gives equation (1.50), whereas substitution of the one-step solubility model, [equation (1.29)], leads to equation (1.51)

$$\delta_m\Delta G^{(I)}_{complex.} + \delta_m\Delta G^{S}_{soln} + \delta_m\Delta G^{L}_{soln}$$

$$= \left(\frac{(-k_BT \ln (K_1^C) + gA^C\gamma')\, K_1^C x_1 x_2 + (-k_BT \ln (K_1^C K_2^C) + 2gA^C\gamma')\, K_1^C K_2^C (x_2)^2}{(x_1)^2 + K_1^C x_1 x_2 + K_1^C K_2^C (x_2)^2} \right)$$

(1.50)

$$\delta_m\Delta G^{(l)}_{complex.} + \delta_m\Delta G^{S}_{soln} + \delta_m\Delta G^{L}_{soln}$$

$$= \frac{\left(gA^C\gamma' - k_B T \ln K_1^C\right)K_1^C x_2}{x_1 + K_1^C x_2} \qquad (1.51)$$

Equation (1.50) has only three adjustable parameters: K_1^C, K_2^C, and gA^C , and equation (1.51) has only two adjustable parameters: gA^C, and K_1^C. To use these equations, $\delta_m\Delta G^{(l)}_{complex.}$, $\delta_m\Delta G^{S}_{soln}$, and $\delta_m\Delta G^{L}_{soln}$ are measured as a function of x_2, and non-linear regression is performed on these data to extract the adjustable parameter values.

A second treatment is called the *full cancellation approximation* (5,6,7), in which we assume that the substrate, the ligand, and the complex are solvated equally, giving $K_1^C = K_1^S = K_1^L = K_1$; applying this condition to equations (1.47) and (1.48) leads to equations (1.52) and (1.53) respectively.

$$\delta_m \Delta G^{(1)}_{complex.} = \frac{\left(\Delta g A \gamma' + k_B T \ln K_1\right) K_1 x_2}{x_1 + K_1 x_2} \qquad (1.52)$$

$$\delta_m \Delta G^{(1)}_{complex.}$$

$$= \left(\frac{(k_B T \ln (K_1) + \Delta g A \gamma')\, K_1 x_1 x_2 + (k_B T \ln (K_1 K_2) + 2 \Delta g A\, \gamma')\, K_1 K_2 (x_2)^2}{(x_1)^2 + K_1 x_1 x_2 + K_1 K_2 (x_2)^2} \right) \qquad (1.53)$$

where $\Delta gA = gA^C - gA^S - gA^L$. (Equation (1.52) has two adjustable parameters, and equation (1.53) has three adjustable parameters.)

The justification for equating the solvation constants lies in our results on 56 solubility studies comprising 36 different solutes and 10 different cosolvents that were subjected to analysis by the phenomenological model. The average value for K_1 is 4.5 with a standard deviation of 3.0 and a range of 1.5 to 15.1 (7). The solutes were structurally very disparate (for example sucrose and dibromobiphenyl), and from this relatively small variation in the solvation exchange constants it seems reasonable to conclude that the exchange constants are not highly sensitive to solute structure. This was discussed earlier in the chapter.

Another special case, where $K_1^C = K_1^S < K_1^L$, leads to a third method called the *partial cancellation approximation* (7). Applying this condition to equation (1.47) gives

$$\delta_m \Delta G^{(1)}_{complex.} = \frac{\left(k_B T \ln K_1^L - gA^L\gamma'\right)K_1^L x_2}{x_1 + K_1^L x_2} + \frac{\left(gA^C - gA^S\right)\gamma' K_1^S x_2}{x_1 + K_1^S x_2} \qquad (1.54)$$

and because $K_1^S < K_1^L$, we write

$$\delta_m \Delta G^{(1)}_{complex.} \equiv \frac{\left(k_B T \ln K_1^L - gA^L\gamma'\right)K_1^L x_2}{x_1 + K_1^L x_2} \qquad (1.55)$$

In Table 1.6 I have summarized these equations.

Table 1.6 The assumptions and equations used to analyze complexation data.

Approximation	No. of Steps in $\delta_m \Delta G^*_{soln}$ equation	Equation no. in this chapter	No. of para-meters	Ref.
Semi-empirical	two-step model	1.50	3	6
Semi-empirical	one-step model	1.51	2	6
Full cancellation	two-step model	1.53	3	5,6,7
Full cancellation	one-step model	1.52	2	5,7
Partial cancellation	one-step model	1.55	2	7

1.5.2 Results

The phenomenological model can quantitatively describe solvent effects on Methyl Orange complexation with α-cyclodextrin (5), theophylline and naphthalene complexation (6), and 4-nitroaniline complexation with α-cyclodextrin (7). In Figure 1.12, a plot of the curve fits to the naphthalene-theophylline complexation data (in ethylene glycol-water mixtures) is presented, as well as fits to naphthalene and theophylline solubility data using the two-step solubility model, equation (1.25). The fits to the other data with the other equations were equally good (5,6,7).

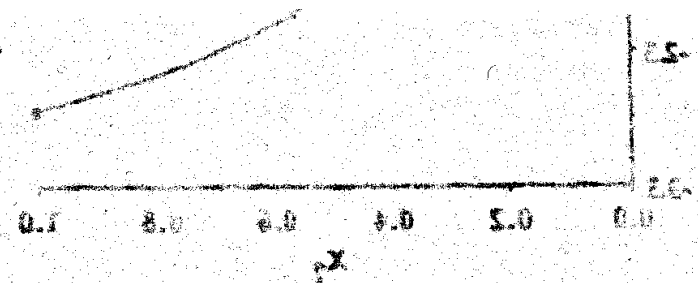

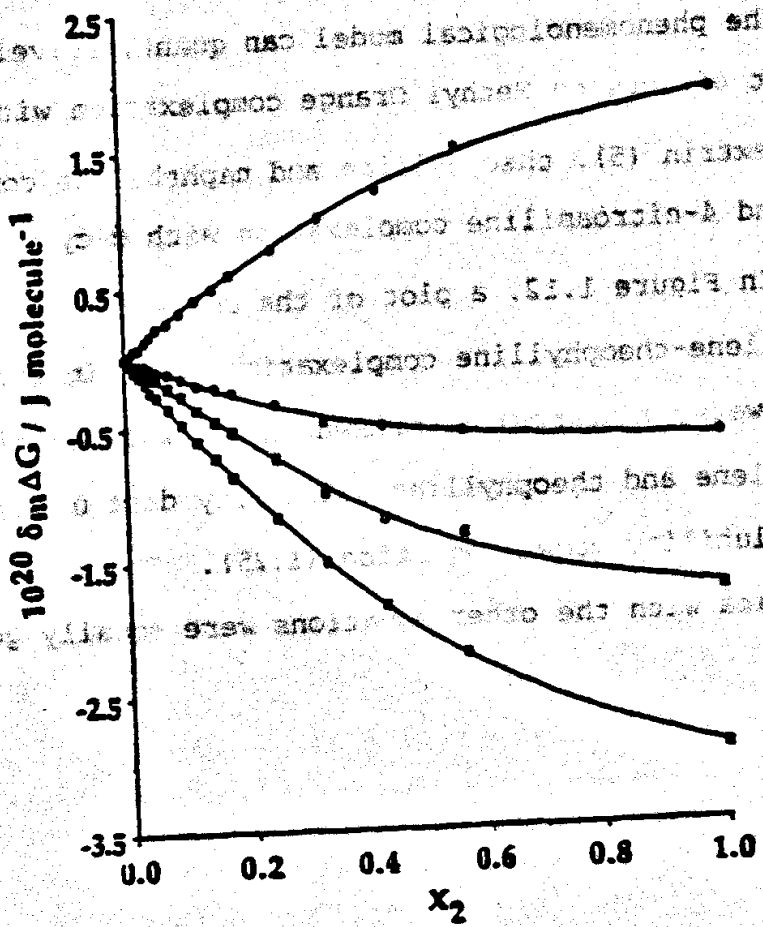

Figure 1.12 Solubility and complexation of naphthalene and theophylline in ethylene glycol-water cosolvent mixtures. In order from top to bottom the lines are: the fit of the complexation data to the equation (1.53), the two-step, full cancellation approximation model; the fit of theophylline solubility data to the two-step solubility model equation (1.25), the fit of the complexation data to the two-step, semi-empirical approximation model equation (1.50), and the fit of the naphthalene solubility data to the two-step solubility model equation (1.25) (6).

An interesting inference of the cyclodextrin solvent effect studies (5,7) is the discontinuous behavior of the solvation exchange constants. When log K_1 for the α-cyclodextrin systems is plotted against log P, a discontinuity at log P = -0.3 is observed. Such a plot for the methyl orange-α-cyclodextrin (5) and the 4-nitroaniline-α-cyclodextrin (7) data is given in Figure 1.13. These results are only pertinent for α-cyclodextrin inclusion complexes.

This discontinuous behavior is also observed from a model-independent, graphical analysis of the data. Connors (7) has estimated the initial slopes of the $\delta_m \Delta G^{(1)}_{complex.}$ *vs.* x_2 plots; when these values were plotted against log P of the organic cosolvent, behavior similar to the log K_1 against log P plots is observed. Figure 1.14 shows such a plot; here again, a discontinuity is observed at log P = -0.3. It was proposed that this value represents the effective log P value of the cyclodextrin cavity.

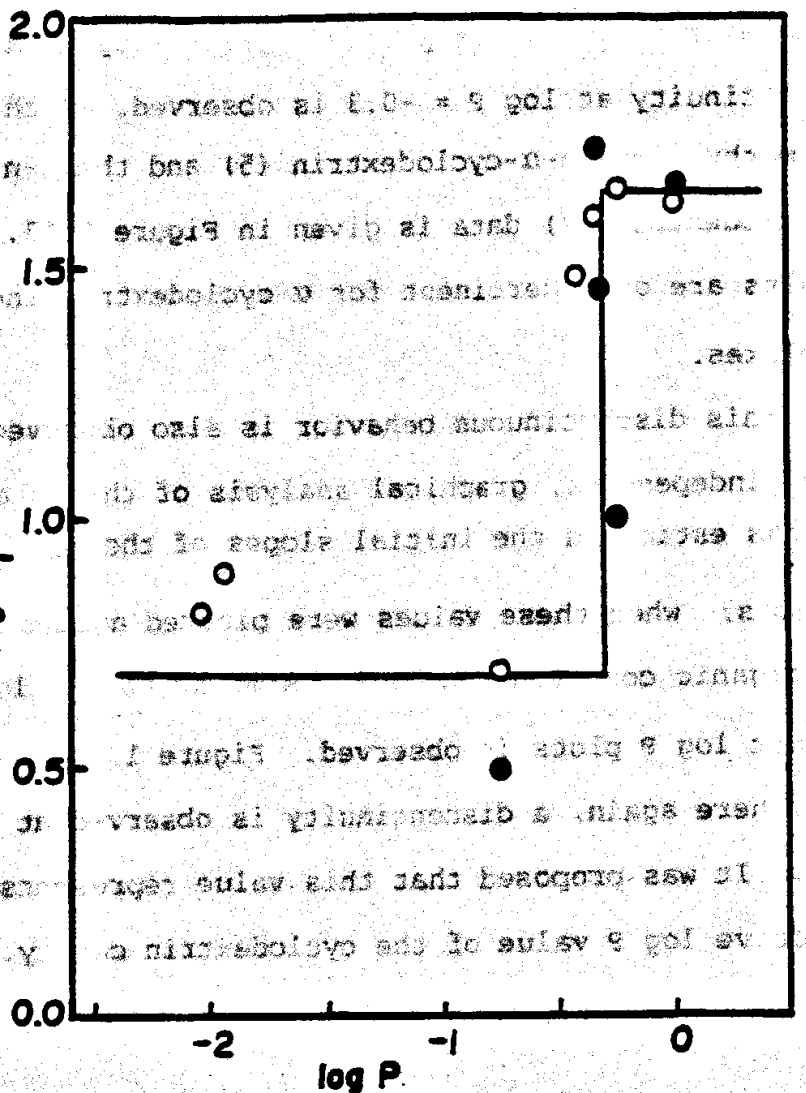

Figure 1.13 Plot of log K_I against log P of the organic cosolvent. The open circles are from the methyl orange-α-cyclodextrin complexation studies (5), and the closed circles are from the 4-nitroaniline-α-cyclodextrin studies.

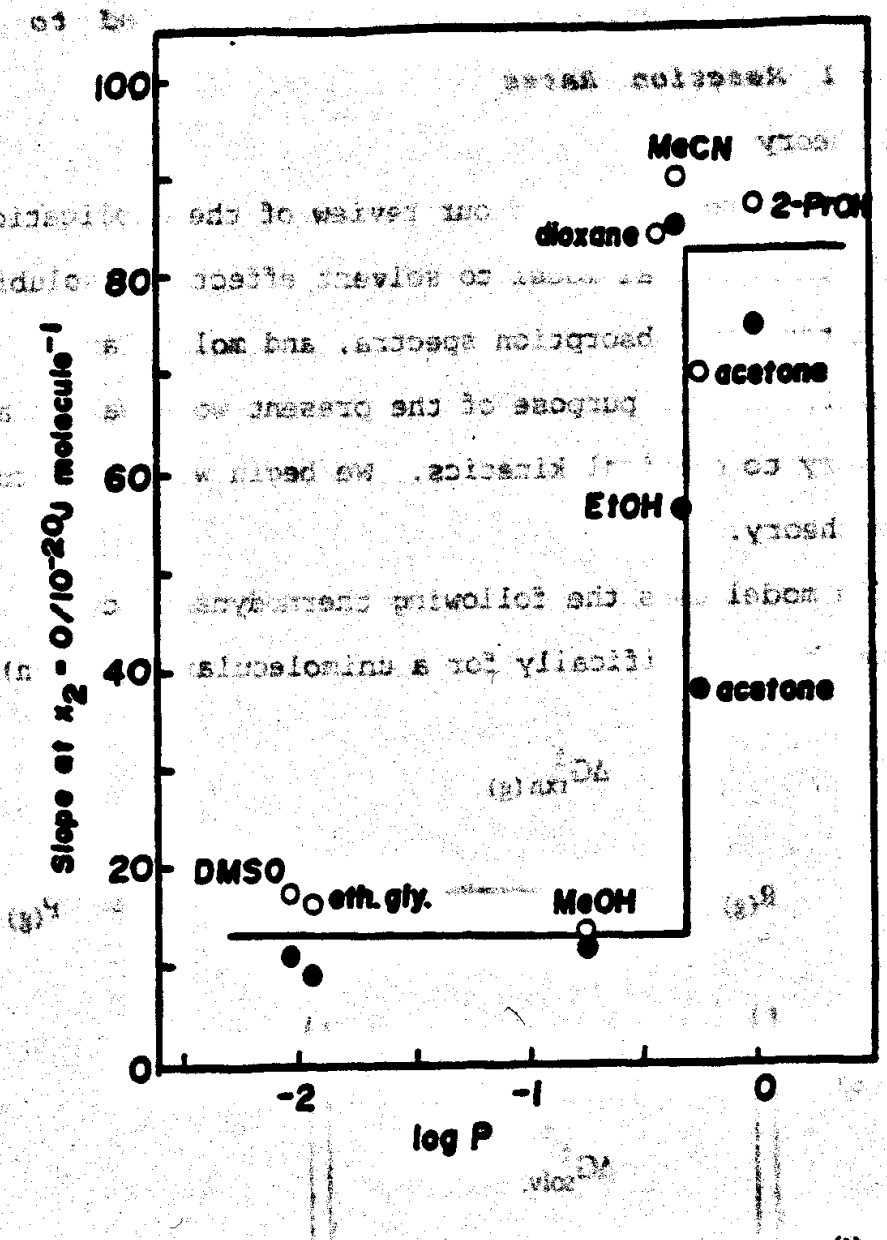

Figure 1.14 Plot of the initial slope of a $\delta_m \Delta G^{(l)}_{complex}$ *vs.* x_2 against log P of the organic cosolvent. Open circles are for methyl orange-α-cyclodextrin complexation (5). Closed circles are from the 4-nitroaniline-α-cyclodextrin complexation system (7). Notice the discontinuous behavior.

1.6 The Phenomenological Model Applied to Chemical Reaction Rates

1.6.1 Theory

We have now completed our review of the application of the phenomenological model to solvent effects on solubility, surface tension, absorption spectra, and molecular complexation. The purpose of the present work was to apply the theory to chemical kinetics. We begin with a discussion of the theory.

The model uses the following thermodynamic cycle (written here specifically for a unimolecular reaction),

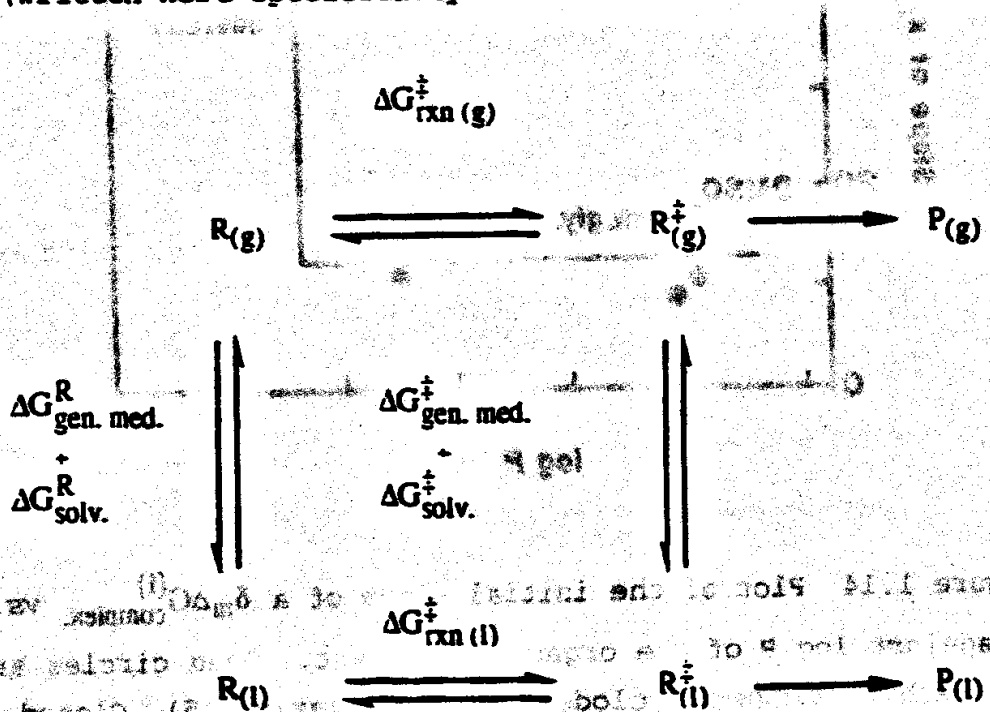

where R is the reactant, $R^{\ddagger}$ the transition state, P the product, and $\Delta G_{gen.\,med.}$ and $\Delta G_{solv.}$ represent the General

Medium Effect (solvent-solvent interactions) and the Solvation Effect (solute-solute interactions) respectively. The superscripts R and ‡ denote the reactant and transition state species respectively.

From this cycle we write equation (1.56)

$$\Delta G^{\ddagger}_{rxn\,(g)} + (\Delta G^{\ddagger}_{gen.\,med.} + \Delta G^{\ddagger}_{solv.}) - \Delta G^{\ddagger}_{rxn\,(l)} - (\Delta G^{R}_{gen.\,med.} + \Delta G^{R}_{solv.}) = 0 \quad (1.56)$$

Rearranging equation (1.56) gives equation (1.57)

$$\Delta G^{\ddagger}_{rxn\,(l)} = \Delta G^{\ddagger}_{rxn\,(g)} + (\Delta G^{\ddagger}_{gen.\,med.} + \Delta G^{\ddagger}_{solv.}) - (\Delta G^{R}_{gen.\,med.} + \Delta G^{R}_{solv.}) \quad (1.57)$$

where $\Delta G^{\ddagger}_{rxn\,(l)}$ is the free energy of activation in solution, which can be calculated from the experimentally determined rate constant. (For simplicity, we will denote $\Delta G^{\ddagger}_{rxn\,(l)}$ as $\Delta G^{\ddagger}_{rxn}$.) $\Delta G^{\ddagger}_{rxn\,(g)}$ is the "intrinsic" gas-phase free energy of activation. Equation (1.57) completely describes the system; however, to apply it to data, the expressions for $\Delta G_{gen.\,med.}$ and $\Delta G_{solv.}$ must be substituted into the equation. $\Delta G^{\ddagger}_{rxn\,(g)}$ is independent of solvent composition and, through application of the Leffler-Grunwald delta operator (9), it will be eliminated from equation (1.57).

The expression for $\Delta G_{solv.}$ was given by equation (1.12)

$$\Delta G_{solv.} = \frac{(-k_B T \ln K_1)\, K_1 x_1 x_2 + (-k_B T \ln K_1 K_2)\, K_1 K_2 (x_2)^2}{(x_1)^2 + K_1 x_1 x_2 + K_1 K_2 (x_2)^2} + \Delta G_{RW_2} \qquad (1.12)$$

and the expression for $\Delta G_{gen.\ med.}$ was given by equation (1.19)

$$\Delta G_{gen.\ med.} = gA\gamma_1 + gA\gamma' \left(\frac{K_1 x_1 x_2 + 2K_1 K_2 (x_2)^2}{(x_1)^2 + K_1 x_1 x_2 + K_1 K_2 (x_2)^2} \right) \qquad (1.19)$$

All terms have been previously defined in sections 1.1.1 and 1.1.2.

The free energy of activation is given by substituting equations (1.12) and (1.19) into equation (1.57) to give equation (1.58)

$$\Delta G^{\ddagger}_{rxn} = \Delta G^{\ddagger}_{rxn\,(g)} + gA^{\ddagger}\gamma_1 + \Delta G^{\ddagger}_{RW_2} \left(\frac{(-k_B T \ln (K_1^{\ddagger}) + gA^{\ddagger}\gamma')\, K_1^{\ddagger} x_1 x_2 + (-k_B T \ln (K_1^{\ddagger} K_2^{\ddagger}) + 2gA^{\ddagger}\gamma')\, K_1^{\ddagger} K_2^{\ddagger} (x_2)^2}{(x_1)^2 + K_1^{\ddagger} x_1 x_2 + K_1^{\ddagger} K_2^{\ddagger} (x_2)^2} \right)$$

$$- \Delta G^{R}_{RW_2} - gA^{R}\gamma_1 - \qquad (1.58)$$

$$\left(\frac{(-k_B T \ln (K_1^{R}) + gA^{R}\gamma')\, K_1^{R} x_1 x_2 + (-k_B T \ln (K_1^{R} K_2^{R}) + 2gA^{R}\gamma')\, K_1^{R} K_2^{R} (x_2)^2}{(x_1)^2 + K_1^{R} x_1 x_2 + K_1^{R} K_2^{R} (x_2)^2} \right)$$

In a pure aqueous medium ($x_2 = 0$) this equation reduces to

$$\Delta G^{\ddagger}_{rxn} = \Delta G^{\ddagger}_{rxn(g)} + gA^{\ddagger}\gamma_1 + \Delta G^{\ddagger}_{RW_2} - \Delta G^{R}_{RW_2} - gA^{R}\gamma_1 \quad (1.59)$$

Using the Leffler-Grunwald operator (9), the solvent effect is defined as

$$\delta_m \Delta G^{\ddagger}_{rxn} = \Delta G^{\ddagger}_{rxn(x_2 = x_2)} - \Delta G^{\ddagger}_{rxn(x_2=0)} \quad (1.60)$$

Application of this operator to equation (1.58) eliminates the solvent independent terms, and allows equation (1.58) to be reduced to

$$\delta_m \Delta G^{\ddagger}_{rxn} = \left(\frac{(-k_B T \ln (K_1^{\ddagger}) + gA^{\ddagger}\gamma')\, K_1^{\ddagger} x_1 x_2 + (-k_B T \ln (K_1^{\ddagger} K_2^{\ddagger}) + 2gA^{\ddagger}\gamma')\, K_1^{\ddagger} K_2^{\ddagger} (x_2)^2}{(x_1)^2 + K_1^{\ddagger} x_1 x_2 + K_1^{\ddagger} K_2^{\ddagger} (x_2)^2} \right)$$

$$- \left(\frac{(-k_B T \ln (K_1^{R}) + gA^{R}\gamma')\, K_1^{R} x_1 x_2 + (-k_B T \ln (K_1^{R} K_2^{R}) + 2gA^{R}\gamma')\, K_1^{R} K_2^{R} (x_2)^2}{(x_1)^2 + K_1^{R} x_1 x_2 + K_1^{R} K_2^{R} (x_2)^2} \right) \quad (1.61)$$

where $\gamma' = \frac{\gamma_1 - \gamma_2}{2}$ and γ_1 and γ_2 retain their definitions.

This equation has six adjustable parameters, namely the

solvation exchange constants K_1^R, K_2^R, $K_1^\ddagger$, and $K_2^\ddagger$ and the products, gA^R and $gA^\ddagger$, of the surface area and the curvature correction factor for the solvent cavities enclosing the reactant and transition state species. These parameters are, in principle, obtained by fitting rate data ($\delta_m \Delta G_{rxn}^\ddagger$ as a function of x_2) using nonlinear regression.

For a one-step solvation scheme equation (1.61) becomes equation (1.62)

$$\delta_m \Delta G_{rxn}^\ddagger = \frac{(gA^\ddagger\gamma' - k_B T \ln K_1^\ddagger) K_1^\ddagger x_2}{x_1 + K_1^\ddagger x_2} - \frac{(gA^R\gamma' - k_B T \ln K_1^R) K_1^R x_2}{x_1 + K_1^R x_2} \qquad (1.62)$$

where $\gamma' = \gamma_1 - \gamma_2$. This equation has four adjustable parameters, namely the solvation exchange constants for the reactant and transition state, and the general medium term for both species.

The full cancellation approximation that was applied to the complexation model to reduce the number of adjustable parameters can also be applied to equations (1.61) and (1.62). For the two-step solvation scheme, this gives $K_1^R = K_1^\ddagger = K_1$ and $K_2^R = K_2^\ddagger = K_2$, and equation (1.61) simplifies to

$$\delta_m \Delta G_{rxn}^\ddagger = \left(\frac{\Delta gA^\ddagger\gamma' K_1 x_1 x_2 + 2\Delta gA^\ddagger\gamma' K_1 K_2 (x_2)^2}{(x_1)^2 + K_1 x_1 x_2 + K_1 K_2 (x_2)^2} \right) \qquad (1.63)$$

where $\Delta gA^{\ddagger} = gA^{\ddagger} - gA^{R}$; this is the difference between the curvature-corrected molecular surface areas of the cavities containing the transition state and the reactant. Depending on the reaction, this quantity may be negative or positive. Notice that the number of parameters in equation (1.61) has been reduced from six to three; these are $\Delta gA^{\ddagger}$, K_1, and K_2.

For the one-step solvation scheme subject to the approximation $K_1^{\ddagger} = K_1^{R} = K_1$, equation (1.62) simplifies to give equation (1.64)

$$\delta_m \Delta G_{rxn}^{\ddagger} = \frac{\Delta gA^{\ddagger} \gamma \, K_1 x_2}{x_1 + K_1 x_2} \qquad (1.64)$$

where all symbols have been previously defined. Notice that the number of parameters in equation (1.62) has been reduced from four to two; the parameters in the new equation are $\Delta gA^{\ddagger}$ and K_1. These several levels of approximation generate more tractable equations; their acceptability must be tested against experimental data.

1.7 Statement of the Problem

Despite the previous success of the model in describing solvent effects on solubility, surface tension, solvatochromism, and complexation, its extension to the more difficult problem of the description of solvent effects on chemical reaction rates had not yet been accomplished, and

so the problem, and the goal of this project, is defined - to test the applicability of the phenomenological model to solvent effect data on chemical reaction rates.

To this end, the decarboxylative-dechlorination of two N-chloro-α-amino acids was studied in many aqueous-organic binary cosolvent systems. The decomposition of N-chloroalanine was studied in eight aqueous-organic cosolvent systems, namely acetonitrile, 1,4-dioxane, 1-propanol, 2-propanol, methanol, ethanol, 1,2-propanediol (propylene glycol), and 1,2-ethanediol (ethylene glycol). The decomposition of N-chloroleucine was examined in four aqueous-organic binary cosolvent systems; these organic cosolvents were methanol, acetonitrile, 2-propanol, and ethylene glycol.

This reaction possesses several features that made it well suited for this study, among them, its pH independence (in the pH range from 5 to 13), its insensitivity to ionic strength in this pH range, its sensitivity to solvent effects, its unimolecularity, and its first-order decomposition kinetics. These properties simplified the interpretation of the solvent effects. A more detailed description of its chemistry is presented in the following chapter.

1.8 Chapter 1 References

(1) Khossravi, D.; Connors, K.A. *J. Pharm. Sci.* (1992), **81**, 371.

(2) Khossravi, D.; Connors, K.A. *J. Pharm. Sci.* (1993), **82**, 817.

(3) LePree, J.M.; Mulski, M.J.; Connors, K.A. *J. Chem. Soc. Perkin Trans. 2* (1994), 1491.

(4) Khossravi, D.; Connors, K.A. *J. Soln. Chem.* (1993), **22**, 321.

(5) Connors, K.A.; Mulski, M.J.; Paulson, A. *J. Org. Chem.* (1992), **57**, 1794.

(6) Khossravi, D.; Connors, K.A. *J. Soln. Chem.* (1993) **22**, 677.

(7) Mulski, M.J.; Connors, K.A. *Supramolecular Chemistry*, (1995), in press.

(8) Skwierczynski, R.D.; Connors, K.A. *J. Chem. Soc. Perkin Trans. 2* (1994), 467.

(9) Leffler, J.E.; Grunwald, E. "Rates and Equilibria of Organic Reactions" Wiley: New York, 1963.

(10) Uhlig, H.H. *J. Phys. Chem.* (1937), **41**, 125.

(11) Li, A. Ph.D. Thesis, University of Wisconsin-Madison, Madison, WI 1993.

(12) Pearlman, R.S. In "Partition Coefficient: Determination and Estimation"; Dunn, W.J.; Block, J.H.; Pearlman, R.S., Eds.; Pergamon: New York (1986) Chapter 1.

(13) Tolman, R.C.; *J. Chem. Phys.* (1949), **3**, 333.

(14) Vogelsberger, W.; Sonnefeld, J.; Rudekoff, G. *Z. Phys. Chem. (Leipzig)* (1985), **266**, 225.

(15) Ahn, W.S.; Jhon, M.S.; Pak, H.; Chang, S. *J. Colloid Interface Sci.* (1972), **38**, 605.

(16) Goncalves, R.M.C.; Simões, A.M.N.; Moura-Ramos, J.J. *J. Soln. Chem.* (1993), **22**, 507.

(17) Hooper, M.A.; Nordholm, S. *J. Chem. Phys.* (1987), **87**, 675.

(18) Choi, D.S.; Jhon, M.S.; Egring, H. *J. Chem. Phys.* (1970), **53**, 2608.

(19) Mahnke, R.; Schmelzer, *J. Z. Phys. Chem. (Leipzig)* (1985), **266**, 1028.

(20) Sinanoglu, O.J. *J. Chem. Phys.* (1981), **75**, 463.

(21) Fischer, L.R.; Isrealachvili, J.N. *Nature*, (1979), **277**, 548.

(22) Fischer, L.R.; Isrealachvili, J.N. *Chem. Phys. Letters* (1980), **76**, 325.

(23) Fischer, L.R.; Isrealachvili, J.N. *Colloids Surf.* (1981), **3**, 303.

(24) Yalkowski, S.H.; Amidon, G.L.; Zografi, G.; Flynn, G.L. *J. Pharm. Sci.* (1975), **64**, 48.

(25) Yalkowski, S.H.; Valvani, S.C.; Amidon, G.L. *J. Pharm. Sci.* (1976), **65**, 1488.

(26) Leo, A.; Hansch, C.; Elkins, D. *Chem. Rev.* (1971), **71**, 525.

(27) Connors, K.A.; Wright, J.L. *Anal. Chem.* (1989), **61**, 194.

(28) LePree, J.M. M.S. Thesis; University of Wisconsin-Madison, Madison, WI (1993).

(29) Dimroth, K.; Reichardt, C.; Sipemann, T.; Bohlmann, F. *Liebigs Ann. Chem.* (1963), **661**, 1.

(30) Kamlet, M.J.; Abboud, J.-L. M.; Abraham, M.H.; Taft, R.W. *J. Org. Chem.* (1983), **48**, 2877.

(31) Maria, P.-C.; Gal, J.F. *J. Phys. Chem.* (1985), **89**, 1296.

(32) Acree, W.E.; Powell, J.R.; Tucker, S.A. *J. Chem. Soc. Perkin Trans. 2*, (1995) 529.

Chapter 2. The Decarboxylative-Dechlorination of N-Chloro-α-Amino Acids

2.1 Chemistry of the Reaction

To test the validity of the model, a chemical reaction well suited for solvent effect studies was needed. The desired characteristics of such a test reaction are that it be unimolecular, that its rate be pH independent (to avoid the complication of measuring and interpreting the pH of aqueous-organic cosolvent systems), and that its rate display a significant solvent effect; other attractive features are first-order kinetics, and a reaction rate that is independent of ionic strength.

The decarboxylative-dechlorination of N-chloro-α-amino acids (Scheme 2.1) met the aforementioned criteria, and though the mechanism of this reaction was not the focus of this project, a brief review concerning its chemistry is warranted. I shall restrict this discussion to studies that were conducted in pH ranges similar to our own studies, that is between 5 and 13. (Actually, the pH of our reaction solutions was usually between 7 and 9). For descriptions of work conducted in more acidic regions the reader is referred to the work of Armesto and coworkers (1) and for the alkaline regions the reader is referred to the work of Armesto *et al.* (2) and Abia *et al* (3).

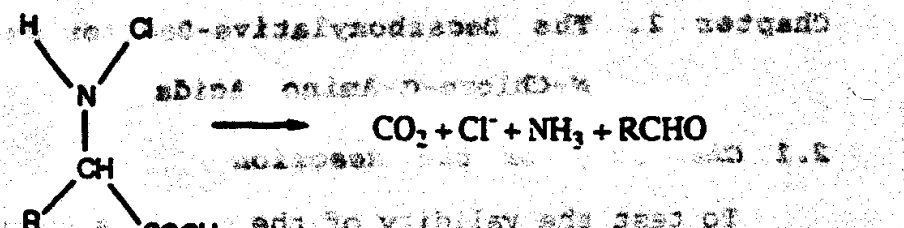

Scheme 2.1 Decarboxylative-dechlorination of N-chloro-α-amino acids.

The reaction has been well studied (4-11), and the following information is known: the N-chloroamino acids form rapidly (within seconds) when a chlorinating agent such as hypochlorous acid (4-6), chlorine (6), or monochloramine (7,8) is added to a solution of the amino acid, and then the chlorinated amino acid decomposes by first-order kinetics as shown for the overall process in Scheme 2.1 (3,9,10). Hand and coworkers (9) have reported quantitative yields of the aldehydes and ammonia formed from the more reactive N-chloro-α-amino acids, namely N-chloroalanine, N-chloro-α-aminoisobutyric acid, and N-chloro-1-amino-1-carboxycyclohexane.

It is also known that the reaction rate is independent of pH in the range of 5 to 13 (3,9,10). Hand and coworkers (9) reported that N-chloroalanine decomposition did not undergo general base catalysis by acetate, phosphate, and

borate buffers ranging in concentration from 0 to 0.25 M. The reaction rate was also unaffected by changes in ionic strength. In support of this work, Awad and coworkers (10) have also reported that the decomposition is not significantly affected by changes in the initial N-chloro-α-amino acid concentrations, phosphate buffer concentrations (0.05 to 0.5 M at pH 7) and ionic strengths (0.2 to 1.6 M -adjusted with NaCl and at pH 7). Our preliminary studies are in agreement with these claims. (Contrary to these findings, Aria and coworkers (3) reported that N-chlorovaline undergoes general base catalysis when buffer concentrations exceed 0.02 M. Their study will be reviewed later in this chapter.)

The decomposition of N-chloro-α-amino acids is usually monitored spectrophotometrically by following the decrease in absorbance (at about 250 nm) corresponding to N-chloro bond cleavage. Awad and coworkers (10) have used additional methods to follow the decomposition including iodometric analysis to monitor N-chloro bond cleavage, and entrapment of CO_2 in $Ba(OH)_2$ solution followed by acid-base titration. They also measured the initial rates of decomposition, and used these data to determine the decomposition rate constants. All four methods gave similar rate constant values for each amino acid; for comparison, the data are listed in Table 2.1.

Table 2.1. First order rate constant values for the decomposition of some N-chloro-α-amino acids determined by four different methods. Data are from reference (10).

	First-Order Rate Constants/ min^{-1} at pH 7 and 25°C			
Amino Acid	Spectro-photometric method	Iodometric Method	Initial Rate Method	CO_2 Trapping Method
N-Chloro-N-methylglycine	0.005	0.005	0.005	0.005
N-Chloroalanine	0.016	0.015	0.015	0.014
N-Chloroglycine	0.002	0.002	-	0.01
2-Amino-N-chloroisobutyric acid	0.63	0.70	-	0.65

Several reaction mechanisms have been proposed, and I will discuss the most plausible ones in this chapter, restricting the discussion to solution conditions in which the pH was between 5 and 13. Fox and Bullock (12) have suggested the mechanism shown in Scheme 2.2. It involves the loss of an α-proton as the first and rate determining step in the reaction.

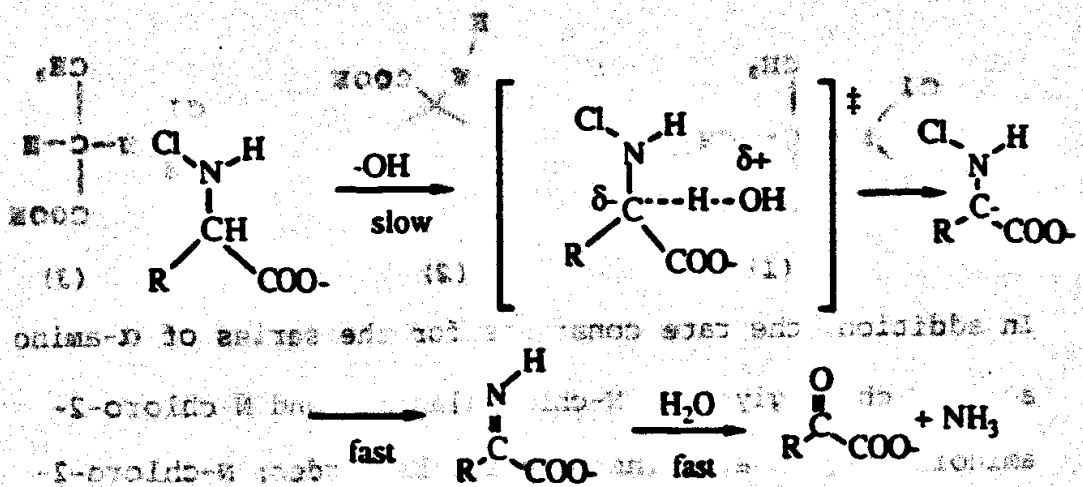

Scheme 2.2.

This mechanism is not supported by currently known experimental data, specifically the pH independence of the reaction. Hand and coworkers (9) and Awad and coworkers(10) offer some experimental data which discredit this mechanism. The most convincing is that N-chloro-2-aminoisobutyric acid (*1*) ($k = 0.77\ min^{-1}$(9); $k = 0.61\ min^{-1}$(10)), and N-chloro-1-amino-1-carboxycyclohexane (*2*) ($k = 5.4\ min^{-1}$ (9)), α-amino acids that do not have α-protons, decompose more rapidly than N-chloroalanine (*3*) ($k = 0.016\ min^{-1}$ (9,10)) which does possess an α-proton. Clearly, the loss of an α-proton cannot be involved in the decomposition of (*1*) or (*2*).

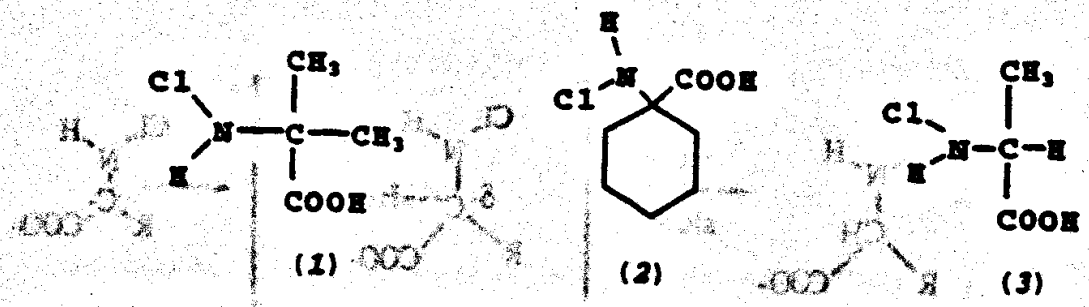

(1) (2) (3)

In addition, the rate constants for the series of α-amino acids N-chloroglycine, N-chloroalanine, and N-chloro-2-aminoisobutyric acid increase in that order; N-chloro-2-aminoisobutyric acid, the amino acid with the greatest number of α-carbon methyl substituents, possesses the fastest rate of decomposition. The opposite order should have been observed if the mechanism involved carbanion formation through α-proton loss via an anionic-like transition state because the methyl substituents would destabilize the transition state and therefore decrease the reaction rate.

Two other mechanisms discussed by Awad and coworkers (10) involve the loss of carbon dioxide as the first step in the mechanism; in Scheme 2.3, the decarboxylation is the rate determining step, whereas in Scheme 2.4 it is not.

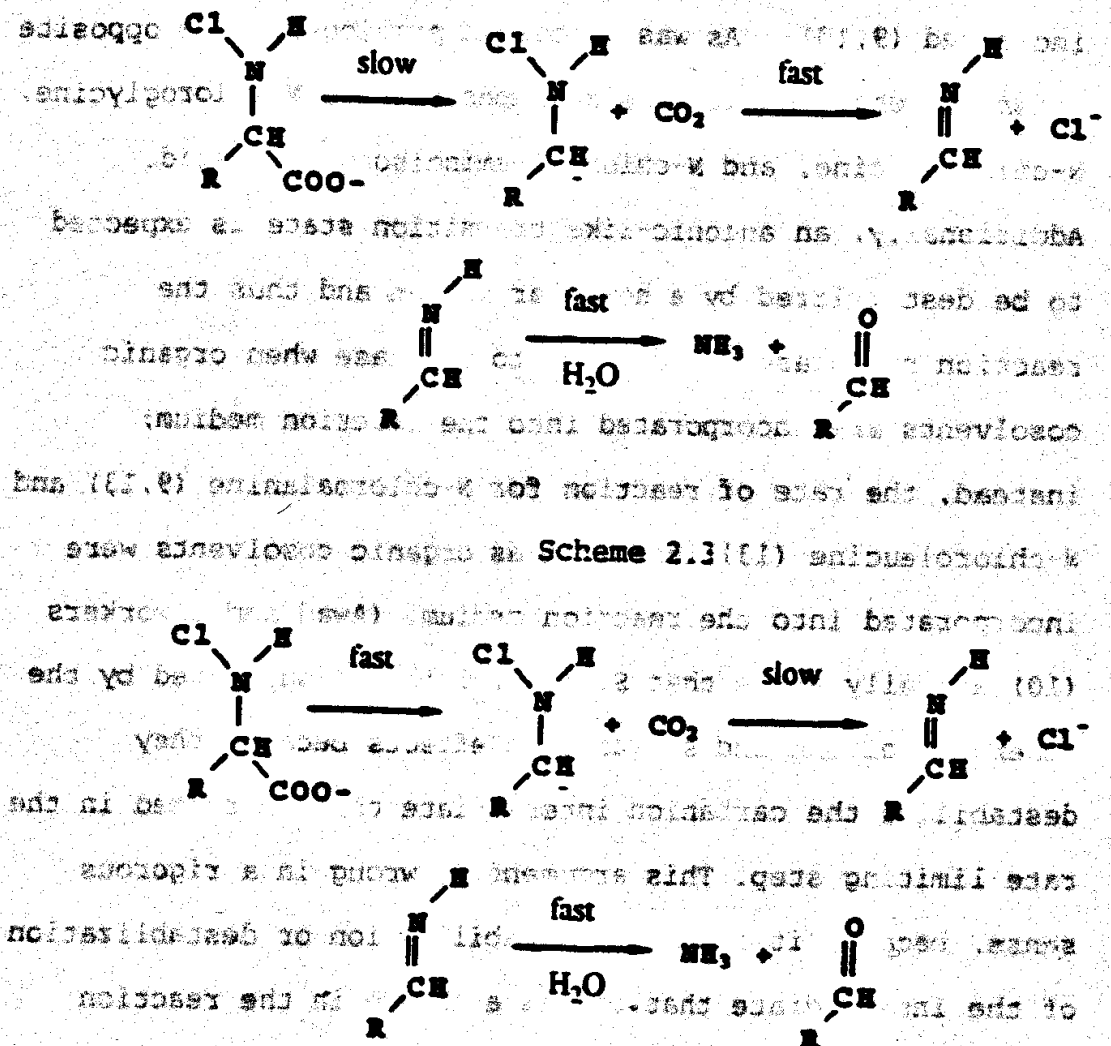

Scheme 2.4

Scheme 2.3 involves formation of an anionic intermediate in the rate determining step. Several observations do not support this mechanism, namely that an anionic-like transition state is destabilized by methyl substituents, thus the rate of reaction should be slowed as the number of methyl substituents on the α-carbon is

increased (9,10). As was discussed previously, the opposite order was observed for the decomposition of N-chloroglycine, N-chloroalanine, and N-chloro-2-aminoisobutyric acid. Additionally, an anionic-like transition state is expected to be destabilized by a nonpolar medium and thus the reaction rates are anticipated to decrease when organic cosolvents are incorporated into the reaction medium; instead, the rate of reaction for N-chloroalanine (9,13) and N-chloroleucine (13) increased as organic cosolvents were incorporated into the reaction medium. (Awad and coworkers (10) actually argue that Scheme 2.3 is not supported by the observed solvent and substituent effects because they destabilize the carbanion intermediate that is formed in the rate limiting step. This argument is wrong in a rigorous sense, because it is not the stabilization or destablization of the intermediate that causes a change in the reaction rate, but rather the increase or decrease in the stability of the transition state relative to the intermediate's stability.)

Awad (10) argues that Scheme 2.4 is supported by the observed solvent and substituent effects, but Scheme 2.4 is not consistent with the experimental observation that the rate of decarboxylation is equal to the rate of dechlorination.

Hand and coworkers (9) have discussed the mechanism depicted in Scheme 2.5, where the loss of chloride leads to the formation of a nitrenium ion intermediate. This intermediate would be born of a cation-like transition state. Electron donating groups such as methyl substituents would stabilize this transition state and act to increase the reaction rate. Hand observed the opposite trend-the rate of decomposition for N-chlorosarcosine (4) was 5 times slower than the decomposition rate of N-chloroalanine (3).

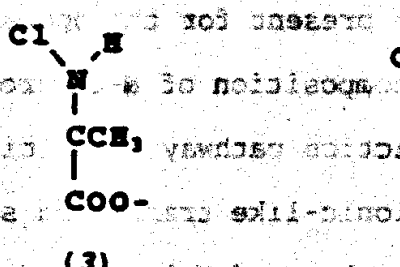

(3) (4)

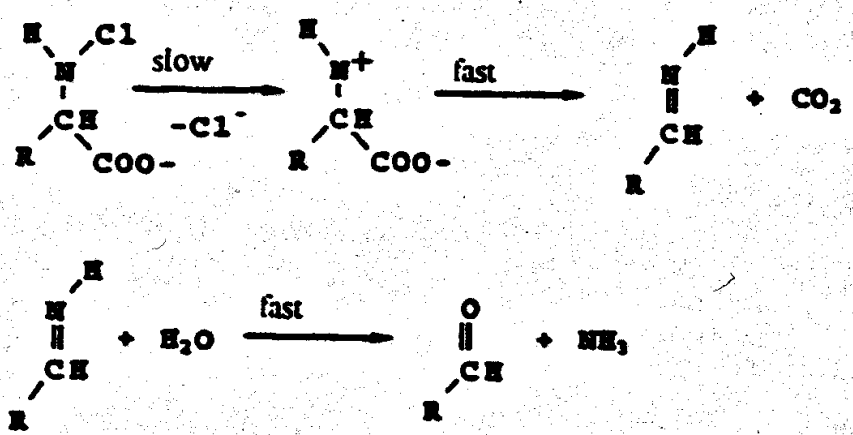

Scheme 2.5.

Though their reasoning is logical, it is based on only one rate study. As previously discussed, the solvent effect work performed by Awad and coworkers (10) and this laboratory (13), and our pressure effect studies (13) (to be described later) indicate that a cationic or anionic-like transition state species is probably not formed during the rate determining step of the reaction.

In this discourse, we must also consider the initial loss of an amino proton as depicted in Scheme 2.6. Clearly an N-proton must be present for the operation of this mechanism; the decomposition of N-chlorosarcosine (4) eliminates this reaction pathway. Additionally, the formation of an anionic-like transition state is not compatible with the observed solvent and pressure effects.

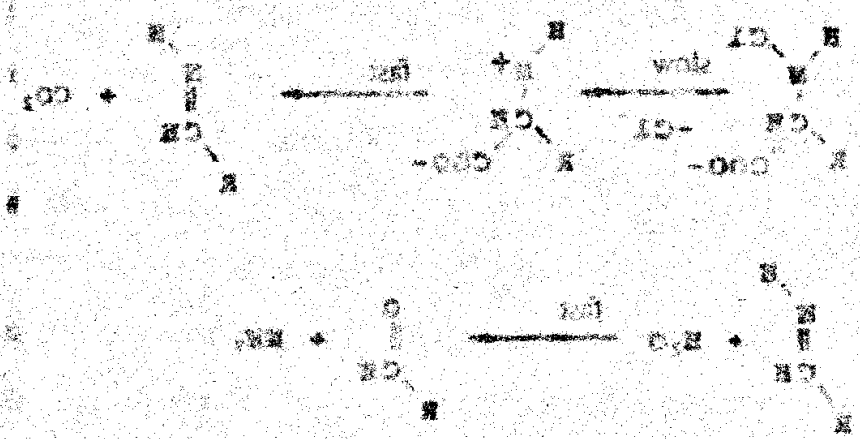

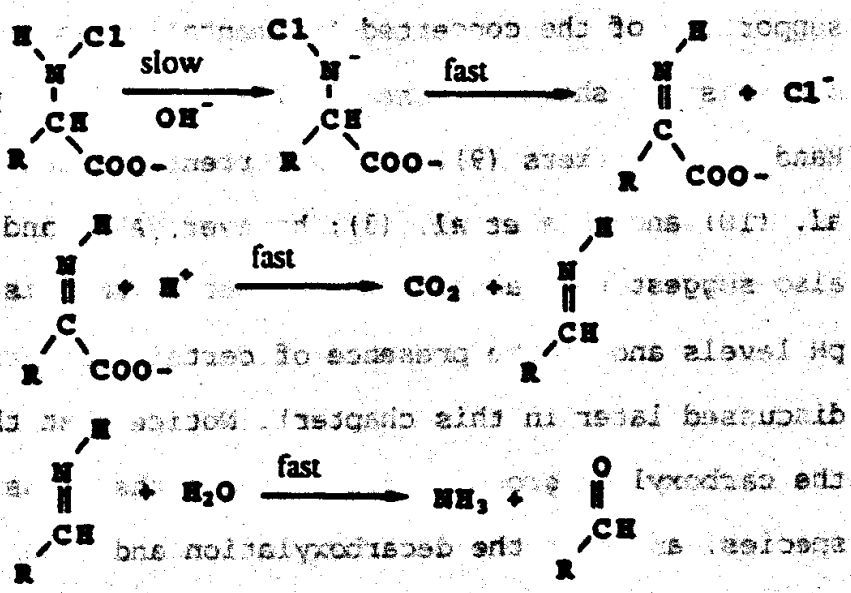

Scheme 2.6.

The mechanisms that we have reviewed are not consistent with all experimental observations, namely that the reaction is insensitive to pH changes in the range of 5 to 13, that the decarboxylation and dechlorination occur simultaneously, and that the rate increases when organic cosolvents are added to the solution (which suggests that the transition state is stabilized by a less polar medium and has some nonpolar characteristics itself). Given these facts, the most likely mechanism appears to be a concerted fragmentation mechanism in which dechlorination and decarboxylation occur simultaneously via an imine-like transition state. It should be noted that the entropy of activation, $\Delta S^{\ddagger}$, of the reaction is positive [for example $\Delta S^{\ddagger}$ = 10 kcal/mole for N-chloroalanine decomposition (9)] which is suggestive of simultaneous bond cleavage (9), and

supportive of the concerted fragmentation as well. The mechanism is shown in Scheme 2.7 and was first proposed by Hand and coworkers (9). It is currently accepted by Awad *et al.* (10) and Abia *et al.* (3); however, Abia and coworkers also suggest that a competing E_2 mechanism exists at higher pH levels and in the presence of certain buffers (to be discussed later in this chapter). Notice that the charge on the carboxylate group is dispersed in the transition state species, and that the decarboxylation and dechlorination occur simultaneously. Notice also that negatively charged reactant is probably the predominantly charged form in solutions of pH 5 to 13. (The pK_a of alanine's carboxylic acid group is 2.35 (14), the pK_a of N-chlorodimethylamine is 0.46 (15), and that of N-chlorodiethylamine is 1.02 (15); it is reasonable to assume that the pK_a's of N-chloroamine groups of the α-amino acids are somewhat similar.) This probably accounts for the pH independent rate of reaction. The charge dispersion that occurs in the transition state species could explain the solvent and pressure effects on the reaction rate. This mechanism seems to be consistent with all reported experimental observations.

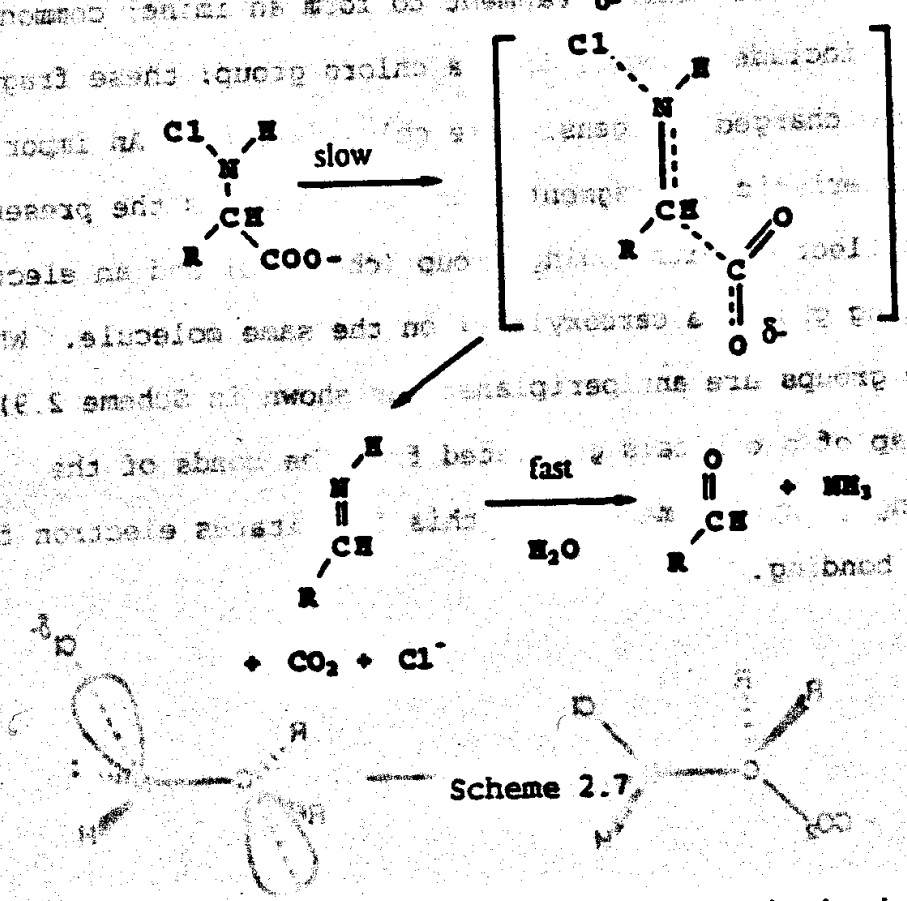

Scheme 2.7

Hand (9) justified this mechanism on the basis of work presented by Grob and coworkers(16-18), who have classified fragmentation reactions as those that occur through Scheme 2.8 (16-18).

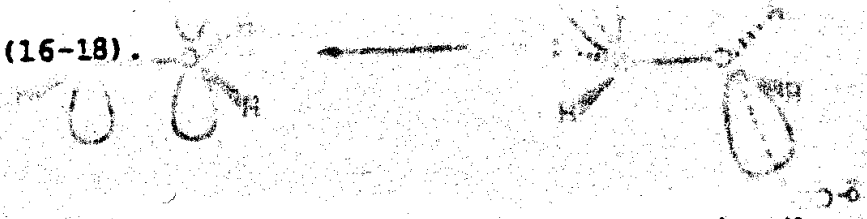

Scheme 2.8

Common a–b— groups include carboxylates, which fragment to carbon dioxide; common —c–d— groups include carbon to

nitrogen bonds, which fragment to form an imine; common —X: groups include halogens like a chloro group; these fragment to form charged halogens, like chloride ions. An important characteristic of fragmentation mechanisms is the presence of an electron withdrawing group (chlorine) and an electron donating group (a carboxylate) on the same molecule. When these groups are antiperiplanar (as shown in Scheme 2.9), overlap of p orbitals generated from the bonds of the leaving groups is maximized; this facilitates electron flow and π bonding.

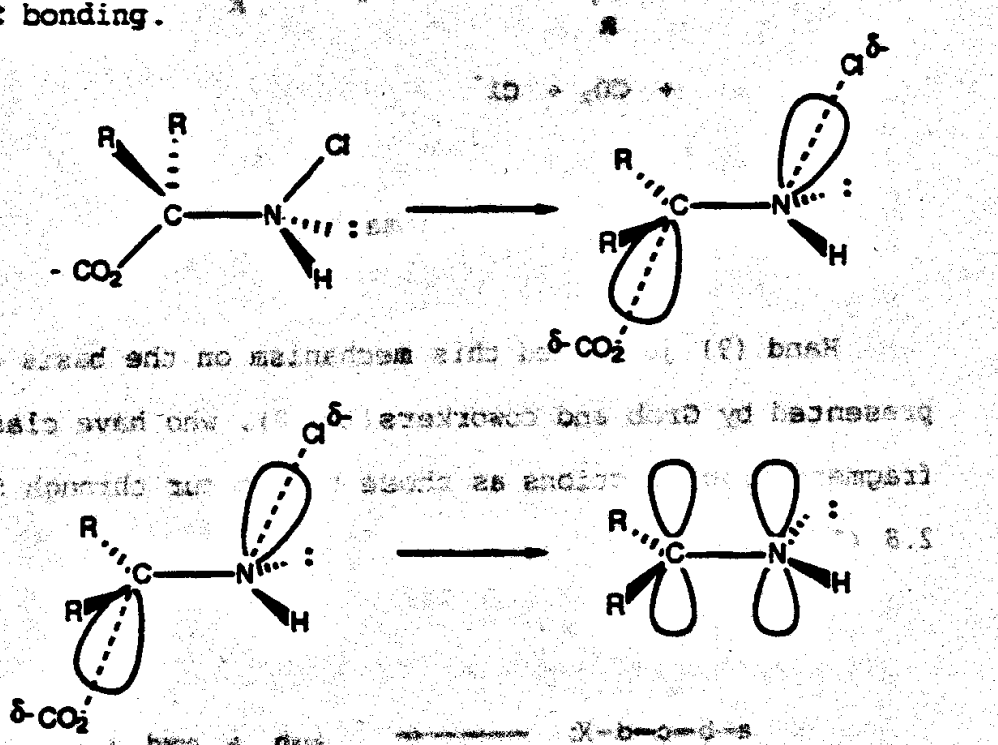

Scheme 2.9 The chloro and carboxylate groups are antiperiplanar, which facilitates p orbital overlap in the transition state (9, 16-18).

Table 2.2 contains a summary of interesting data from Hand's study. Seven different amino acids were examined: glycine (Gly), sarcosine (Sar), threonine (Thr), alanine (Ala), proline (Pro), α-aminoisobutyric acid (Aib), and 1-amino-1-carboxycyclohexane (Acc); the rates varied by a factor of 21,000, with the chloroamine of Gly being the least reactive and the chloroamine of Acc being the most reactive species.

Table 2.2. Rate constants and relative rates for the decomposition of N-chloro-α-amino acids in aqueous solution. All data are from reference (9); the studies were conducted at 25°C in pH 6.85, 0.01 M phosphate buffer and an ionic strength of 0.5 M.

Chloroamine of	k / 10^{-4} min^{-1}	Relative k
Gly, $NH_2CH_2COO^-$	2.5 (0.25)[a]	1
Sar, $CH_3NHCH_2COO^-$	30.4 (0.42)	12
Thr, $NH_2CH(CH(OH)CH_3)COO^-$	120 (60)	50
Ala, $NH_2CH(CH_3)COO^-$	160[b] (1.2)	64
Pro, 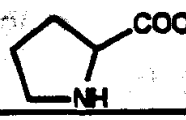	530 (12)	210
Aib, $NH_2C(CH_3)_2COO^-$	7700 (480)	3100
Acc 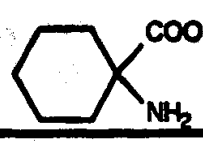	54000 (600)	22000

[a] Numbers in parentheses are the standard deviation.
[b] Value from our study was 149 (1.7) x 10^{-4} min^{-1}.

Clearly the substituent effects for this reaction series are dramatic. Hand believes that disubstitution on the α-carbon increases the reaction rate because it promotes the existence of the antiperiplanar conformation, which favors fragmentation reactions as was previously discussed. He also argues that substituents which promote expansion of the α-carbon bond angles would increase the reaction rate because the angles at the α-carbon and at the nitrogen must increase from 109° to 120° when the imine is formed. (This argument was supported by *ab initio* calculations performed by Bhattacharjee (19).) For example, reaction rates of N-Cl-Aib and N-Cl-Acc would be influenced by this effect, but in opposite directions. The repulsion between the two methyl groups of N-Cl-Aib would promote the expansion of the bond angle at the α-carbon and increase the reaction rate, while the cyclic structure of N-Cl-Acc would deter the expansion, and inhibit the rate. Hand further postulates that increased carbon substitution may also stabilize the imine-like transition state, resulting in a lower activation energy and increased reaction rate. (His basis for this argument is the well known stabilization of olefin double bonds by carbon substitution.)

He reasons that all three factors must be considered when exploring the substituent effects on the reaction. These arguments seem plausible, but they are highly

speculative. Many more amino acids of varying structure should be studied before any conclusions are drawn.

Prior to concluding this chapter a discussion of some new findings is warranted. Abia and coworkers (3) reported that N-chlorovaline decomposition is similar to other N-chloro-α-amino acids, in that the N-chlorovaline decomposition rate is independent of pH from 5 to 13; it is independent of initial N-chlorovaline concentration, and *l*-valine concentration; it is independent of ionic strength. However, they report that N-chlorovaline is general base catalyzed in this pH range in the presence of certain buffers. This observation is contradictory to the findings of Hand and coworkers (9), Awad and coworkers (10), and this laboratory's preliminary findings. The report of general base catalysis therefore may be important. However, the results of Abia and coworkers' studies are questionable. Figures 2.1 and 2.2 are plots of their observed rate constants against base concentration. In Table 2.3, I have presented the maximum base concentration that was used in each study, along with the maximum reported value of the rate constant.

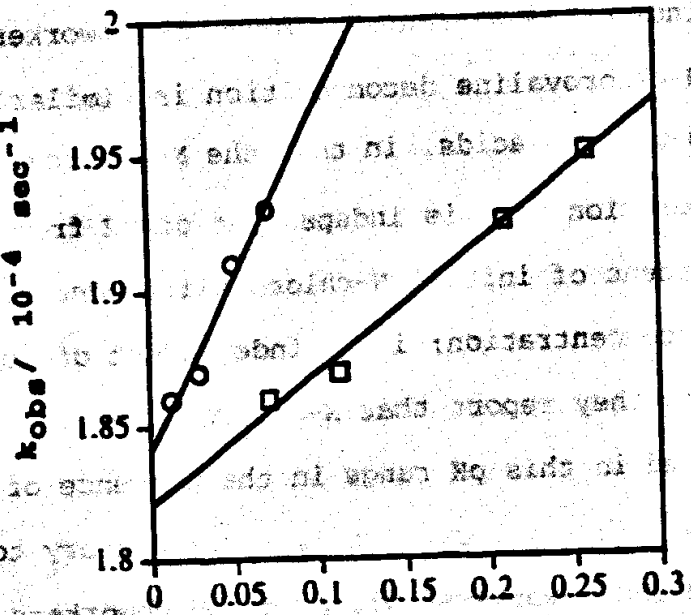

Figure 2.1 Plot of observed first order rate constant against molar concentration of dibasic phosphate. Circular points: pH = 7.6, Square points: pH = 6.3. Ionic strength adjusted to 1 molar with NaCl. Data are from reference (3). Error in each point was unreported, but experimental error was said to be never greater than 5 %.

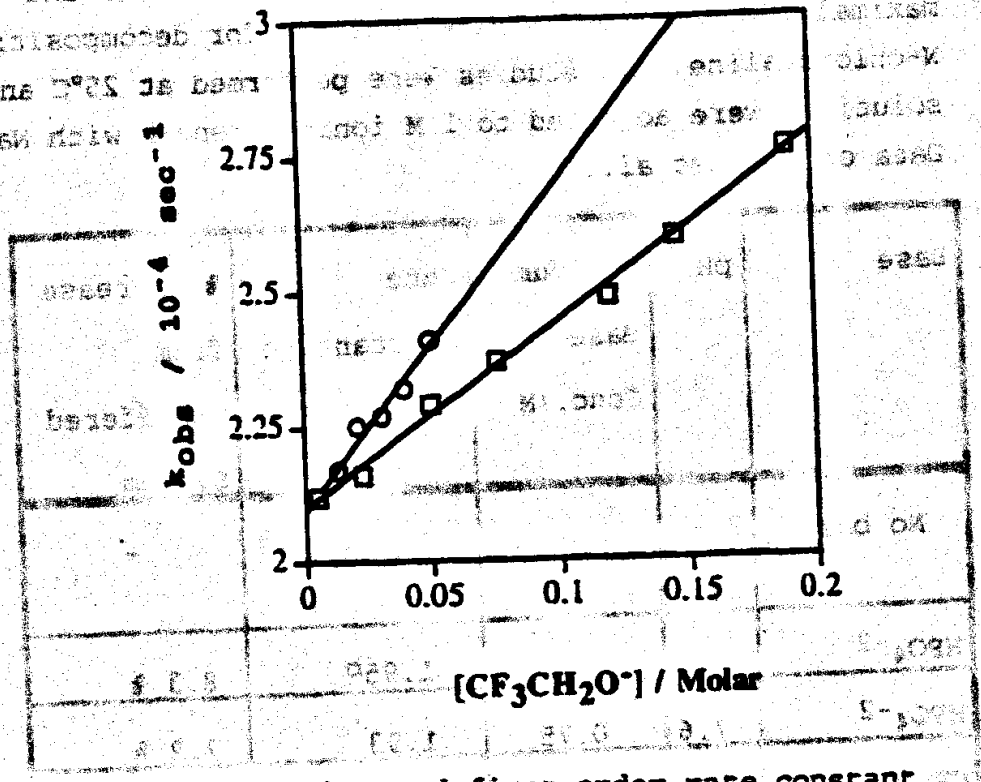

Figure 2.2 Plot of observed first order rate constant against molar concentration of (2,2,2)-trifluoroethoxide. Circular points: pH = 12.7, Square points: pH = 11.6. Ionic strength adjusted to 1 molar with NaCl. Data are from reference (3). Error in each point was unreported, but experimental error was said to be never greater than 5 %.

Table 2.3 Bases, their maximal concentrations, and the maximal increase in the rate constant for decomposition of N-chlorovaline. All studies were performed at 25°C and all solutions were adjusted to 1 M ionic strength with NaCl. Data of Abia *et al.*(3).

Base	pH	Maximum Base Conc./M	Rate Constant, k /10^{-4} sec^{-1}	% increase from Unbuffered System
No base	4 to 13	-	1.8 (0.1)[a]	-
HPO_4^{-2}	6.3	0.26	1.95[b]	8.3 %
HPO_4^{-2}	7.6	0.75	1.93	7.2 %
$CF_3CH_2O^-$	11.6	0.05	2.4	33.3 %
$CF_3CH_2O^-$	12.7	0.19	2.76	53.3 %

[a]Standard error in parentheses
[b]Standard error unreported, but error in determinations reportedly never exceeded 5 %

From their studies these workers conclude that N-chlorovaline undergoes base catalyzed abstraction of an α-carbon proton (Scheme 2.2), and this reaction competes with the concerted fragmentation mechanism (Scheme 2.7). I find some flaws in their arguments.

Though Figure 2.1 shows an increase in observed rate constant with increasing dibasic phosphate concentration,

the increase never exceeds 10 % of the uncatalyzed rate constant value. This seems insignificant relative to the 5% error in their experimental rate constant determinations. I believe these workers should have pursued this general base catalysis more aggressively by using higher HPO_4^{-2} concentrations. The rate increase shown in Figure 2.2 is more significant, indicating that general base catalysis by $CF_3CH_2O^-$ may be occurring in this system, but they are neglecting the possibility of a solvent effect from the addition of (2,2,2)-trifluoroethanol to the system. For example, the pK_a of (2,2,2)-trifluoroethanol is 12.43 (3), therefore at pH = 11.6 the ratio of (2,2,2)-trifluoroethanol to (2,2,2)-trifluoroethoxide is 6.76. The concentration of trifluoroethanol in a system with 0.15 M trifluoroethoxide would be 1.014 M in trifluoroethanol; we have observed solvent effects on the decomposition of N-chloroalanine and N-chloroleucine with ethanol at these concentrations (13). The effect observed by Abia and coworkers may be a combination of general base catalysis, and a medium effect, and it is difficult to distinguish between the two.

To substantiate their claim of general base catalysis, and the proposed α-carbon proton abstraction, they should have investigated possible general base catalysis of N-chloro-2-aminoisobutyric acid (1) or a similar N-chloroamino

acid, which has no α-carbon proton. A lack of catalysis would be consistent with their proposed competing mechanism. These authors also do not discuss the results of Awad and coworkers (10) and Hand and coworkers (9), which were mentioned earlier in this chapter, namely that at pH 7 and a phosphate buffer concentration of 0.5 M (10), and with phosphate, carbonate, or borate concentrations of 0.25 M, no catalysis of N-chloroalanine decomposition was observed (9). I believe that N-chlorovaline may be showing some unusual substituent effects that promote a base catalyzed reaction, and these studies should be pursued further. These workers have made an interesting and important find, but they did not pursue it far enough.

In conclusion, the concerted reaction shown in Scheme 2.7 seems to be consistent with all the experimental observations. But areas of possible future exploration should include studies in the highly basic and highly acidic region. Such studies are being pursued in this laboratory (20). Additional work should be conducted to better understand the substituent effects on the reaction.

2.2 Chapter 2 References

(1) Armesto, X.L; Canle, L.; Losda, M.; Santaballa, J.A. *Int. J. Chem. Kinetics* (1993), **25**, 331.

(2) Armesto, X.L; Canle, L.; Losda, M.; Santaballa, J.A. *J. Chem. Soc. Perkin Trans. 2* (1993) 181.

(3) Abia, L.; Armesto, X.L; Canle, L.; Garcia, M.V.; Losda, M.; Santaballa, J.A. *Int. J. Chem. Kinetics*, (1994), **26**, 1041.

(4) Langheld, K. *Chem. Ber.* (1909), **42**, 2360.

(5) Palin, A.T. *Water Waste Eng.* (1950), **54**, 151-159, 189-200, 248-256.

(6) Margerum, D.W.; Gray, E.T., Jr.; Huffman, R. P. "Organometals and Organometalloids, Occurrence and Fate in the Environment"; Brickman, F.E.; Bellma, J.M., Eds.; American Chemical Society: Washington D.C. (1978); A.C.S. Symposium Ser. No. 82, pp. 278-291.

(7) Synder, M.P.; Margerum, D.W.; *Inorg. Chem.* (1982), **21**, 2545.

(8) Issac, R.A.; Morris, J.C. " Water Chlorination, Environmental Impact and Health Effects"; Jolley, R.L.; Brungs, W.A.; Cummings, R.B., Eds.; Ann Arbor Science: Ann Arbor, MI (1980) Vol. III, Chapt. 17.

(9) Hand, V.C.; Synder, M.P.; Margerum, D.W. *J. Am. Chem. Soc.* (1983), **105**, 4022.

(10) Awad, R.; Hussain, A.; Crooks, P.A. *J. Chem. Soc. Perkin Trans. 2* (1990), 1233.

(11) Kaminski, J.J.; Bodor, N.; Higuchi, T. *J. Pharm. Sci.* (1976), **65**, 553.

(12) Fox, S.W.; Bullock, M.W. *J. Am. Chem. Soc.* (1951), **73**, 2754.

(13) Le Pree, J.M.; Connors, K.A., unpublished results.

(14) Budavari, S.; O'Neil, M.J.; Smith, A.; Heckelman, P.E., Eds.; "The Merck Index" Merck and Co.: Rahway, NJ, (1989).

(15) Weil, I.; Morris, J.C. *J. Am. Chem. Soc.* (1949), **71**, 3123.

(16) Grob, C.A.; Schiess, P.W. *Angew. Chem. Int. Ed. Engl.* (1967), **6**, 1.

(17) Grob, C.A. *Angew. Chem. Int. Ed. Engl.* (1969), **8**, 535.

(18) Becker, K.B.; Grob, C.A. "Supplement A: The Chemistry of Double Bonded Functional Groups"; Patai, S., Ed.; Wiley: New York, (1977).

(19) Bhattachatjee, A.K. *Indian, J. Chem.* (1993), **32B**, 942.

(20) Brown, M.C., personal communication.

Chapter 3. Pressure Effects

Though the majority of this work focused on solvent effects on chemical kinetics, I have performed two pressure effect studies. High pressure kinetic studies are not commonly performed, and this material may be foreign to the reader. To provide some background, I have included a brief discussion on high pressure kinetic work. This discussion is limited to pressure effects on small organic molecule reaction kinetics, more specifically the calculation of activation volumes from pressure effect data, and the mechanistic inferences which may be obtained from this information. More detailed descriptions of this field are given in the review literature (1-4).

3.1 Activation Volumes

A general chemical reaction is shown in Scheme 3.1.

$$aA + bB + \ldots \rightleftharpoons [aA\text{--}bB\text{-}\ldots]^{\ddagger} \longrightarrow \text{Products}$$

Scheme 3.1

Here the reactants combine to form the transition state, $[aA\text{--}bB\text{-}\ldots]^{\ddagger}$, which decomposes to give the products.

The volume of activation for a reaction is the difference between the partial molar volumes of the transition state and the reactants of a chemical reaction and is given by equation (3.1),

$$\Delta V^{\ddagger} = V^{\ddagger} - \sum V_{reactants} \quad (3.1)$$

where $V^{\ddagger}$ is the partial molar volume of the transition state, and $\sum V_{reactants}$ is the sum of the partial molar volumes of the reactants.

From thermodynamics, the volume of activation is related to the free energy of activation, $\Delta G^{\ddagger}$, by equation (3.2),

$$\Delta V^{\ddagger} = \left(\frac{\partial \Delta G^{\ddagger}}{\partial P}\right)_T = -RT\left(\frac{\partial \ln K^{\ddagger}}{\partial P}\right)_T \quad (3.2)$$

where $K^{\ddagger}$ is the equilibrium constant for a postulated equilibrium between the reactant and the transition state, RT is the product of the gas constant and absolute temperature, and P is the pressure.

Using transition state theory, $K^{\ddagger}$ is related to the rate constant, k, by equation (3.3)

$$K^{\ddagger} = \frac{kh}{k_B T} \quad (3.3)$$

where h is Planck's constant, k_B is the Boltzmann constant, and T is the temperature. Substitution of equation (3.3) into equation (3.2) gives equation (3.4). According to

equation (3.4) a decrease in the rate constant with an increasing pressure indicates a positive volume of activation, and a rate increase indicates a negative volume of activation. This is in accord with Le Chatelier's principle.

$$\Delta V^{\ddagger} = -RT\left(\frac{\partial \ln k}{\partial P}\right)_T \qquad (3.4)$$

The activation volumes for many reactions have been determined and are reported in the review literature (1-4). From these data, average activation volumes for various mechanistic features have been determined and tabulated. These values can be compared to values for newly studied reactions to gain mechanistic information; however, comparison of activation volumes must be done cautiously as will be discussed in the next two sections.

3.2 Concentration Units

It is important to realize that equation (3.4) applies only to rate constants in pressure independent concentration units such as molal or mole fraction units. These rate constants are denoted by k_m and k_x respectively, and using equation (3.4) we write

$$\Delta V^{\ddagger} = -RT\left(\frac{\partial \ln k_m}{\partial P}\right)_T = -RT\left(\frac{\partial \ln k_x}{\partial P}\right)_T \qquad (3.5)$$

If the rate constant for this reaction is expressed in molar concentration units (k_c), then a correction term is added to equation (3.5). This term can be derived as follows (5). The molar concentration for any solute is given by equation (3.6)

$$c_i = \frac{n_i}{V} \qquad (3.6)$$

where V is the volume of the solution and n_i is the number of moles of solute. In a dilute solution the volume of the solution is approximately equal to the volume of the pure solvent in the solution, thus we may rewrite equation (3.6) to give

$$c_i = \frac{d_s n_i 1000}{n_s M_s} \qquad (3.7)$$

where n_s, d_s, and M_s are the number of moles, the density, and the molecular weight of the solvent in solution. In a dilute solution, the number of moles of solvent and solute are approximately equal to the moles of pure solvent; therefore, the mole fraction of the solute is given by equation (3.8).

$$x_i = \frac{n_i}{n_s + n_i} = \frac{n_i}{n_s} \qquad (3.8)$$

Combination of equations (3.7) and (3.8) gives

$$c_i = \frac{x_i d_s 1000}{M_s} = \frac{x_i 1000}{V_s^o} \qquad (3.9)$$

where V_s^o is the molar volume of the solvent used in the solution.

If the equilibrium constant for the reaction in Scheme 3.1 is expressed in molar concentration units, then it is given by equation (3.10)

$$K_c^{\ddagger} = \frac{[[A--B--...]^{\ddagger}]}{[A]^a[B]^b...} \qquad (3.10)$$

where the brackets denote molar concentrations. This equilibrium constant is related to $K_x^{\ddagger}$, the equilibrium constant expressed in mole fraction concentration units, by equation (3.11)

$$K_c^{\ddagger} = \frac{x^{\ddagger} 1000 / V_s^o}{\left(x_A 1000 / V_s^o\right)^a \left(x_B 1000 / V_s^o\right)^b ...} = K_x^{\ddagger} \left(V_s^o / 1000\right)^{-(1-a-b...)} \qquad (3.11)$$

where x denotes mole fraction concentration.

Substitution of equation (3.3) into equation (3.11) gives

$$k_c = \frac{x^{\ddagger} 1000 / V_s^o}{\left(x_A 1000 / V_s^o\right)^a \left(x_B 1000 / V_s^o\right)^b \ldots} = k_x \left(V_s^o / 1000\right)^{-(1-a-b\ldots)} \qquad (3.12)$$

Differentiating the natural logarithm of equation (3.12) with respect to pressure and multiplying this result by -RT leads to equation (3.13)

$$-RT\left(\frac{\partial \ln k_c}{\partial P}\right)_T = -RT\left(\frac{\partial \ln k_x}{\partial P}\right)_T + RT(1-a-b-\ldots)\left(\frac{\partial \ln V_s^o}{\partial P}\right)_T \qquad (3.13)$$

Combination of equations (3.5) and (3.13) gives equation (3.14)

$$-RT\left(\frac{\partial \ln k_c}{\partial P}\right)_T = \Delta V^{\ddagger} - RT(1-a-b-\ldots)\kappa_s^o \qquad (3.14)$$

where κ_s^o is the compressibility of the pure solvent and

$$\kappa_s^o = -\left(1/V_s^o\right)\left(dV_s^o/dP\right)_T \qquad (3.15)$$

Notice that equation (3.14) differs from equation (3.5) only by the compressibility term, and that when this term is equal to zero, as it is for a first-order reaction,

$$\Delta V^{\ddagger} = -RT\left(\frac{\partial \ln k_m}{\partial P}\right)_T = -RT\left(\frac{\partial \ln k_x}{\partial P}\right)_T = -RT\left(\frac{\partial \ln k_c}{\partial P}\right)_T \qquad (3.16)$$

LeNoble, Asano, and Hamann (3-6) discussed another and less obvious case where the compressibility term is equal to zero. In this case, the rate constant is calculated from molarities at one atmosphere, thus V_s^o at one atmosphere is a constant and its derivative with respect to pressure is equal to zero; therefore the compressibility term should not be included in the activation volume calculation and equation (3.16) still holds.

A typical laboratory scenario can be used to illustrate when the compressibility term is not needed. Suppose a second order reaction is studied at various pressures, and samples are withdrawn for spectrophotometric analysis at ambient pressure. This analysis will give molar concentrations at one atmosphere, and thus corrections for compressibility must not be used in the data analysis.

Values for activation volumes typically range from ±(10 to 50) cm^3/mole (5), and the compressibility term can amount to 1 to 5 cm^3/mole, depending on the solvent used.

This is not negligible, and so improper inclusion (or exclusion) of the compressibility term in data analysis can cause significant errors in $\Delta V^{\ddagger}$. Workers in this field should always check for the correctness of activation volume calculations before using them for comparative purposes.

3.3 Data Treatment and Calculation of $\Delta V^{\ddagger}$

If the activation volume is independent of pressure it is easily calculated from the slope of an ln k vs. P plot and equation (3.17)

$$\Delta V^{\ddagger} = -RT\left(\frac{\partial \ln k}{\partial P}\right)_T = -RT\left(\frac{\partial \ln k/k_{1\ bar}}{\partial P}\right)_T \qquad (3.17)$$

where $k_{1\ bar}$ is the rate constant at ambient pressure. However, the activation volumes for many reactions are usually pressure dependent, as is evident from the non-linearity of the ln k vs. P plot shown in Figure 3.1 (7). It is difficult to accurately determine the slopes of these plots and this dilemma complicates the calculation of activation volumes. The situation is even worse than this, because there is no quantitative theory of the dependence of $\Delta V^{\ddagger}$ on pressure.

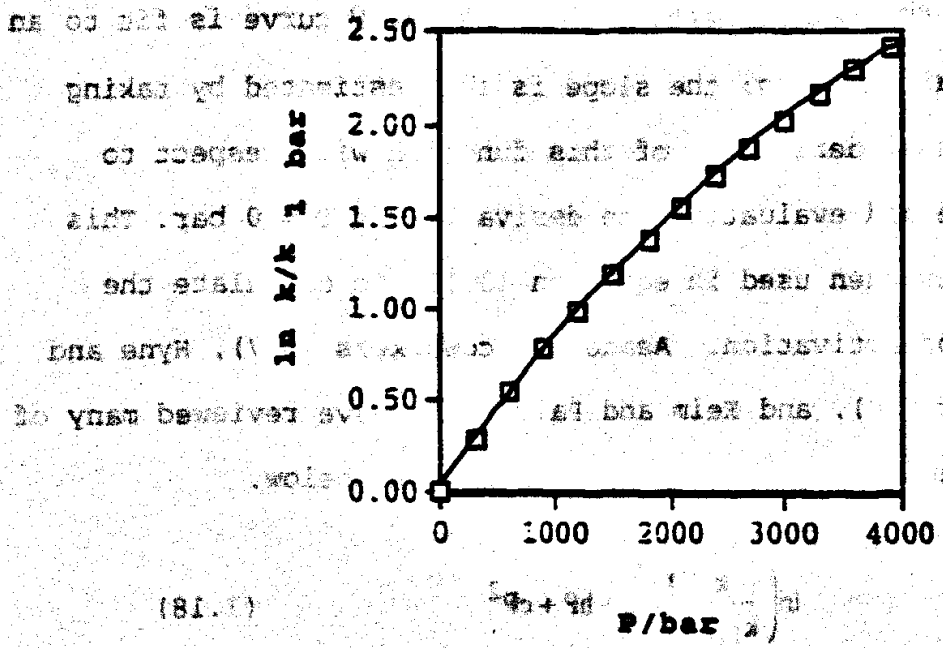

Figure 3.1) The pressure effect on the thermal isomerization of (Z)-4-(dimethylamino)-4'-nitrobenzene in chloroform at 25°C (7). The line has no theoretical significance.

Two methods have been used to determine the slopes of such curves, and hence the volume of activation. In the first method, the slope of the ln k vs. P curve at 0 or one atmosphere (for all practical work, P=0 and P=1 atmosphere may be taken as the same condition) is determined and then substituted into equation (3.17). To properly employ this method, the data collection should be concentrated at lower pressures.

In the second method, the ln k vs. P curve is fit to an empirical function; the slope is then estimated by taking the partial derivative of this function with respect to pressure and evaluating the derivative at P = 0 bar. This result is then used in equation (3.17) to calculate the volume of activation. Asano and coworkers (5,7), Hyne and coworkers (8), and Kelm and Palmer (9) have reviewed many of these functions. Some of them are given below.

$$\ln\left(\frac{k}{k_{1\ bar}}\right) = a + bP + cP^2 \qquad (3.18)$$

$$\ln\left(\frac{k}{k_{1\ bar}}\right) = a + bP + cP^2 + dP^3 \qquad (3.19)$$

$$\ln\left(\frac{k}{k_{1\ bar}}\right) = bP + cP^2 \qquad (3.20)$$

$$\ln\left(\frac{k}{k_{1\ bar}}\right) = bP + cP^{1.523} \qquad (3.21)$$

$$\left(\frac{\ln\left(k_{P_{i+1}} / k_{P_i}\right)}{P_{i+1} - P_i}\right) = a + \frac{b}{2}\left(P_{i+1} + P_i\right) \qquad (3.22)$$

$$\ln\left(\frac{k}{k_{1\ bar}}\right) = a + b\left(1 - \left(e^{-cP}\right)\right) \qquad (3.23)$$

$$\ln\left(\frac{k}{k_{1\ bar}}\right)=a+\frac{bP}{c+P} \qquad (3.24)$$

$$\ln\left(\frac{k}{k_{1\ bar}}\right)=aP+\frac{bP}{1+cP} \qquad (3.25)$$

$$\ln\left(\frac{k}{k_{1\ bar}}\right)=aP+b\ln(1+cP) \qquad (3.26)$$

Hyne and coworkers (8) examined the pressure effects on benzyl chloride hydrolysis and used two methods of data analysis. The first method was graphical; they took the initial slope of the ln $k/k_{1\ bar}$ vs. P curve. In the second method, they fit the data to equations (3.18-3.22). Kelm and Palmer (9) analyzed data on a Diels-Alder reaction and a ligand substitution reaction using equations (3.18, 3.19, 3.21, 3.23, and 3.24). Both groups found that these equations gave equally good quantitative fits to the data and similar values for the activation volumes; however, they noticed that the quadratic equations (3.18) and (3.20) gave somewhat smaller activation volume values than the other functions. This is disturbing because much of the work in this field has been analyzed with quadratic equations (references 3, 4); hence, many reported activation volumes may actually be underestimated. (This is assuming the other equations are not overestimating the volume.)

Even more disturbing are Asano's findings (7), which are presented in Tables 3.1 and 3.2. These data show that $\Delta V^{\ddagger}$ values estimated from the quadratic equation (3.18) depend on the upper pressure limit that is used in the data analysis. The activation volumes in Table 3.1 are calculated for the thermal isomerization of (Z)-4-(dimethylamino)-4'-nitroazobenzene in chloroform at 25°C, and the plot of these kinetic data is shown in Figure 3.1 (7). The activation volumes in Table 3.2 are calculated for the Diels-Alder reaction between isoprene and maleic anhydride (7,10).

Table 3.1 The activation volumes at zero pressure for the thermal isomerization of (Z)-4-(dimethylamino)-4'-nitroazobenzene in chloroform at 25°C estimated from various equations and data including different pressure limits (7).

Upper Pressure limit used in data analysis/bar	$\Delta V^{\ddagger}$/cm^3/mole estimated from quadratic equation (3.18)	$\Delta V^{\ddagger}$/cm^3/mole estimated from equation (3.25)	$\Delta V^{\ddagger}$/cm^3/mole estimated from equation (3.26)
1,500	-24.6 (0.36)[a]	-25.5 (0.57)	-25.5 (0.59)
2,100	-23.6 (0.45)	-25.9 (0.42)	-26.0 (0.46)
2,700	-22.7 (0.44)	-25.8 (0.29)	-25.9 (0.32)
3,300	-22.1 (0.38)	-25.4 (0.27)	-25.5 (0.29)
3,900	-21.6 (0.34)	-25.0 (0.25)	-25.1 (0.26)

[a]Numbers in parentheses are standard deviations.

Table 3.2 The activation volumes at zero pressure for the Diels-Alder reaction between isoprene and maleic anhydride estimated from various equations and data including different pressure limits (7,10).

Upper Pressure limit used in data analysis/bar	$\Delta V^{\ddagger}$/cm^3/mole estimated from quadratic equation (3.18)	$\Delta V^{\ddagger}$/cm^3/mole estimated from equation (3.25)	$\Delta V^{\ddagger}$/cm^3/mole estimated from equation (3.26)
1000	-38.1 (0.57)[a]	-36.6 (0.61)	-38.0 (2.1)
2100	-35.5 (0.77)	-38.7 (0.88)	-38.7 (0.97)
3100	-33.3 (0.90)	-39.2 (0.71)	-39.5 (0.88)
4100	-32.5 (0.70)	-36.6 (0.80)	-37.9 (0.86)
5200	-31.6 (0.62)	-36.7 (0.66)	-37.0 (0.69)
6200	-30.3 (0.74)	-37.1 (0.61)	-37.5 (0.68)

[a]Numbers in parentheses are standard deviations.

Notice that the activation volumes calculated with the quadratic equation (3.18) show a dependence on the pressure ranges that are used in the data analysis; the volumes do not exhibit this dependence when equations (3.25) and (3.26) are used. For this reason, Asano (7) has recommended that equation (3.25) or (3.26) be used for data analysis rather than a quadratic equation.

Yet, as stated before, much of the data in this field have been analyzed with a quadratic equation, and the activation volumes reported in these papers must be regarded with some skepticism. The data can still be used comparatively for mechanistic inferences; however, I agree

with Isaacs (2) that their best use should be restricted to distinguishing between mechanisms that would lead to activation volumes of opposite sign rather than just different magnitudes.

3.4 Interpretation of Activation Volumes

Many workers (2,3,11-15) interpret the activation volume for a reaction as the sum of two individual volume changes as given in equation (3.27).

$$\Delta V^{\ddagger} = \Delta V^{\ddagger}_{intr} + \Delta V^{\ddagger}_{solv} \qquad (3.27)$$

where $\Delta V^{\ddagger}_{intr}$ (intrinsic volume change) is the difference in the van der Waals volumes between the transition state and the reactants and originates from bond formations, bond cleavages, bond stretchings and changes in bond angles; and $\Delta V^{\ddagger}_{solv}$ (solvation volume change) is the difference in the solvation volumes between the transition state and the reactants and originates from various solute-solvent interactions.

(Some authors (2,3,12) have discussed an additional volume change, called the void volume change ($\Delta V^{\ddagger}_{v}$), which is the difference in intermolecular spaces that are occupied by the transition state and the reactants as a result of thermal vibrations. In dilute solution, $\Delta V^{\ddagger}_{v}$ is thought to

be small so its contribution to the activation volume is neglected (3,12).

Mechanistic interpretation of $\Delta V^{\ddagger}$ is as follows; bond formation leads to negative volume changes, bond cleavage and stretching lead to positive volume changes; charge formation leads to negative volume changes, while charge dispersion and charge neutralization cause positive volume changes. The overall volume of activation is the sum of volume contributions from all the events that occur during the formation of the transition state from the reactants.

Activation volumes for some common mechanistic events are given in Table 3.3 (4). These are only averages, and given the discussion in the previous sections, the magnitudes of the numbers may not be very accurate.

Table 3.3 Activation volumes for various mechanistic features(4).

Mechanistic feature	Contribution to $\Delta V^{\ddagger}$/cm^3 mole^{-1}
Neutralization	20
Bond cleavage	10
Charge dispersion	5
Bond deformation	0
Cyclization	0
Displacement	-5
Charge concentration	-5
Bond formation	-10
Ionization	-20

Solvation can contribute greatly to the volume of activation, and may even be more important than the intrinsic volume change. This was shown by Hamann and coworkers, who studied the S_N1 solvolysis of tert-butyl chloride in a 80% (v/v) ethanol-water system at 15°C (16). The reaction is shown in Scheme 3.2. In this scheme, the C-Cl bond is stretching thus increasing the volume of the transition state relative to the reactant volume and thereby increasing $\Delta V^{\ddagger}$; however, the volume of activation for this reaction was -20 cm^3/mole. This result was explained by an electrostatic attraction of the solvating molecules to the cation-like transition state that caused the solvating molecules to form a dense arrangement around the transition state, thereby reducing its volume. The volume reduction caused by dense packing of solvent molecules around a ion or dipole is called electrostriction. Hamann's study showed the importance of the solvation volume's contribution to the activation volume, and in a broader sense, the importance of solvation effects on chemical reactions.

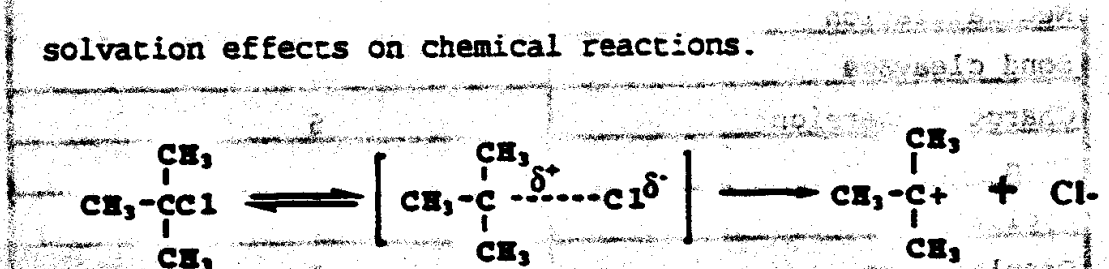

Scheme 3.2

Another interesting phenomenon, attributable to solvation effects, is the solvent effect on activation volumes. Volumes of activation for a Menshutkin reaction are presented in Table 3.4 (2).

Table 3.4 Solvent Effect on the Volumes of Activation for a Menshutkin Reaction (2).

$Et_3N + EtI \longrightarrow Et_4N^+ + I^-$

Solvent	$\Delta V^{\ddagger}$ / cm^3 $mole^{-1}$
Aqueous Dioxane	-13
Methanol	-38
Nitrobenzene	-30
Acetone	-54
Benzene	-50
Hexane	-58

The magnitude of the volumes increases with the nonpolarity of the solvent because the electric field around an ion decreases less rapidly with distance in a solvent of lower dielectric constant than it does in a solvent with a higher dielectric constant; therefore, the electrostriction is greater in solvents of low dielectric constant than in solvents of higher dielectric constant.

These data are also consistent with the Drude-Nernst equation [equation (3.28)],

$$\Delta V_{el} = -\frac{(ze)^2}{2r\varepsilon^2}\frac{1}{\varepsilon^2}\left(\frac{\partial \varepsilon}{\partial P}\right)_T \qquad (3.28)$$

where ΔV_{el} is the volume change induced by electrostriction of solvent around an ion, ze is the total charge on the ion, ε is the dielectric constant of the medium, and r is the ionic radius. Values for $\frac{1}{\varepsilon^2}\left(\frac{\partial \varepsilon}{\partial P}\right)_T$ were shown by Hamann to increase in going from water to less polar solvents (17); this finding is in agreement with the activation volumes in Table 3.4, which show some electrostrictive effects. Values of $\frac{1}{\varepsilon^2}\left(\frac{\partial \varepsilon}{\partial P}\right)_T$ for water, methanol, ethanol, and acetone are presented in Table 3.5.

Table 3.5 Values for $\frac{1}{\varepsilon^2}\left(\frac{\partial \varepsilon}{\partial P}\right)_T$ at 1 bar and 25°C (17).

Solvent	$10^7 \frac{1}{\varepsilon^2}\left(\frac{\partial \varepsilon}{\partial P}\right)_T$ /bar^{-1}
Water	5.01
Methanol	32.4
Ethanol	37.6
Acetone	59.1

The last topic to be discussed in this section is the relationship between the entropy of activation, $\Delta S^{\ddagger}$, and $\Delta V^{\ddagger}$. These might be expected to be related because events which increase freedom of motion or disorder in the system cause an increase in $\Delta S^{\ddagger}$ and they also usually lead to increases in $\Delta V^{\ddagger}$. For example, bond stretching and bond cleavage would allow for greater motional freedom and thus increase $\Delta S^{\ddagger}$, and, as shown in Table 3.3, these events also increase the activation volume. Formation of charge in going from the initial state to the transition state creates an ordering of solvent molecules around the transition state, and thus decreases the order in the system, thereby lowering $\Delta S^{\ddagger}$; these events are associated with decreases in $\Delta V^{\ddagger}$ as shown in Table 3.3. The opposite processes would lead to opposite effects. Such correlations have been observed for entropies and activation volumes of inorganic chemical reactions (18-20), but van Eldick (3) has warned that there are also many exceptions to this general correlation. He and his coworkers conclude that a large, positive entropy of activation will generally correspond to a large, positive volume of activation.

3.5 Chapter 3 References

(1) Matsumoto, K.; Acheson, R.M.; Eds.; "Organic Synthesis at High Pressures"; John Wiley and Sons, Inc.: New York, (1991).

(2) Isaacs, N.S. *Tetrahedron* (1991), **47**, 8463.

(3) van Eldik, R.; Asano, T.; Le Nobel, W.J. *Chem. Rev.* (1989), **89**, 549.

(4) Asano, T.; LeNoble, W.J. *Chem. Rev* (1978), **78**, 407.

(5) Asano, H. "Organic Synthesis at High Pressures"; Matsumoto, K.; Acheson, R.M.; Eds.; John Wiley and Sons, Inc.: New York, (1991), Chapter 2.

(6) Hamann, S.D.; Le Noble, W.J. *J. Chem. Educ.*, (1984), **61**, 558.

(7) Asano, T.; Okada, T. *J.Phys. Chem.* (1984), **88**, 238.

(8) Lohmüller, R.; Macdonald, D.D.; Mackinnon, M.; Hyne, J. B. *Can. J. Chem.* (1978), **56**, 1739.

(9) Kelm, H.; Palmer, D.A. "High Pressure Chemistry"; Kelm, H., Ed.; Reidel: Dordrecht, (1978); pp. 281-309.

(10) Grieger, R.A.; Eckert, C.A. *AIChE J.* (1970), **16**, 766.

(11) Evans, M.G.; Polanyi, M. *Trans. Faraday Soc.* (1935) **31**, 875.

(12) Hamann, S.D. *Rev. Phys. Chem. Jpn.* (1980), **50**, 47.

(13) le Noble, W.J.; Kelm, H. *Angew. Chem. Int. Ed. Engl.* (1986), **19**, 841.

(14) Kotowski, M.; Palmer, D.A.; Kelm, H. *Inorg. Chem.* (1979), **18**, 2555.

(15) Asano, T. *Rev. Phys. Chem. Jpn.* (1979), **49**, 109.

(16) Buchanan, J.; Hamann, S.D. *Trans. Faraday Soc.* (1953), **49**, 1425.

(17) Hamann, S.D. "Modern Aspects of Electrochemistry"; Conway, B.E.; Bockris, J. O'M. Eds.; Plenum Press: New York (1974). Vol. 9. Chapter 2.

(18) Twigg, M.V. *Inorg. Chem. Acta.* (1977), **24**, L84.

(19) Lawrance, G.A.; Suvachittunout, S. *Inorganic Chim. Acta.* (1979), **32**, L13.

(20) Phillips, J.C. *J. Phys. Chem.* (1985), **89**, 3060.

Chapter 4 Experimental

4.1 Materials

The organic cosolvents, acetonitrile, dioxane, ethanol, methanol, 2-propanol, 1-propanol, 1,2-ethanediol (ethylene glycol), and 1,2-propanediol (propylene glycol), used in these studies were of HPLC grade and were obtained from EM Science (Gibbstown, NJ).

Distilled, deionized water was obtained from an in-house Sybron-Barnstead PCS water purification system which consisted of prefilter, organic, ion-exchange, and microfilter (0.2 μm) cartridges (Barnstead Co., Dubuque, IA).

l-Alanine was purchased from Aldrich Chemical Co. (Milwaukee, WI) and was recrystallized from 1:1 ethanol-water solution. l-leucine (99%) was purchased from Aldrich Chemical Co. and was used as received.

Sodium hypochlorite solution (5% minimum concentration) was purchased from Aldrich Chemical Co. The solution was standardized according to the procedures given in the National Formulary XII (1).

The following salts were purchased from Mallinkrodt (Paris, KY).

Sodium Bicarbonate ($NaHCO_3$)

Sodium Carbonate (Na_2CO_3)

Sodium Phosphate, Dibasic (Na_2HPO_4)

Sodium Phosphate, Monobasic (NaH_2PO_4)

Sodium Chloride (NaCl)

Sodium Dichromate ($Na_2Cr_2O_7$)

Sodium borate, decahydrate ($Na_2B_4O_7 \cdot 10\ H_2O$) was purchased from Anachemia LTD (Champlain, NY).

Sodium Thiosulfate, ($Na_2S_2O_3$) was purchased from Baker and Adamson (Morristown, NJ).

All salts were of analytical reagent grade and used as received.

Starch TS solution was purchased from Aldrich Chemical Co. (Milwaukee, WI).

4.2 Apparatus

A Hitachi U-3000 spectrophotometer with circulating water cell compartment (San Jose, CA) was used for all rate constant determinations at atmospheric pressure. Temperature was maintained to 25 ± 0.1 °C with a Polyscience Model 9100 (Niles, IL) refrigerated circulating water bath. Hellma 1.00 cm, quartz cuvettes were used for the spectrophotometric analyses.

The pressure effect studies were conducted with the following equipment. Pressure was generated by a motorized and automated piston and cylinder arrangement that was connected to a Gateway computer (North Sioux City, SD) via a computer controller from Advanced Pressure Products

(Ithaca, NY). The controller regulated the pressure to ± 2 % during each study. The system was connected to a high pressure cell fitted with sapphire windows purchased from SLM-Aminco (Ithaca, NY). A Gilford Model 240 spectrophotometer was used as the light source and was placed in front of the pressure cell. An end-on photomultiplier tube was placed in front of and connected directly to the opposite window. PMT voltages were collected and manipulated by an Olis Spectrophotometer Operating System (Bogart, GA), where the absorbances were calculated and stored on a computer.

4.3 Procedures

4.3.1 Preliminary Studies

All preliminary studies were conducted in fully aqueous solutions at 25°C. The solution conditions for each study are presented in Table 5.1 of Chapter 5 Results. Typically, each experimental solution contained 0.01 to 0.03 M *L*-alanine. To initiate the reaction, NaOCl solution was pipetted into a flask containing *L*-alanine solution. The flask was swirled to form N-chloroalanine in situ. Alanine was present in a 5 to 10 fold excess over NaOCl to avoid forming the dichlorinated amino acid. An aliquot of this solution was placed in a cuvette and the absorbance decrease at 253 nm was monitored to determine the first-order rate

constant for N-chloroalanine decomposition. The results of these studies were in agreement with the results of studies conducted by other workers (2,3); specifically, that the reaction rate was insensitive to solution pH and ionic strength and these solution conditions did not require any control. These experiments revealed that it was not necessary to add buffers and salts to the aqueous-organic binary cosolvent solutions used in the solvent effect studies.

4.3.2 Solvent Effect Studies

A given volume of organic cosolvent was pipetted into each of three 50.00 ml volumetric flasks, and the weight of the organic cosolvent was recorded. One of the flasks was labeled "amino acid", a second flask was labeled "NaOCl", and the third was labeled "spectrophotometric blank". A given quantity of alanine or leucine was weighed into the "amino acid" flask, and the weight of the amino acid was recorded. The three flasks were brought to near volume with water, and the weight of water added to each flask was recorded. The flasks were sonicated for 15 to 30 minutes and then equilibrated to 25°C. After equilibration, the "amino acid" and the "spectrophotometric blank" flasks were brought to full volume with water, and the weight of this additional water was recorded. A given volume of NaOCl

solution (typically 0.3 ml) was pipetted into the "NaOCl" flask and then this flask was brought to full volume with water. The weight of water and NaOCl solution was recorded. The amino acid concentration was usually between 0.06 and 0.03 M, and the NaOCl concentration was usually about 0.006 M.

The spectrophotometer was zeroed with the "spectrophotometric blank" solution. To initiate a study, 10.00 ml of the amino acid solution was pipetted into a 50.00 ml erlenmeyer flask, and then 10.00 ml of the NaOCl solution was pipetted slowly into the flask. The flask was swirled during this process to assure proper mixing. (Assuming the chlorination reaction went to completion, the intial concentration of N-chloroamino acid in the reaction solution was approximately 0.003 M.) An aliquot of this solution was then transferred to a cuvette, and the absorbance decrease, corresponding to the decomposition of the N-chloroamino acid, was recorded over time. Data points were recorded at equal intervals for at least three half-lives. All studies were carried out in triplicate.

4.3.3 Blank studies

To assure that the N-chloroamino acid was not reacting with the organic cosolvent, the following two studies were performed. A 0.006 M solution of NaOCl was prepared in a

50% v/v solution of the organic cosolvent. The solution was assayed spectrophotometrically; a decrease in the absorbance at 294 nm, the analytical wavelength of NaOCl (4), indicated that NaOCl was reacting with the organic cosolvent (probably via an oxidation-reduction reaction). Because the N-chloro group is also in a -1 oxidation state, a second study, described in the next paragraph, was performed to assure that the N-chloroamino acid was not reacting with the organic cosolvent.

In the second study, a solution containing equal concentrations of the N-chloroamino acid and organic cosolvent was prepared, and the decomposition of the N-chloroamino acid was monitored. If the N-chloroamino acid reacted with the organic cosolvent, the reaction would not be unimolecular and deviations from first order kinetics would be observed. Though the alcohols and dioxane did react with NaOCl, the second study demonstrated that dioxane, methanol, 2-propanol, ethylene glycol, and propylene glycol did not react with N-chloroalanine and that methanol did not react with N-chloroleucine.

4.3.4 Effect of Ultra-Violet Radiation on the Decomposition of N-Chloroalanine.

To assure that ultra-violet radiation did not affect the decomposition rate of N-chloroalanine, a solution of N-

chloroalanine was stored in darkness and only exposed to light while absorbance readings were taken. The results from this study were compared with the results from other studies in which the solution was exposed to UV radiation throughout three half-lives of decomposition. No significant differences were observed, indicating that UV light at 253 nm did not affect the rate of decomposition.

4.3.5 Pressure effect studies

All pressure effect studies were conducted in fully aqueous solutions. The alanine studies were conducted at 26°C, and the leucine studies were conducted at 25°C. A 0.06 M solution of the amino acid was prepared in a 50.00 ml volumetric flask. In a second 50.00 ml volumetric flask, a 0.006 M NaOCl solution was prepared. Both solutions were degassed. To initiate a study, 2.00 ml of the amino acid solution was pipetted into a 5 ml Erlenmeyer flask, then 2.00 ml of NaOCl solution was slowly pipetted into the flask. The flask was swirled to assure proper mixing.

A 3 ml syringe was used to fill the pressure cuvette with the N-chloroamino acid solution. Care was taken not to introduce air into the cuvette. The cuvette was placed in the cell, and the cell was closed. The system was pressurized using ethanol. The reaction was followed for at least one-half life; however, when the pressure fell below

2% of its initial value, the piston motor automatically engaged to re-establish the pressure. This would often cause "spikes" in the absorbance versus time curve. To obtain a smooth curve covering a considerable time span, it was usually necessary to follow the reaction for two to three half-lives, and the smoothest portion of the absorbance versus time curve was used to determine the rate constant; typically 0.5 to 1 half-lives of "spike-free" data could be collected.

4.4 *Calculations*

4.4.1 Rate constant calculations

The first-order rate constants for solvent effect and pressure effect studies were determined by plotting the solution absorbances at time = t against the absorbances at a later time, t + Δt, where Δt is a constant time interval. This method of analysis was developed by Kezdy and coworkers (5). (See Figure 5.3 in the results section for a typical plot.) The rate constant, k, was calculated from the slope of this plot using equation (4.1),

$$k = \frac{\ln \text{slope}}{\Delta t} \qquad (4.1)$$

where Δt is the time interval between absorbance readings. Δt was usually between 0.25 and 0.75 of the half-life.

4.4.2 Mole fraction of Organic Cosolvent in Reaction Solution

The mole fraction of organic cosolvent in the reaction solution, x_2, was calculated from the average weights of water and organic cosolvent in the amino acid and NaOCl solutions using equation (4.2).

$$x_2 = \frac{\frac{(A+B)/2}{C}}{\frac{(A+B)/2}{C} + \frac{(D+E)/2}{18.016}} \qquad (4.2)$$

where:

A = the weight of organic cosolvent in the "amino acid" flask;

B = the weight of organic cosolvent in the "NaOCl" solution flask;

C= the molecular weight of the organic cosolvent used in the study;

D = the total weight of water added to the "amino acid" solution flask;

E = the total weight of water added to the "NaOCl" solution flask, including the weight of water in the standardized NaOCl solution; the weight of NaOCl in this solution was negligible and was not subtracted from this total.

4.4.3 Calculation of $\delta_m\Delta G^{\ddagger}$

The solvent effect on the free energy of activation was calculated with equation (4.3),

$$\delta_m\Delta G^{\ddagger} = -k_B T \ln(k/k_w) \qquad (4.3)$$

where k_B is Boltzmann's constant, T is the temperature, k is the first order rate constant for the reaction in the aqueous-organic cosolvent system, and k_w is the first order rate constant for the decomposition in the fully aqueous system.

4.4.4 Calculation of the Volume of Activation, $\Delta V^{\ddagger}$

To calculate the volume of activation, a plot of $\ln\left(k/k_{1\ bar}\right)$ against P was made, where $k_{1\ bar}$ is the rate constant at ambient pressure. The data were fit to

$$\ln\frac{k}{k_{1\ bar}} = aP + bP^2 \qquad (4.4)$$

where a and b are adjustable parameters. The volume of activation is then calculated from equation (4.5)

$$\Delta V^{\ddagger} = -RTa \qquad (4.5)$$

Fits of the data to three-parameter equations such as equations (4.6) and (4.7) [from reference (6)] were unsuccessful, as the parameter estimates were highly correlated and sensitive to starting values.

$$\ln k/k_{1\ bar} = aP + \frac{bP}{1+cP} \qquad (4.6)$$

$$\ln k/k_{1\ bar} = aP + b\ln(1+cP) \qquad (4.7)$$

4.5 Chapter 4 References

(1) NF XII; "The National Formulary," 12th ed., Mack Publishing Co., Easton, PA, (1965) 365.

(2) Hand, V.C.; Synder, M.P.; Margerum, D.W. *J. Am. Chem. Soc.* (1983), **105**, 4022

(3) Awad, R.; Hussain, A.; Crooks, P.A. *J. Chem. Soc. Perkin Trans. 2*, (1990), 1233.

(4) Hussain, A.; Trudell, P.; Repta, A.J. *J. Pharm. Sci.* (1970) **59**, 1169.

(5) Kezdy, F.J.; Jaz, J.; Bruylants, A. *Bull. Chem. Soc. Belg.* (1958) **67**, 687.

(6) Asano, T; Okada, T. *J. Phys. Chem.* (1984) **88**, 238.

Chapter 5 Results

In this chapter, results from the solvent effect and pressure effect experiments are presented. Section 5.1 contains kinetic data from preliminary studies, Section 5.2 from the solvent effect rate studies, and Section 5.3 gives the parameter values obtained by fitting the kinetic rate data to the phenomenological model (equations 1.63 and 1.64). Section 5.4 gives plots of the data and curve fits generated from these models. Section 5.5 contains the results from the pressure effect studies.

5.1 Preliminary studies

Table 5.1.1 provides a summary of various preliminary studies that were performed to investigate the effects of altering the reaction solution conditions. All studies were performed in fully aqueous solution at 25 ± 0.1°C. The rate constant was not significantly affected as solution conditions were altered, in agreement with results reported in the literature (1,2), some of which are also given in Table 5.1.

Figure 5.1 shows a representative plot of the absorbance of N-chloroalanine against time. In Figure 5.2 a first-order plot of the data is presented, and in Figure 5.3 the data are plotted according to the method of Kezdy and coworkers (3). Notice that both methods give the same rate constant.

Table 5.1 Preliminary data summary. All studies were performed at 25°C.

Solution conditions prior to start of reaction; pH values were measured upon completion of the reaction.	$k^{a,b}$ /min^{-1}	Notebook Reference
0.08 M phosphate buffer; pH = 6.69 0.01 M alanine; 0.001 M NaOCl	0.0150	36c-123
0.08 M phosphate buffer; pH = 6.9 0.03 M alanine; 0.003 M NaOCl	0.0158	36c-127
0.08 M phosphate buffer; pH unrecorded 0.03 M alanine; 0.003 M NaOCl 0.3 M NaCl	0.0154	36c-132
0.03 M alanine; 0.003 M NaOCl; solution was **not** exposed to UV radiation	0.0152	40c-129
0.03 M alanine; 0.003 M NaOCl added	0.0154	40c-128
0.08 M phosphate buffer; pH unrecorded 0.03 M alanine; 0.003 M NaOCl 0.3 M NaCl; Solution was **not** exposed to UV radiation	0.0153	36c-137
0.08 M carbonate buffer; pH = 9.51 0.03 M alanine; 0.003 M NaOCl 0.3 M NaCl	0.0151	36c-149
0.05 M phosphate buffer; pH = 6.79 0.03 M alanine; 0.003 M NaOCl	0.0141 0.0152	36c-153 36c-157
0.01 M phosphate buffer; pH unrecorded 0.03 M alanine; 0.003 M NaOCl	0.0154 0.0151 0.0150	36c-160 37c-12 37c-13
Self-buffered solution; pH = 8.3 0.03 M alanine; 0.003 M NaOCl	0.0150 0.0150 0.0148 0.0148	37c-15 37c-16 37c-17 37c-18
pH = 6.85, 0.01 M phosphate buffer, 0.5 M ionic strength	0.0160 (0.00012)[a]	Reference (1)
pH = 7.0 phosphate buffer	0.0160	Reference (2)

[a] Standard deviation

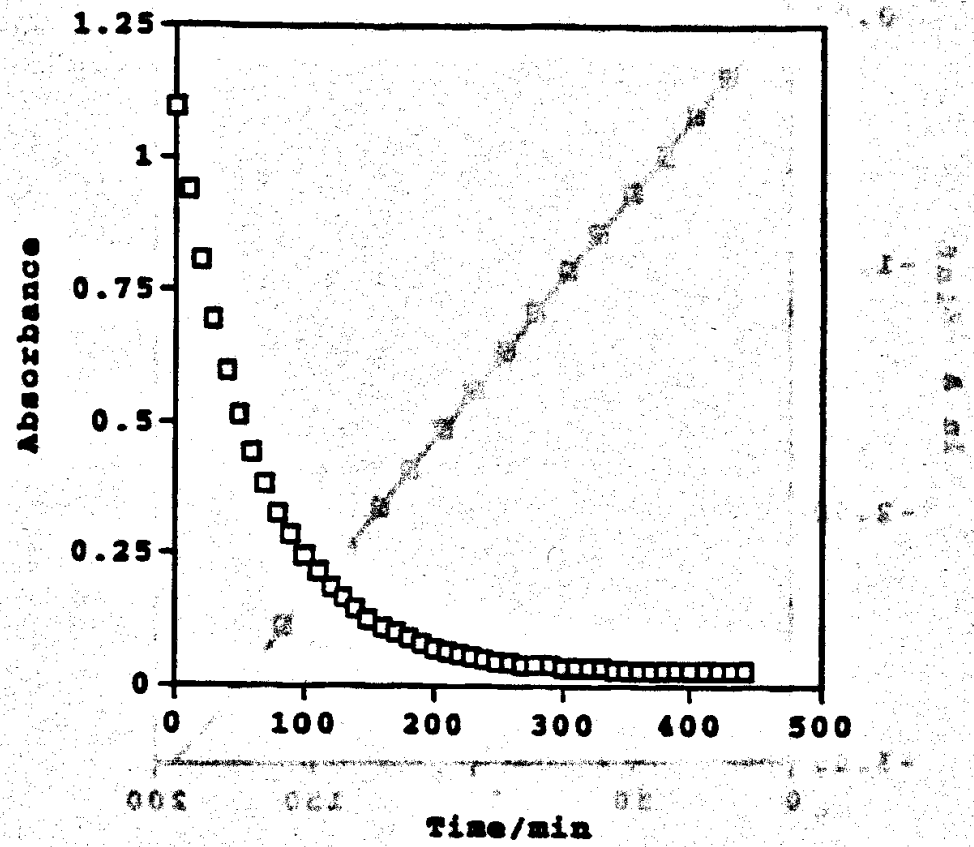

Figure 5.1 A plot of absorbance (253 nm) against time for the decomposition of N-chloroalanine. The study was conducted at 25°C in a pH 6.69, 0.02 M phosphate-buffered solution. The initial concentration of alanine was 0.03 M, and the initial concentration of the chlorinating agent, NaOCl, was 0.003 M. The molar absorptivity, estimated from the initial concentration (0.003 M) and absorbance reading at time = 0 minutes, is 370 L $mole^{-1}$ cm^{-1}. Metcalf reported a value of 385 L $mole^{-1}$ cm^{-1} (4).

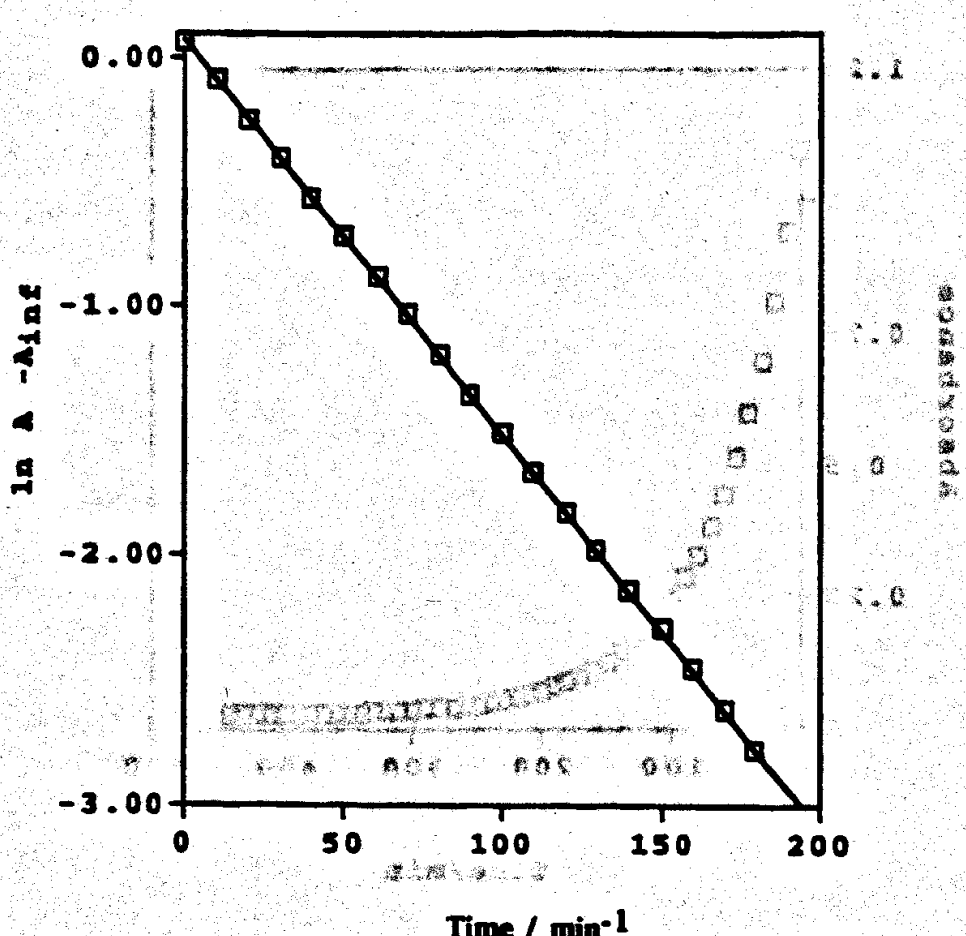

Figure 5.2 A first-order plot of the data from Figure 5.1 (decomposition of N-chloroalanine). The rate constant is 0.0158 min-1. The study was conducted at 25°C in a pH 6.69, 0.02 M phosphate buffered solution. The initial concentration of alanine was 0.03 M, and the initial concentration of the chlorinating agent, NaOCl, was 0.003 M.

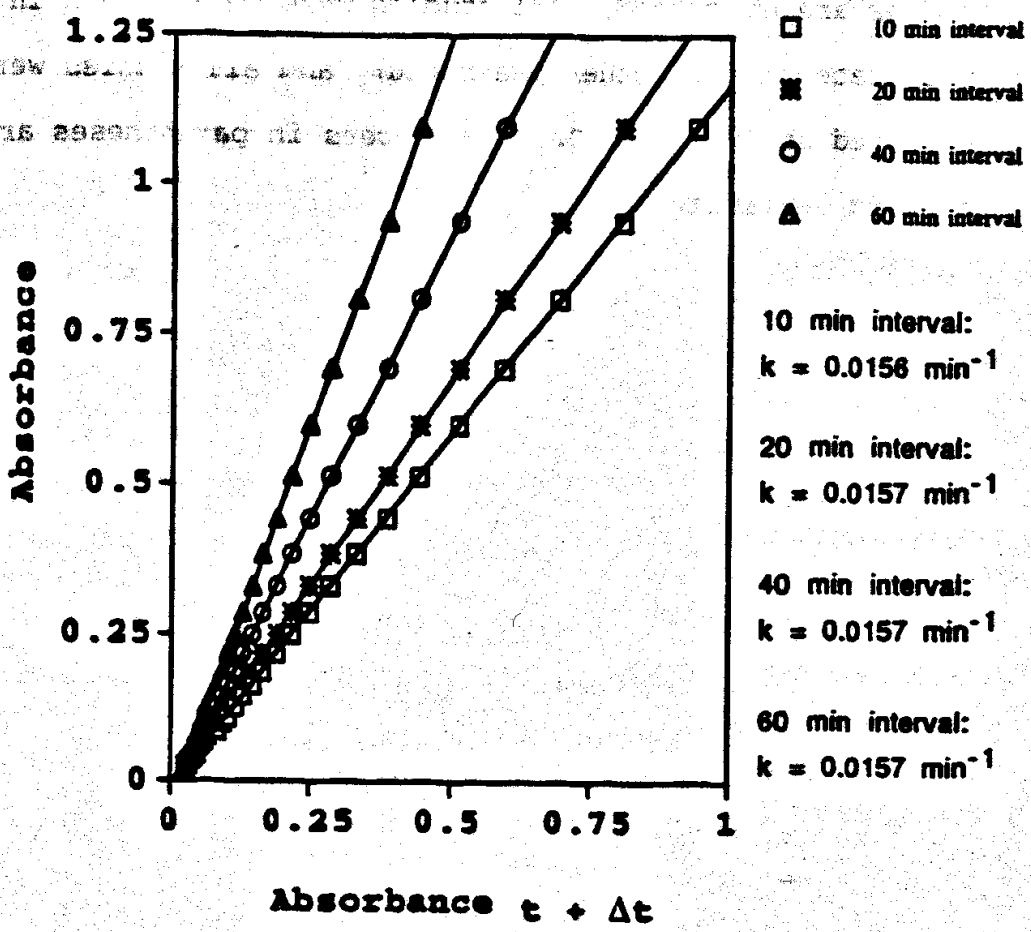

Figure 5.3 A plot of the data in Figure 5.1 according to the method of Kezdy and coworkers (3). As described in Chapter 4, the absorbance in real time is plotted against the absorbance at some later, but equally spaced, time interval. Notice that using different time intervals does not significantly affect the value of the rate constant.

5.2 Solvent Effect Studies

In this section, the data from N-chloroamino acid studies are presented. All studies were carried out in triplicate (unless otherwise noted), and all studies were conducted at 25 ± 0.1 °C. The numbers in parentheses are standard deviations.

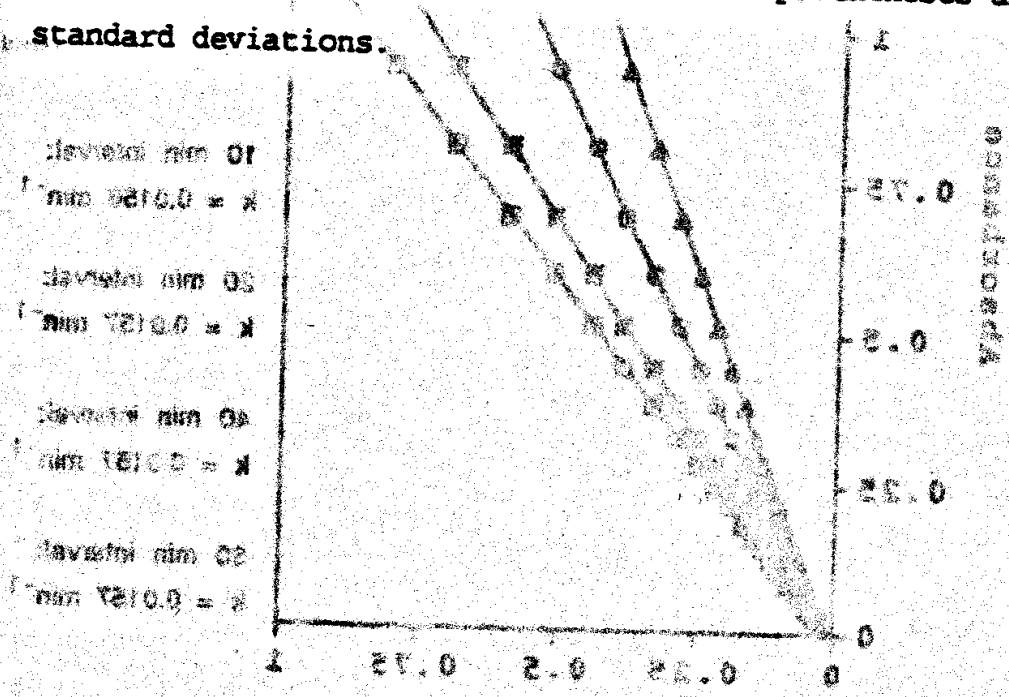

Figure 5.1 A plot of the data in Figure 3.1 according to the method of Zady and Cookerly (1). As described in Chapter 4, the absorbance in this case is plotted against the absorbance at some later, but equally spaced, time interval. Notice that using different time intervals does not significantly affect the value of the rate constant.

Table 5.2 Solvent effect data for N-chloroalanine decomposition in acetonitrile-water binary cosolvent systems.

x2	Volume percent (post mixing)	Weight of Organic /g	Weight of Water/g	k/min^{-1}	$\delta_m \Delta G^{\ddagger}$ / 10^{-20} J Molecule-1
0	0	0	50	0.0149 (0.00017)	0 (0.0066)[a]
0.0213	6	2.3392	47.1783	0.0197 (0.00037)	-0.115 (0.0090)
0.03615	10	3.8772	45.3547	0.0246 (0.00027)	-0.206 (0.0065)
0.05214	14	5.4494	43.4759	0.0312 (0.00074)	-0.30 (0.011)
0.0778	20	7.8271	40.6229	0.0421 (0.00037)	-0.427 (0.0059)
0.1255	30	11.7158	35.8281	0.0706 (0.00072)	-0.640 (0.0063)
0.1807	40	15.5620	30.9746	0.117 (0.001)	-0.847 (0.0059)
0.2073	44	17.1933	28.8609	0.131 (0.0023)	-0.894 (0.0086)
0.2468	50	19.4137	25.9981	0.176 (0.0032)	-1.0154 (0.0088)
0.2793	54	21.1045	23.9034	0.196 (0.0038)	-1.060 (0.0093)
0.3267	60	23.3229	21.0949	0.263 (0.0081)	-1.18 (0.014)
0.3685	64	24.9538	18.7678	0.321 (0.0069)	-1.26 (0.010)
0.4308	70	27.2411	15.7954	0.419 (0.0025)	-1.372 (0.0053)

[a] Calculated by standard propagation of errors

Table 5.3 Solvent effect data for N-chloroalanine decomposition in dioxane-water binary cosolvent systems.

x_2	Volume Percent (post mixing)	Weight of Organic /g	Weight of Water/g	k/min^{-1}	$\delta_m\Delta G^{\ddagger}$ /10^{-20} J Molecule^{-1}
0	0	0	50	0.0149 (0.00017)	0 (0.0066)[a]
0.0132	6	3.0999	47.5542	0.0198 (0.00015)	-0.117 (0.0056)
0.0226	10	5.2117	45.1706	0.0256 (0.0004)	-0.223 (0.0080)
0.0330	14	7.2131	43.239	0.0322 (0.00079)	-0.32 (0.011)
0.0493	20	10.2724	40.4386	0.046 (0.00066)	-0.464 (0.0075)
0.04920	20	10.2372	40.4504	0.045 (0.0011)	-0.45 (0.011)
0.0815	30	15.4639	35.6385	0.0876 (0.00094)	-0.728 (0.0064)
0.1198	40	20.3722	30.9126	0.154 (0.001)	-0.960 (0.0054)
0.1683	50	25.7385	26.0050	0.28 (0.017)	-1.21 (0.025)
0.1905	54	27.7491	24.1034	0.38 (0.011)	-1.33 (0.013)
0.2307	60	30.8741	21.0517	0.4946 (0.0005)	-1.440 (0.0047)

[a]Calculated by standard propagation of errors

Table 5.4 Solvent effect data for N-chloroalanine decomposition in ethanol-water binary cosolvent systems.

x2	Volume percent (post mixing)	Weight of Organic /g	Weight of Water/g	k/min^{-1}	$\delta_m \Delta G^{\ddagger}$ /10^{-20} J Molecule^{-1}
0	0	0	50	0.0149 (0.00017)	0 (0.0066)[a]
0.0190	6	2.3399	47.1077	0.0179 (0.0005)	-0.075 (0.0012)
0.0328	10	3.9179	45.237	0.0198 (0.00062)	-0.12 (0.0147)
0.0699	20	7.8314	40.7823	0.026 (0.0012)	-0.23 (0.020)
0.1131	30	11.7958	36.1905	0.0368 (0.0008)	-0.37 (0.010)
0.1624	40	15.6660	31.5971	0.051 (0.0015)	-0.51 (0.013)
0.223	50	19.6350	26.7623	0.073 (0.0056)	-0.65 (0.032)
0.2984	60	23.6225	21.7224	0.096 (0.0031)	-0.77 (0.014)
0.392	70	27.4689	16.6639	0.131 (0.0043)	-0.89 (0.014)

[a] Calculated by standard propagation of errors.

Table 5.5 Solvent effect data for N-chloroalanine decomposition in ethylene glycol-water binary cosolvent systems.

x2	Volume Percent (post mixing)	Weight of Organic /g	Weight of Water/g	k/min^{-1}	$\delta_m \Delta G^{\ddagger}$ $/10^{-20}$ J $Molecule^{-1}$
0	0	0	50	0.0149 (.00017)	0 (0.0066)[a]
0.0130	4	2.1779	47.9375	0.0155 (.00021)	-0.016 (0.0073)
0.0342	10	5.5011	45.1207	0.0171 (.00022)	-0.057 (0.0071)
0.0728	20	10.9022	40.2987	0.0203 (.00029)	-0.127 (0.0075)
0.1193	30	16.5233	35.3904	0.025 (.0012)	-0.21 (0.020)
0.1724	40	22.0045	30.6549	0.0301 (.00053)	-0.289 (0.0086)
0.236	50	27.4266	25.7648	0.0372 (.00049)	-0.376 (0.0072)
0.3151	60	32.9754	20.9359	0.0471 (.00071)	-0.473 (0.0078)
0.4151	70	38.5281	15.7560	0.057 (.0013)	-0.55 (0.010)
0.5465	80	44.1649	10.6394	0.072 (.0039)	-0.65 (0.023)
0.7192	90	44.6230	5.6238	0.09 (.0021)	-0.74 (0.011)

[a] Calculated by standard propagation of errors

Table 5.6 Solvent effect data for N-chloroalanine decomposition in 2-propanol-water binary cosolvent systems.

x2	Volume Percent (post mixing)	Weight of Organic /g	Weight of Water/g	k/min^{-1}	$\delta_m\Delta G^{\ddagger}$ $/10^{-20}$ J Molecule^{-1}
0	0	0	50	0.0149 (0.00017)	0 (0.00664)[a]
0.00475	2	0.7797	48.9798	0.0156 (0.00017)	-0.019 (0.0065)
0.00954	4	1.5433	48.0374	0.0164 (0.00023)	-0.039 (0.0074)
0.0145	6	2.3132	47.1067	0.0171 (0.00032)	-0.057 (0.00900
0.0248	10	3.8515	44.3356	0.0192 (0.00034)	-0.104 (0.0087)
0.0305	12	4.6573	44.4010	0.021 (0.00041)	-0.141 (0.0093)
0.0363	14	5.458	43.4975	0.0208 (0.00023)	-0.137 (0.0065)
0.0479	18	7.0047	41.7159	0.0264 (0.00024)	-0.235 (0.0060)
0.0539	20	7.7624	40.8797	0.0272 (0.00077)	-0.25 (0.013)
0.0672	24	4.6787	19.568	0.0326 (0.00076)	-0.32 (0.011)
0.0879	30	11.653	36.2758	0.0425 (0.0016)	-0.43 (0.016)
0.112	36	7.0036	16.7263	0.054 (0.0015)	-0.53 (0.012)
0.128	40	15.5042	31.5326	0.065 (0.0021)	-0.61 (0.014)
0.148	44	8.5418	14.7599	0.074 (0.0022)	-0.66 (0.013)
0.18	50	19.4730	26.5143	0.085 (0.0017)	-0.716 (0.0095)
0.216	56	10.8708	11.8050	0.1013 (0.00053)	-0.788 (0.0052)
0.244	60	23.3206	21.5987	0.11 (0.0073)	-0.82 (0.028)
0.331	70	27.2174	16.4762	0.145 (0.0043)	-0.94 (0.013)

[a] Calculated by standard propagation of errors

Table 5.7 Solvent effect data for N-chloroalanine decomposition in methanol-water binary cosolvent systems.

x2	Volume Percent (post mixing)	Weight of Organic /g	Weight of Water /g	k/min^{-1}	$\delta_m\Delta G^{\ddagger}$ / 10^{-20} J Molecule^{-1}
0	0	0	50	0.0149 (0.00017)	0 (0.0066)[a]
0.0180	4	1.5686	48.0155	0.0167 (0.00031)	-0.047 (0.0090)
0.0462	10	3.9110	45.3708	0.0178 (0.00027)	-0.073 (0.0078)
0.0978	20	7.8349	40.6640	0.0206 (0.00033)	-0.133 (0.0081)
0.1552	30	11.8019	36.1192	0.0275 (0.00052)	-0.252 (0.0091)
0.2205	40	15.7826	31.3727	0.036 (0.00021)	-0.363 (0.0053)
0.2935	50	19.6776	26.6352	0.047 (0.0019)	-0.47 (0.017)
0.3796	60	23.6426	21.7318	0.059 (0.003)	-0.57 (0.021)
0.4798	70	27.5079	16.7682	0.075 (0.0012)	-0.665 (0.0081)
0.6054	80	31.4738	11.5350	0.086 (0.0024)	-0.72 (0.012)

[a] Calculated by standard propagation of errors

Table 5.8 Solvent effect data for N-chloroalanine decomposition in 1-propanol-water binary cosolvent systems.

x_2	Volume Percent (post mixing)	Weight of Organic /g	Weight of Water/g	k/min^{-1}	$\delta_m\Delta G^{\ddagger}$ /10^{-20} J Molecule^{-1}
0	0	0	50	0.0149 (0.00017)	0 (0.0066)[a]
0.0149	6	2.3702	47.1328	0.0184 (0.00013)	-0.087 (0.0055)
0.0256	10	3.9637	45.2482	0.0205 (0.0002)	-0.131 (0.0062)
0.0372	14	5.5847	43.4014	0.0234 (0.00062)	-0.19 (0.012)
0.0557	20	7.9932	40.6265	0.0296 (0.00106)	-0.28 (0.015)
0.0910	30	11.9753	35.8580	0.0403 (0.00022)	-0.409 (0.0052)
0.1341	40	15.9870	30.9381	0.0536 (0.0046)	-0.53 (0.036)
0.1867	50	19.9646	26.0723	0.0624 (0.00085)	-0.589 (0.0073)
0.2560	60	23.9929	20.9009	0.076 (0.0017)	-0.67 (0.010)
0.3453	70	27.9427	15.8814	0.095 (0.0029)	-0.76 (0.013)
0.4689	80	31.9108	10.8348	0.123 (0.0054)	-0.87 (0.019)

[a] Calculated by standard propagation of errors

Table 5.9 Solvent effect data for N-chloroalanine decomposition in propylene glycol-water binary cosolvent systems.

x_2	Volume Percent (post mixing)	Weight of Organic /g	Weight of Water/g	k/min^{-1}	$\delta_m \Delta G^{\ddagger}$ / 10^{-20} J Molecule^{-1}
0	0	0	50	0.0149 (0.00017)	0 (0.0066)[a]
0.0148	6	2.9792	47.0355	0.0172 (0.00019)	-0.059 (0.0065)
0.0257	10	5.0307	45.1979	0.0182 (0.00027)	-0.082 (0.0077)
0.0558	20	10.1864	40.4733	0.0224 (0.00038)	-0.168 (0.0084)
0.0922	30	15.3349	35.7351	0.0309 (0.00017)	-0.300 (0.0052)
0.1342	40	20.356	31.0947	0.04 (0.0014)	-0.41 (0.015)
0.193	50	25.4819	26.2106	0.054 (0.0024)	-0.53 (0.019)
0.2525	60	30.5322	21.4042	0.077 (0.0016)	-0.675 (0.0098)
0.3378	70	35.5406	16.4946	0.094 (0.0081)	-0.76 (0.036)
0.455	80	40.5270	11.4940	0.104 (0.004)	-0.80 (0.017)

[a] Calculated by standard propagation of errors

Table 5.10 Solvent effect data for N-chloroleucine decomposition in acetonitrile-water binary cosolvent systems.

x_2	Volume Percent (post mixing)	Weight of Organic /g	Weight of Water/g	k / min^{-1}	$\delta_m\Delta G^{\ddagger}$ / 10^{-20} J $Molecule^{-1}$
0	0	0	50	0.0201 (0.0002)	0 (0.0058)[a]
0.0140	4	1.5576	48.0885	0.0238 (0.00056)	-0.07 (0.0108)
0.0364	10	3.8921	45.2753	0.0375 (0.00031)	-0.256 (0.0058)
0.0522	14	5.4629	43.557	0.049 (0.0014)	-0.37 (0.013)
0.0772	20	7.7960	40.9102	0.072 (0.0013)	-0.525 (0.0088)
0.0947	24	9.3416	39.1712	0.095 (0.0017)	-0.639 (0.0087)
0.125	30	11.7079	35.9742	0.133 (0.0074)	-0.78 (0.023)
0.157	36	14.0397	33.0746	0.195 (0.0026)	-0.934 (0.0072)
0.1792	40	15.5052	31.1684	0.224 (0.0013)	-0.991 (0.0053)
0.2461	50	19.4303	26.1168	0.364 (0.0068)	-1.191 (0.0090)
0.2676	56	21.7905	25.6678	0.48 (0.028)	-1.30 (0.024)
0.3064	60	21.1045	20.9711	0.564 (0.0045)	-1.371 (0.0057)

[a] Calculated by standard propagation of errors

Table 5.11 Solvent effect data for N-chloroleucine decomposition in ethylene glycol-water binary cosolvent systems.

x2	Volume Percent (post mixing)	Weight of Organic /g	Weight of Water/g	k/min^{-1}	$\delta_m \Delta G^{\ddagger}$ $/10^{-20}$ J $Molecule^{-1}$
0	0	0	50	0.0201 (0.0002)	0 (0.0058)[a]
0.0195	6	3.2286	47.0839	0.023 (0.00049)	-0.055 (0.0097)
0.0334	10	5.4722	45.1333	0.0249 (0.00029)	-0.088 (0.0063)
0.0493	14	7.7042	43.1022	0.0258 (0.00038)	-0.103 (0.0073)
0.0733	20	10.9801	40.2977	0.0293 (0.00047)	-0.155 (0.0078)
0.1196	30	16.5448	35.3630	0.038 (0.0012)	-0.26 (0.014)
0.1721	40	21.9146	30.6075	0.0513 (0.00075)	-0.385 (0.0073)
0.1961	44	24.1382	28.7272	0.057 (0.002)	-0.43 (0.015)
0.2362	50	27.4154	25.7257	0.0686 (0.00021)	-0.505 (0.0043)
0.2811	56	30.7653	22.8401	0.078 (0.003)	-0.56 (0.016)
0.3125	60	32.8389	20.9738	0.085 (0.0033)	-0.59 (0.017)

[a] Calculated by standard propagation of errors

Table 5.12 Solvent effect data for N-chloroleucine decomposition in 2-propanol-water binary cosolvent systems.

x_2	Volume Percent (post mixing)	Weight of Organic /g	Weight of Water/g	k / min^{-1}	$\delta_m\Delta G^{\ddagger}$ / 10^{-20} J Molecule^{-1}
0	0	0	50	0.0201 (0.0002)	0 (0.0058)[a]
0.0096	4	1.5513	48.0614	0.022[b] (0.0012)	-0.04 (0.023)
0.0250	10	3.8686	45.3363	0.0264 (0.00032)	-0.112 (0.0064)
0.0362	14	5.4462	43.5269	0.0337 (0.0002)	-0.213 (0.0048)
0.0534	20	7.7113	40.9848	0.046 (0.0011)	-0.34 (0.011)
0.0730	26	10.0346	38.2269	0.0668 (0.00033)	-0.494 (0.0046)
0.0879	30	11.6706	36.309	0.095 (0.0033)	-0.64 (0.0149)
0.1288	40	15.5711	31.5901	0.161 (0.0015)	-0.856 (0.0056)
0.1786	50	19.4275	26.7862	0.227 (0.0047)	-0.997 (0.0094)
0.2446	56	23.5761	21.8279	0.27 (0.0099)	-1.07 (0.016)
0.2464	60	23.4263	21.4803	0.296 (0.0057)	-1.106 (0.0089)
0.2908	66	25.7740	18.8491	0.337 (0.006)	-1.159 (0.0084)

[a] Calculated by standard propagation of errors
b Average of duplicate experiments rather than triplicate

Table 5.13 Solvent effect data for N-chloroleucine decomposition in methanol-water binary cosolvent systems.

x_2	Volume Percent (post mixing)	Weight of Organic /g	Weight of Water/g	k/min^{-1}	$\delta_m\Delta G^{\ddagger}$ /10^{-20} J Molecule^{-1}
0	0	0	50	0.0201 (0.0002)	0 (0.0058)[a]
0.0181	4	1.5766	48.0946	0.02104 (0.00006)	-0.019 (0.0043)
0.0463	10	3.9254	45.4443	0.0237 (0.00023)	-0.068 (0.0057)
0.0978	20	7.8535	40.7362	0.0316 (0.00022)	-0.186 (0.0050)
0.1556	30	11.8112	36.0494	0.043 (0.0017)	-0.31 (0.017)
0.2194	40	15.7439	31.4935	0.0608 (0.00071)	-0.455 (0.0063)
0.292	50	19.6204	26.7465	0.086 (0.0013)	-0.598 (0.0074)
0.342	56	22.0682	23.8754	0.0923 (0.00044)	-0.627 (0.0045)
0.3762	60	23.604	22.0004	0.112 (0.0056)	-0.71 (0.021)
0.4798	70	27.6051	16.8269	0.139 (0.0038)	-0.80 (0.012)

[a] Calculated by standard propagation of errors

5.3 Parameter estimates

In this section I have compiled the parameter estimates obtained by fitting the data to the one-step and two-step, cancellation approximation models, equations (1.64) and (1.63) respectively. The numbers in parentheses are standard deviations.

Table 5.14 The parameter estimates obtained by fitting the N-chloroalanine data to the one-step model, equation (1.64).

Solvent System	$\Delta gA^{\ddagger}$ / Å^2 Molecule-1	K_1
Methanol-Water	20.1 (0.97)	2.0 (0.22)
1-Propanol-Water	20.7 (0.42)	6.5 (0.36)
Ethanol-Water	27.6 (0.82)	2.9 (0.17)
2-Propanol-Water	28 (1.5)	4.3 (0.43)
Propylene-Glycol	32 (1.6)	3.9 (0.46)
Ethylene-Glycol	36.5 (0.50)	2.45 (0.088)
Acetonitrile-Water	43.4 (0.65)	3.5 (0.12)
Dioxane-Water	68 (1.9)	4.1 (0.21)

Table 5.15 The parameter estimates obtained by fitting the N-chloroalanine data to the two-step model, equation (1.63).

Solvent System	$\Delta gA^{\ddagger}$ / Å^2 Molecule^{-1}	K_1	K_2
Methanol-Water	16.8 (0.54)	2.8 (0.38)	3.1 (0.73)
2-Propanol-Water	20.6 (0.44)	5.9 (0.50)	11 (1.6)
1-Propanol-Water	22 (1.1)	13.0 (0.98)	3.2 (0.89)
Ethanol-Water	23.8 (0.82)	5.7 (0.25)	2.8 (0.45)
Propylene-Glycol	27 (1.1)	5.2 (0.84)	6 (1.6)
Ethylene-Glycol	34.8 (0.45)	4.4 (0.16)	1.7 (0.14)
Acetonitrile-Water	42. (1.8)	7.0 (0.25)	2.0 (0.36)
Dioxane-Water	55 (2.4)	8.9 (0.25)	4.3 (0.72)

Table 5.16 The parameter estimates obtained by fitting t
N-chloroleucine data to the one-step model, equation (1.6

Solvent System	$\Delta gA^{\ddagger}$ / Å^2 Molecule-1	K_1
Methanol-Water	27 (2.0)	1.8 (0.25)
2-Propanol-Water	35 (2.7)	5.1 (0.85)
Acetonitrile-Water	50 (1.6)	3.9 (0.24)
Ethylene Glycol-Water	54 (4.0)	2.0 (0.23)

Table 5.17 The parameter estimates obtained by fitting t
N-chloroleucine data to the two-step model, equation (1.6

Solvent System	$\Delta gA^{\ddagger}$ / Å^2 Molecule-1	K_1	K_2
Methanol-Water	19.3 (0.81)	2.5 (0.39)	4 (1.2)
2-Propanol-Water	24.2 (0.45)	2.7 (0.91)	40 (16)
Ethylene Glycol-Water	38 (3.1)	4.4 (0.33)	3.2 (0.97)
Acetonitrile-Water	43 (2.2)	7.5 (0.46)	3.9 (0.92)

5.4 Curve-Fits

Plots of the solvent effect on the free energy of activation as a function of the mole fraction of organic cosolvent are presented in this section. The solid line in these plots represents the curve fits to the one-step or two-step phenomenological model. The curve fits indicate that the two-step model can fit all the data and the one-step model can fit most, but not all, of the systems.

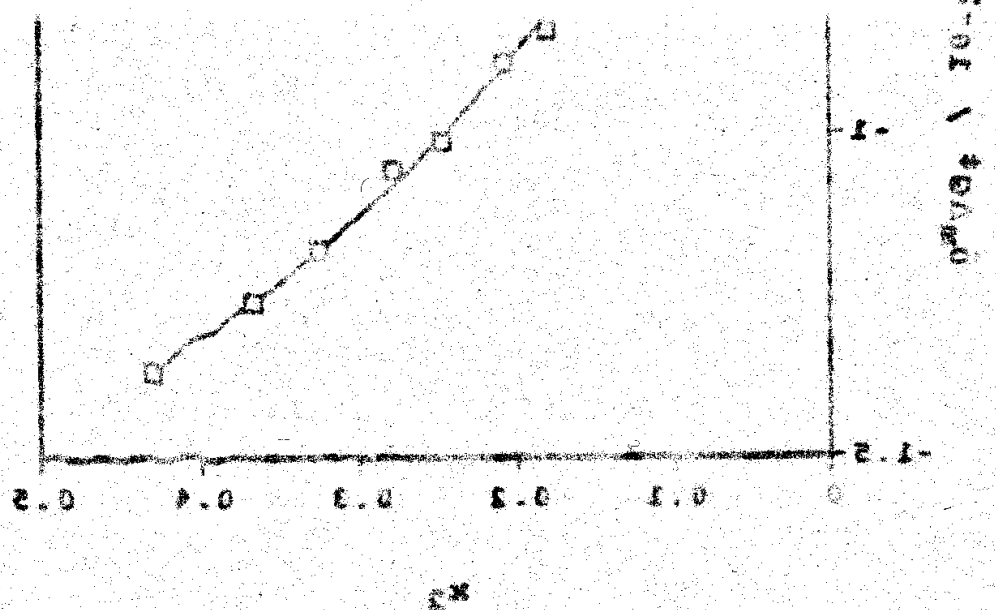

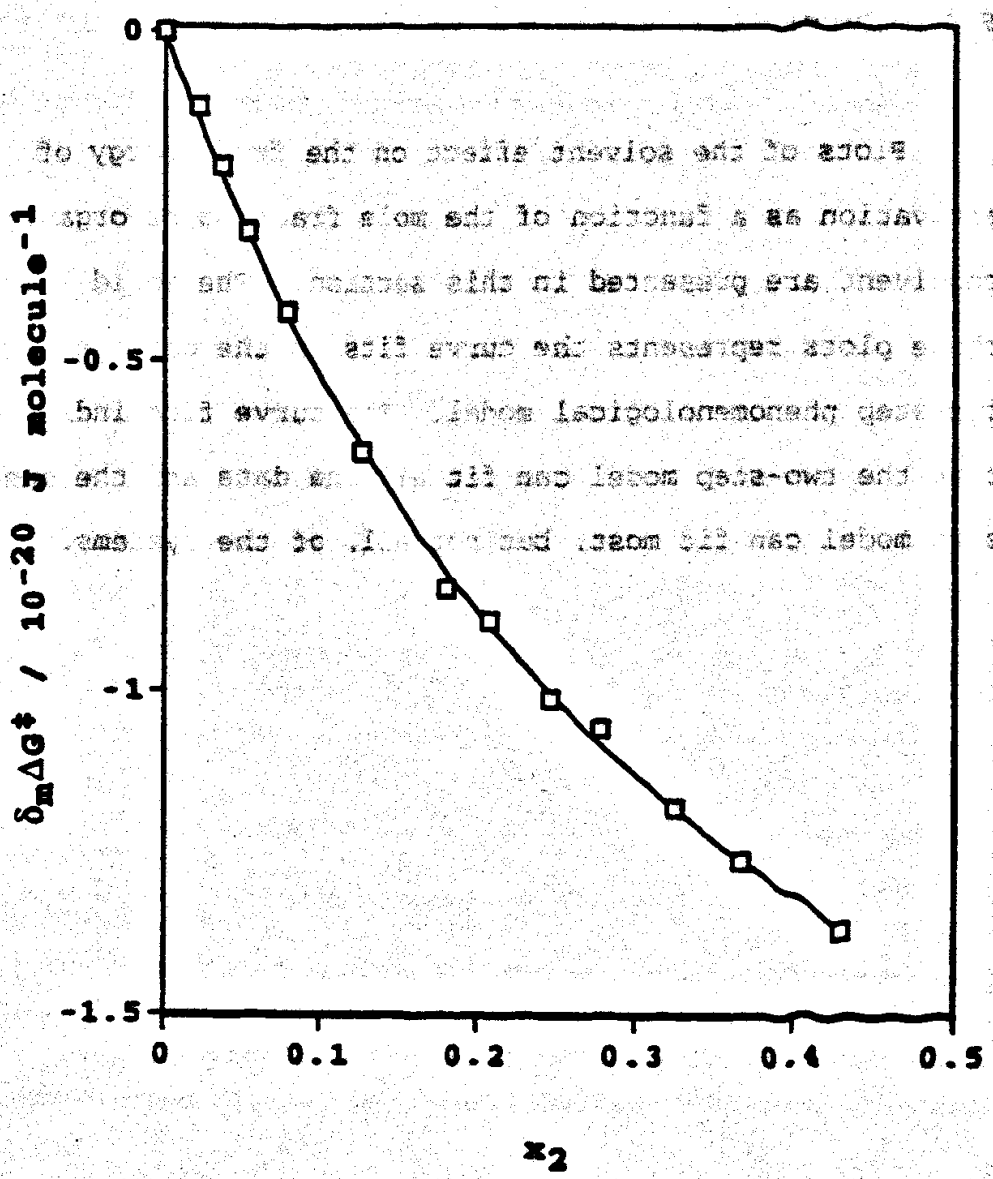

Figure 5.4 Solvent effect on the decomposition of N-chloroalanine in the acetonitrile-water binary cosolvent system showing the experimental data points and the curve fit to the data with the one-step, cancellation approximation phenomenological model (equation 1.64).

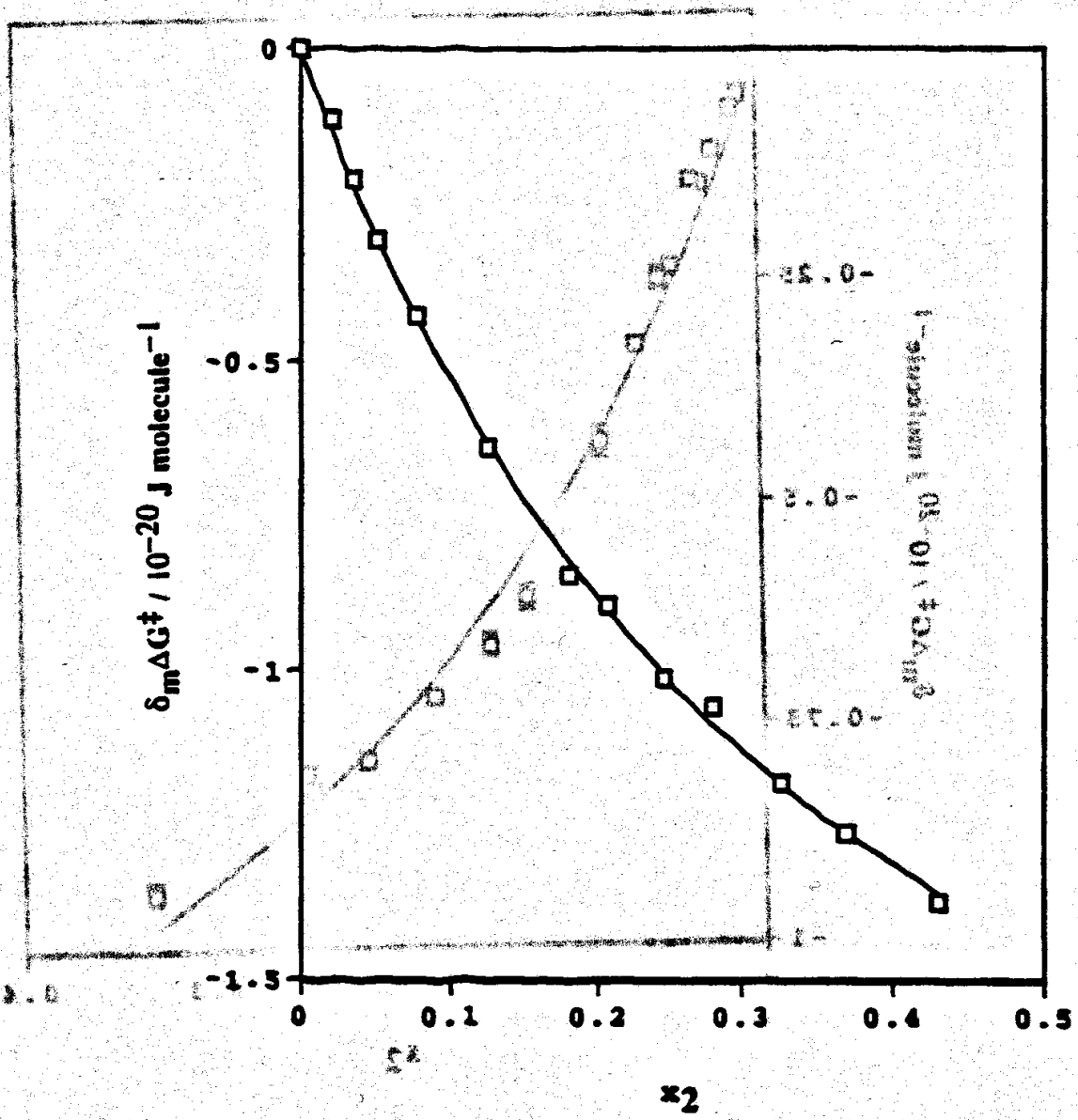

Figure 5.5 Solvent effect on the decomposition of N-chloroalanine in the acetonitrile-water binary cosolvent system showing the experimental data points and the curve fit to the data with the two-step, cancellation approximation phenomenological model (equation 1.63).

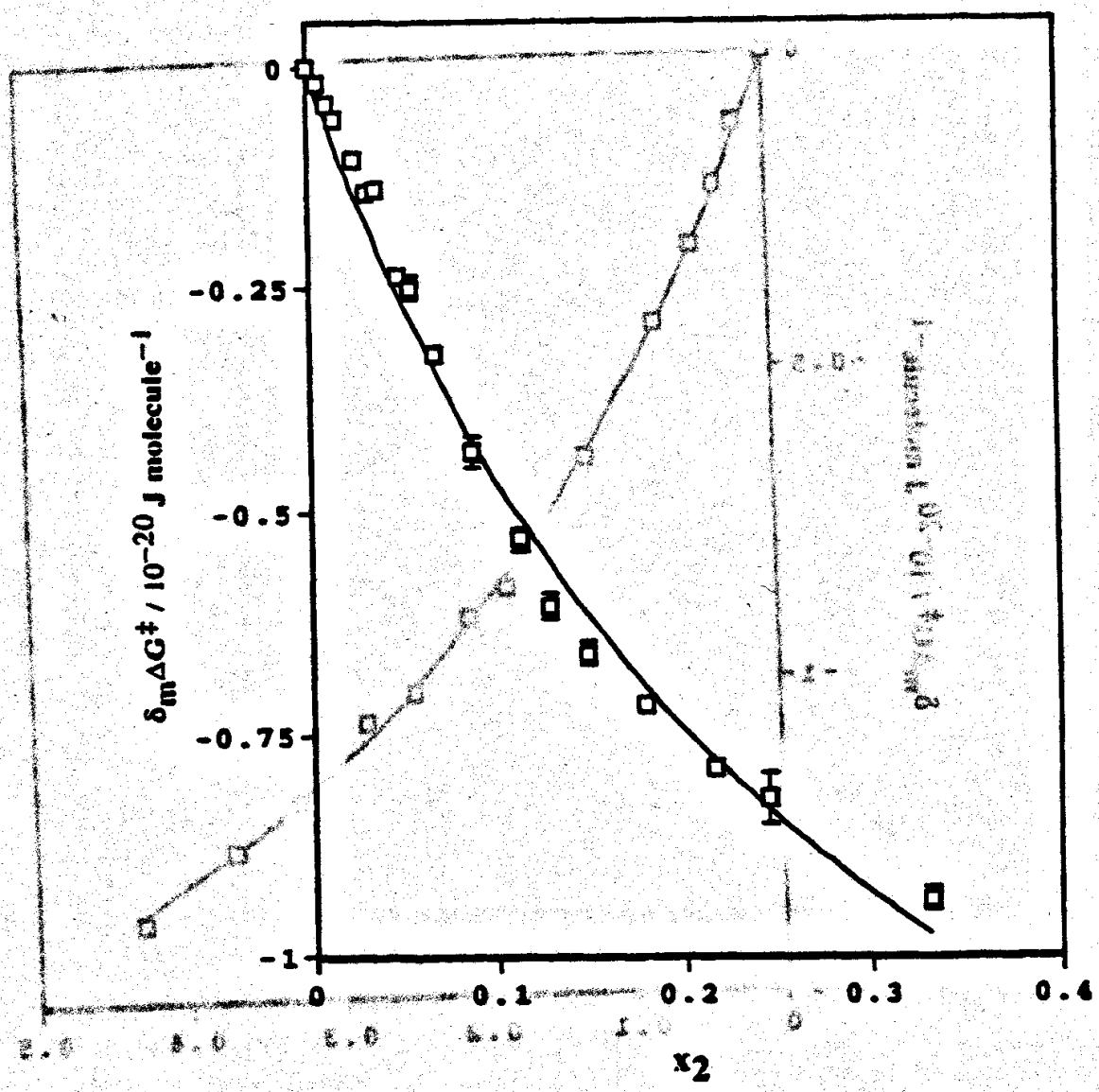

Figure 5.6 Solvent effect on the decomposition of N-chloroalanine in the 2-propanol-water binary cosolvent system showing the experimental data points and the curve fit to the data with the one-step, cancellation approximation phenomenological model (equation 1.64).

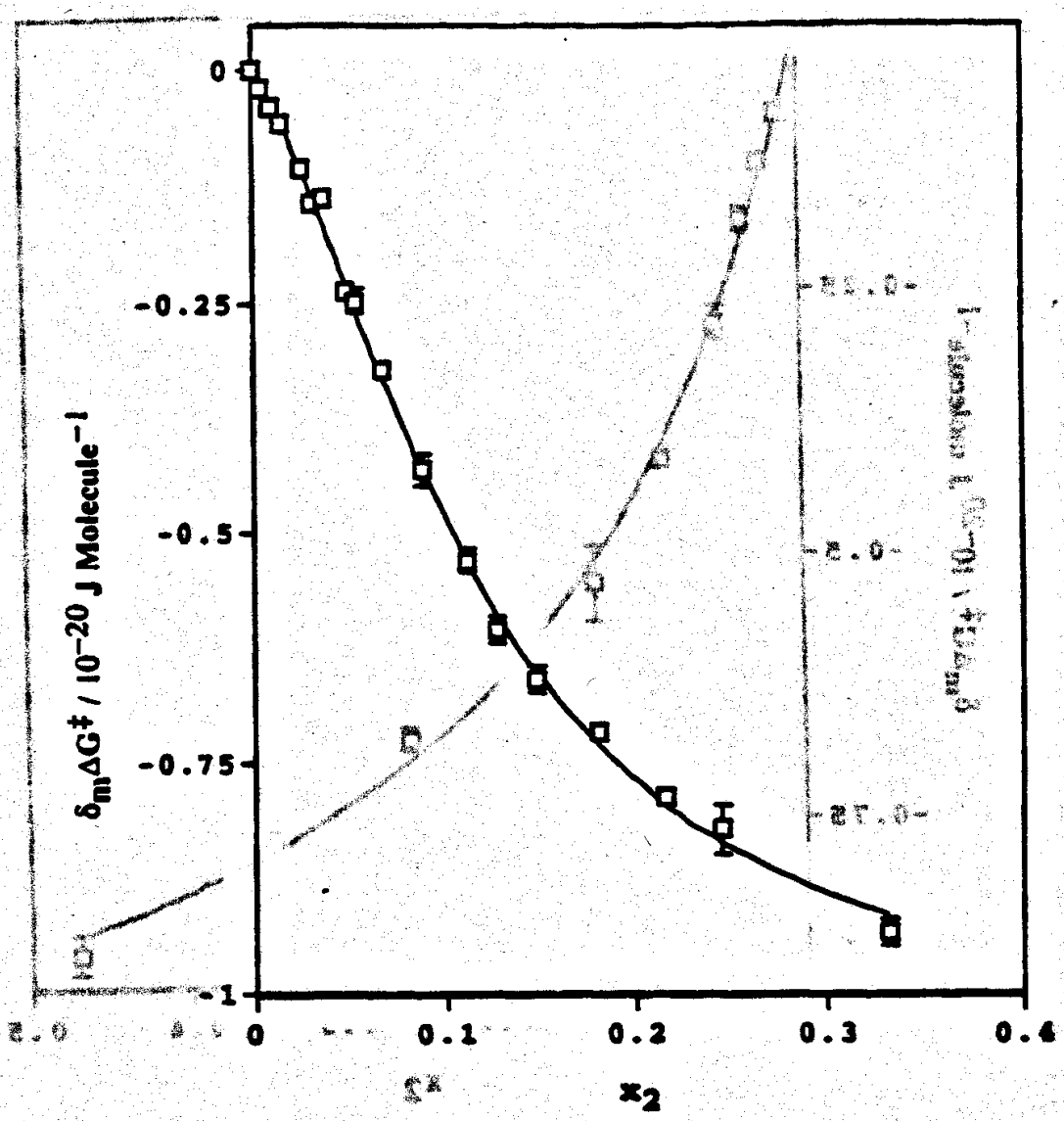

Figure 5.7 Solvent effect on the decomposition of N-chloroalanine in the 2-propanol-water binary cosolvent system showing the experimental data points and the curve fit to the data with the two-step, cancellation approximation phenomenological model (equation 1.63).

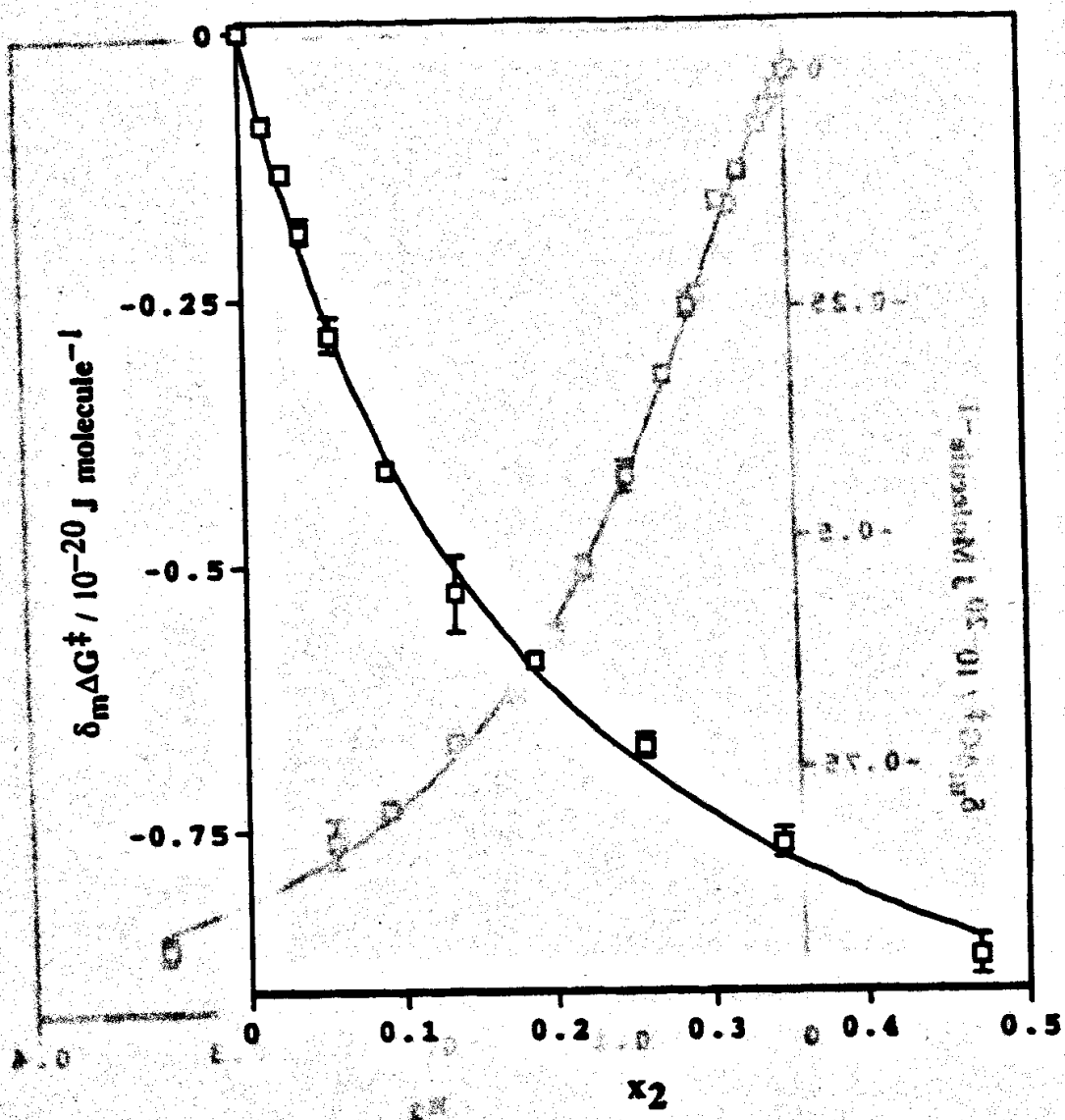

Figure 5.8 Solvent effect on the decomposition of N-chloroalanine in the 1-propanol-water binary cosolvent system showing the experimental data points and the curve fit to the data with the one-step, cancellation approximation phenomenological model (equation 1.64).

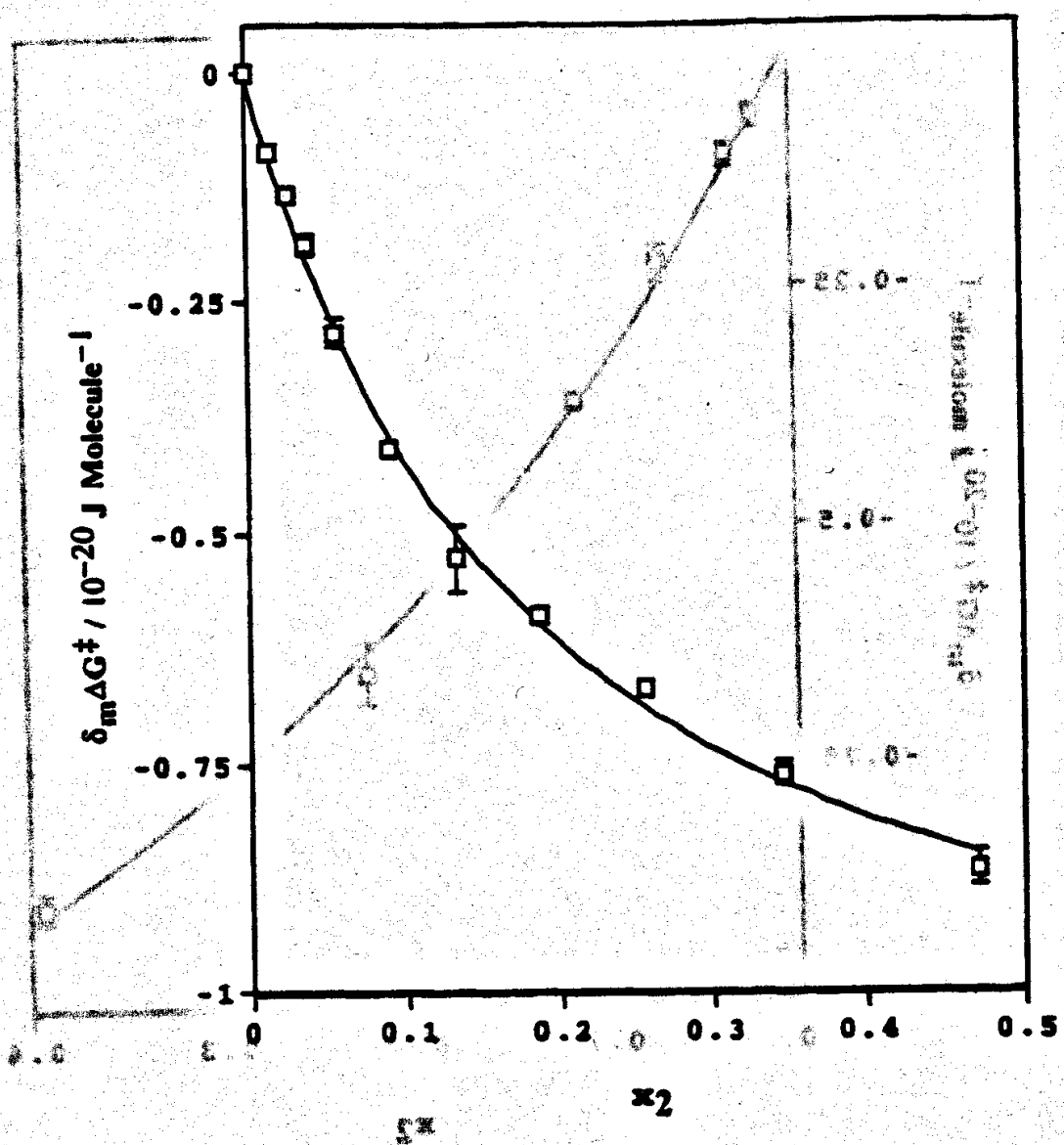

Figure 5.9 Solvent effect on the decomposition of N-chloroalanine in the 1-propanol-water binary cosolvent system showing the experimental data points and the curve fit to the data with the two-step, cancellation approximation phenomenological model (equation 1.63).

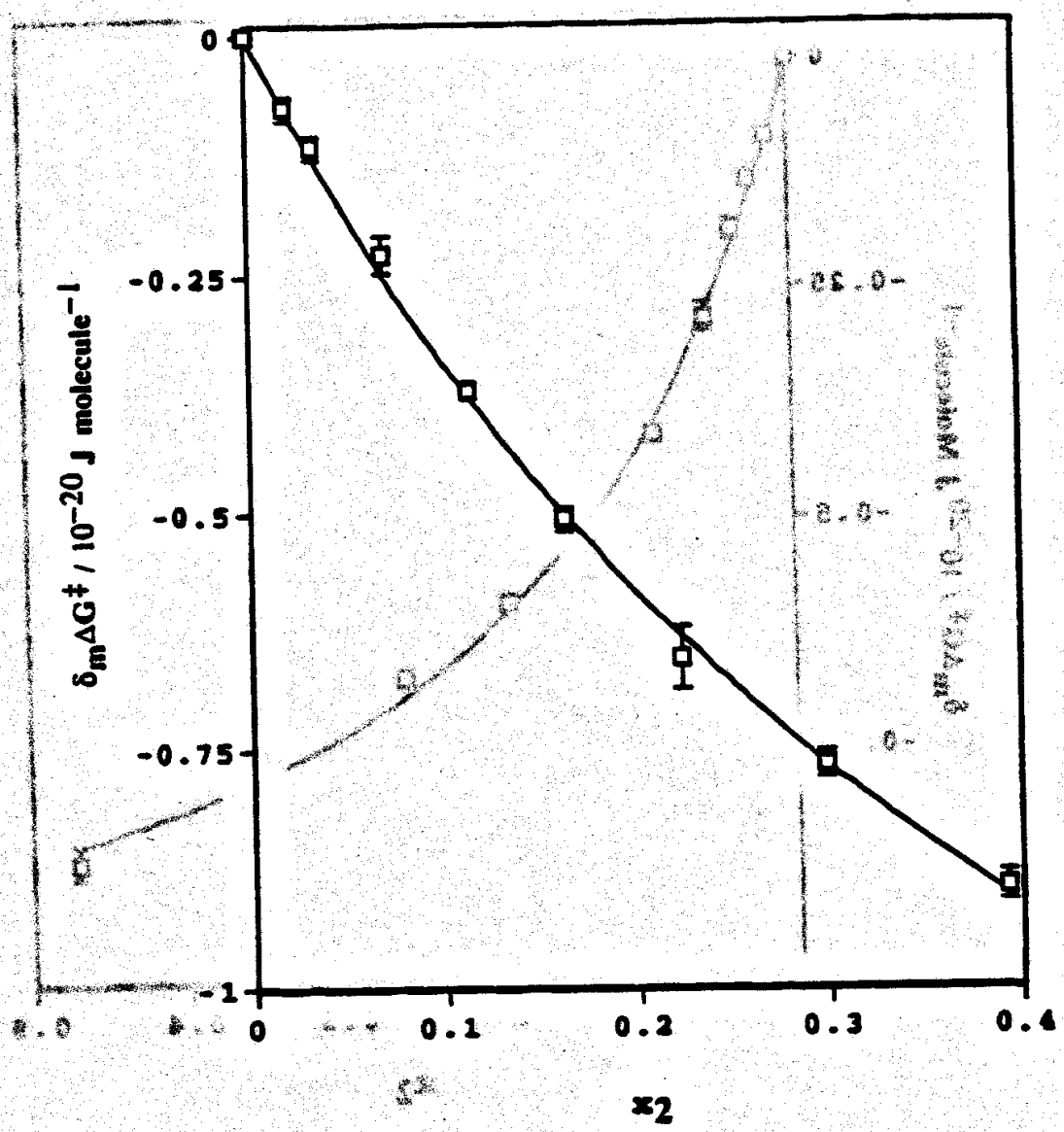

Figure 5.10 Solvent effect on the decomposition of N-chloroalanine in the ethanol-water binary cosolvent system showing the experimental data points and the curve fit to the data with the one-step, cancellation approximation phenomenological model (equation 1.64).

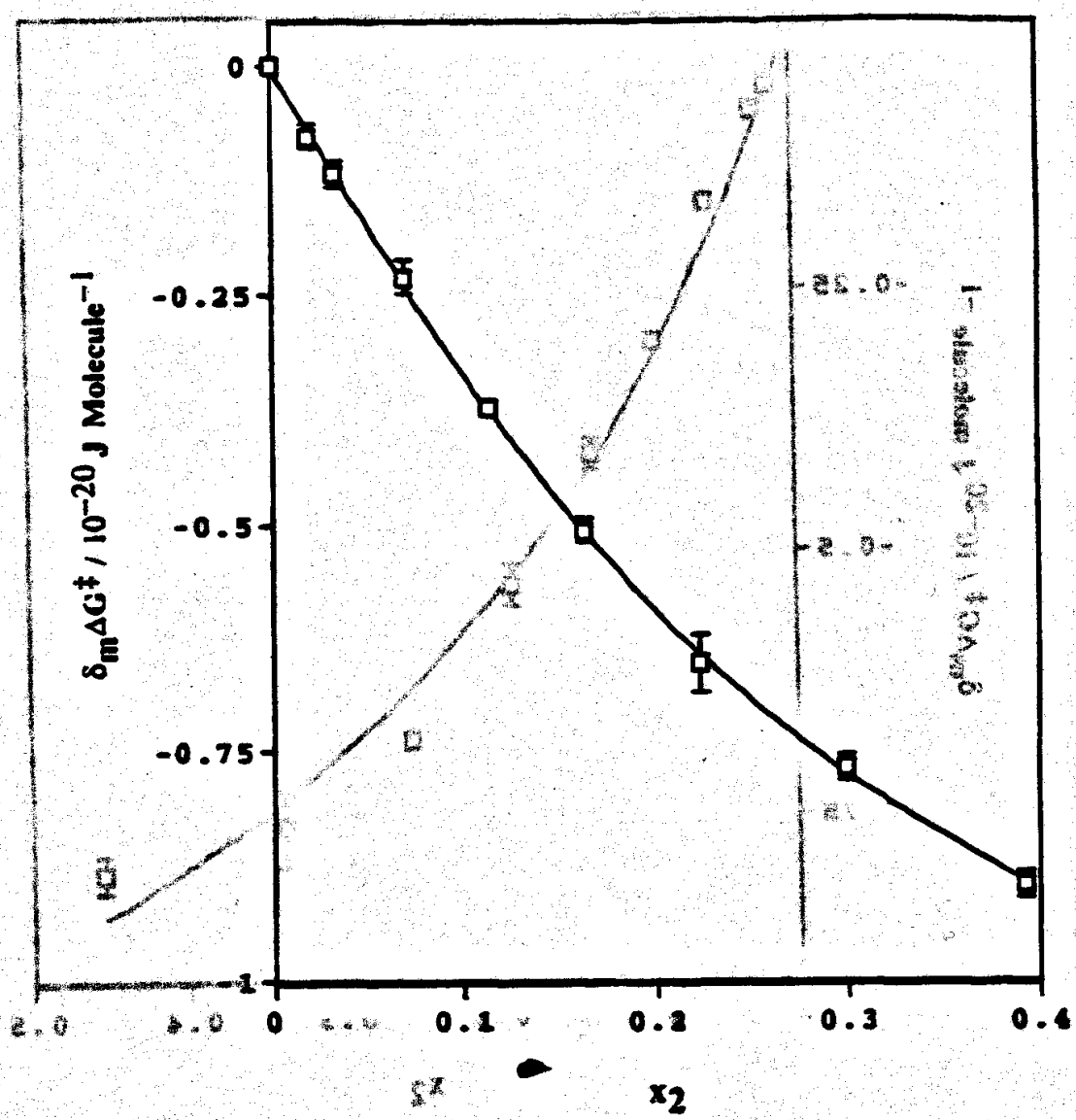

Figure 5.11 Solvent effect on the decomposition of N-chloroalanine in the ethanol-water binary cosolvent system showing the experimental data points and the curve fit to the data with the two-step, cancellation approximation phenomenological model (equation 1.63).

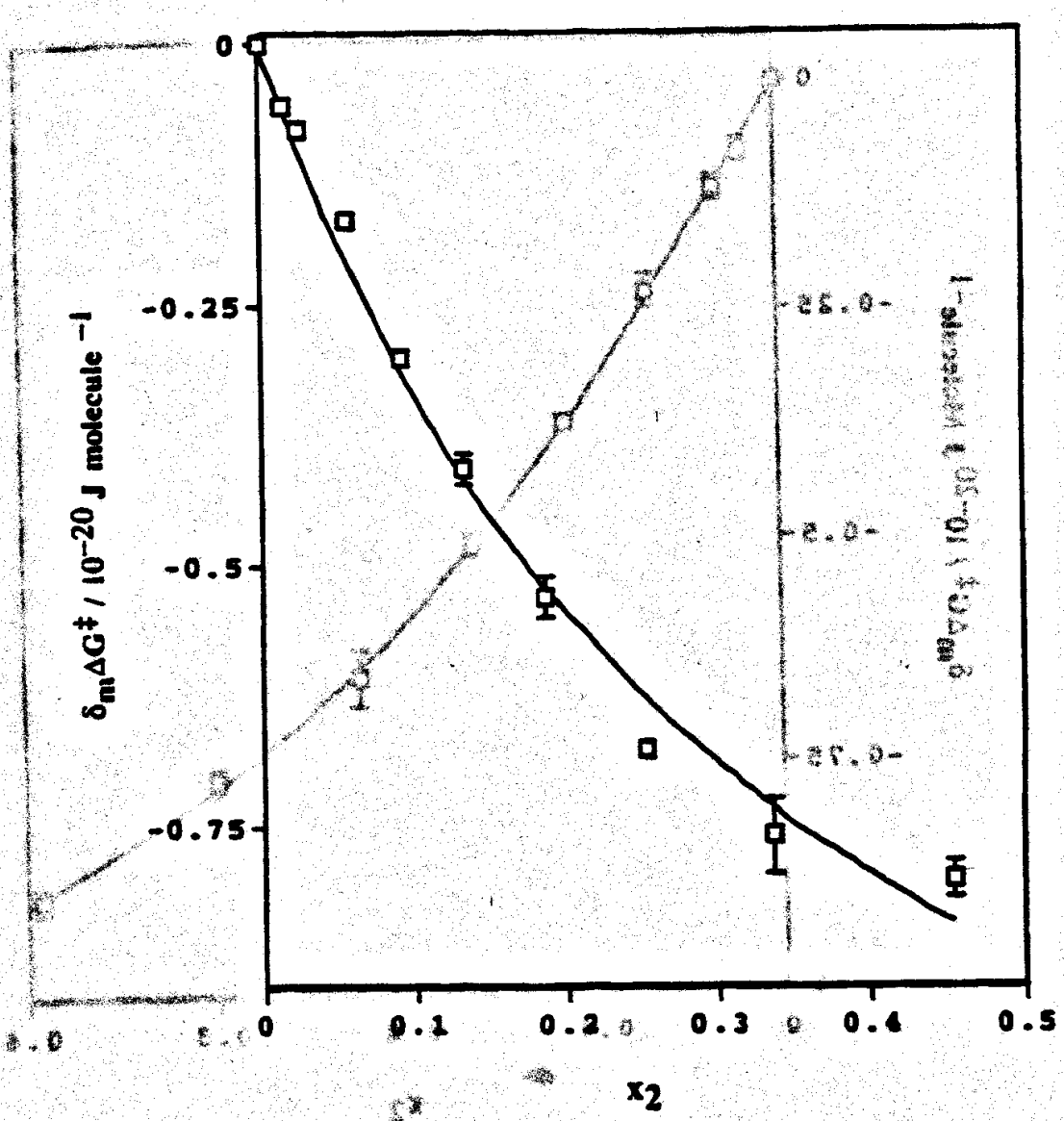

Figure 5.12 Solvent effect on the decomposition of N-[illegible] chloroalanine in the propylene glycol-water binary cosolvent system showing the experimental data points and the curve fit to the data with the one-step, cancellation [illegible] approximation phenomenological model (equation 1.64).

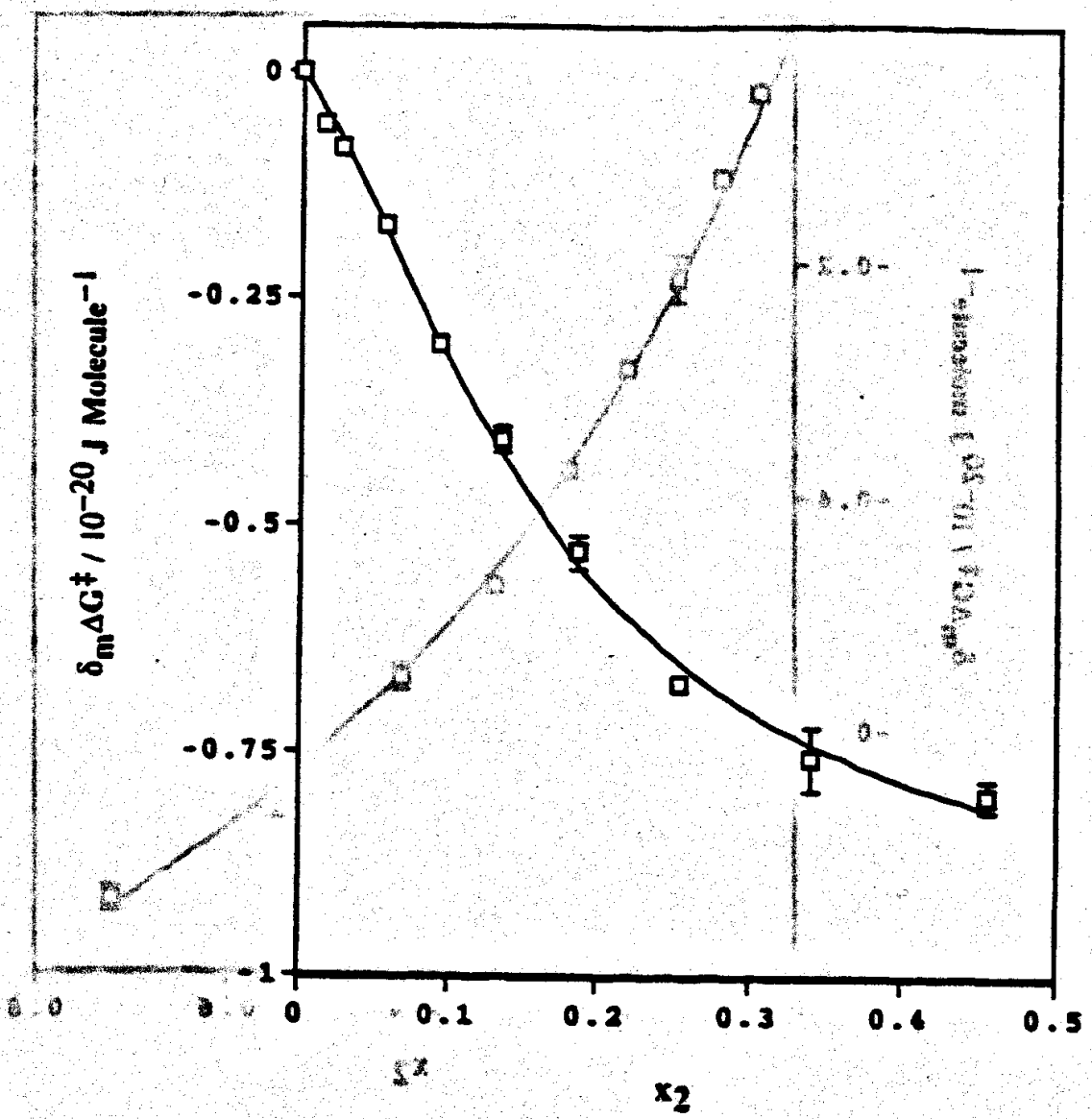

Figure 5.13 Solvent effect on the decomposition of N-chloroalanine in the propylene glycol-water binary cosolvent system showing the experimental data points and the curve fit to the data with the two-step, cancellation approximation phenomenological model (equation 1.63).

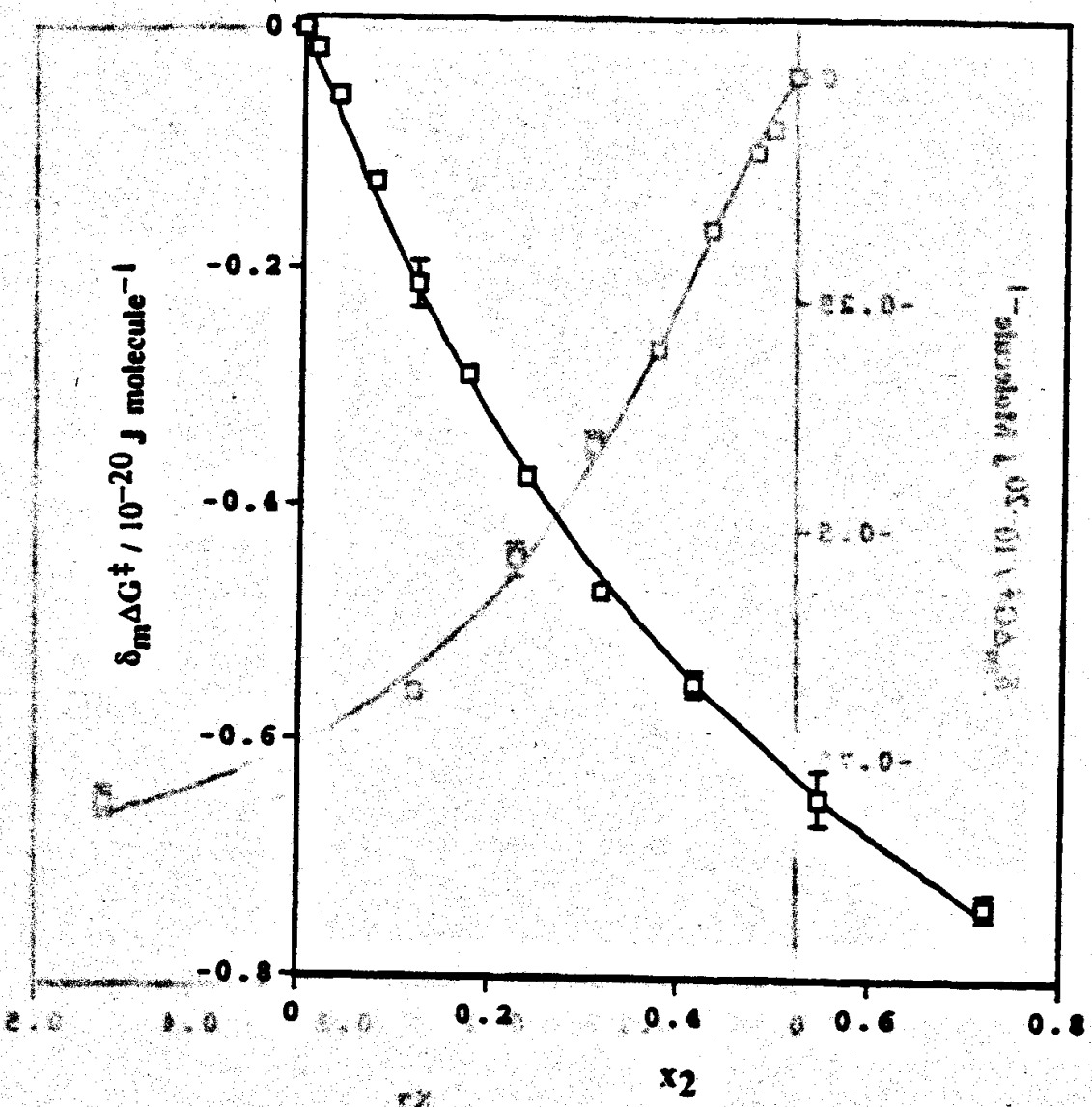

Figure 5.14 Solvent effect on the decomposition of N-chloroalanine in the ethylene glycol-water binary cosolvent system showing the experimental data points and the curve fit to the data with the one-step, cancellation approximation phenomenological model (equation 1.64).

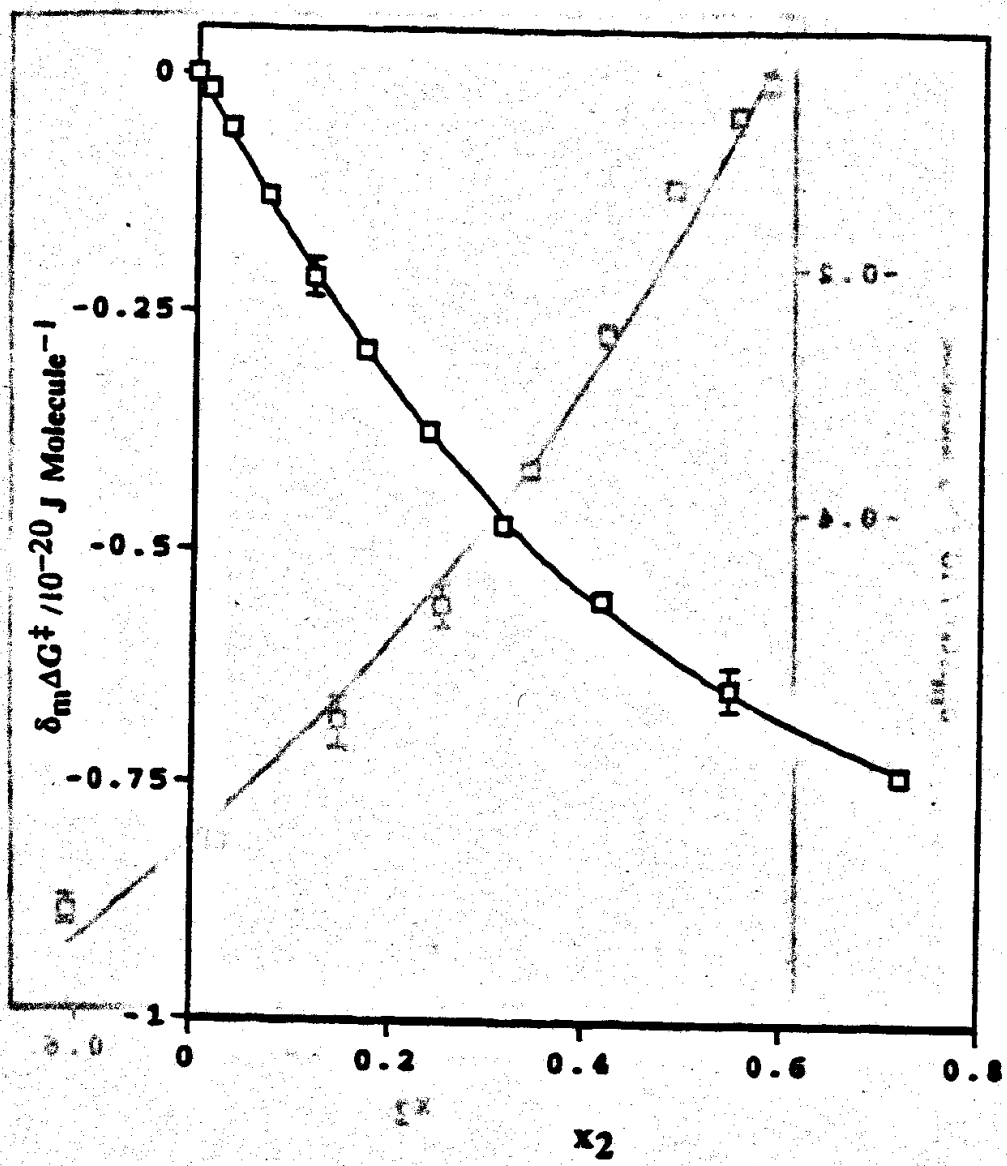

Figure 5.15 Solvent effect on the decomposition of N-chloroalanine in the ethylene glycol-water binary cosolvent system showing the experimental data points and the curve fit to the data with the two-step, cancellation approximation phenomenological model (equation 1.63).

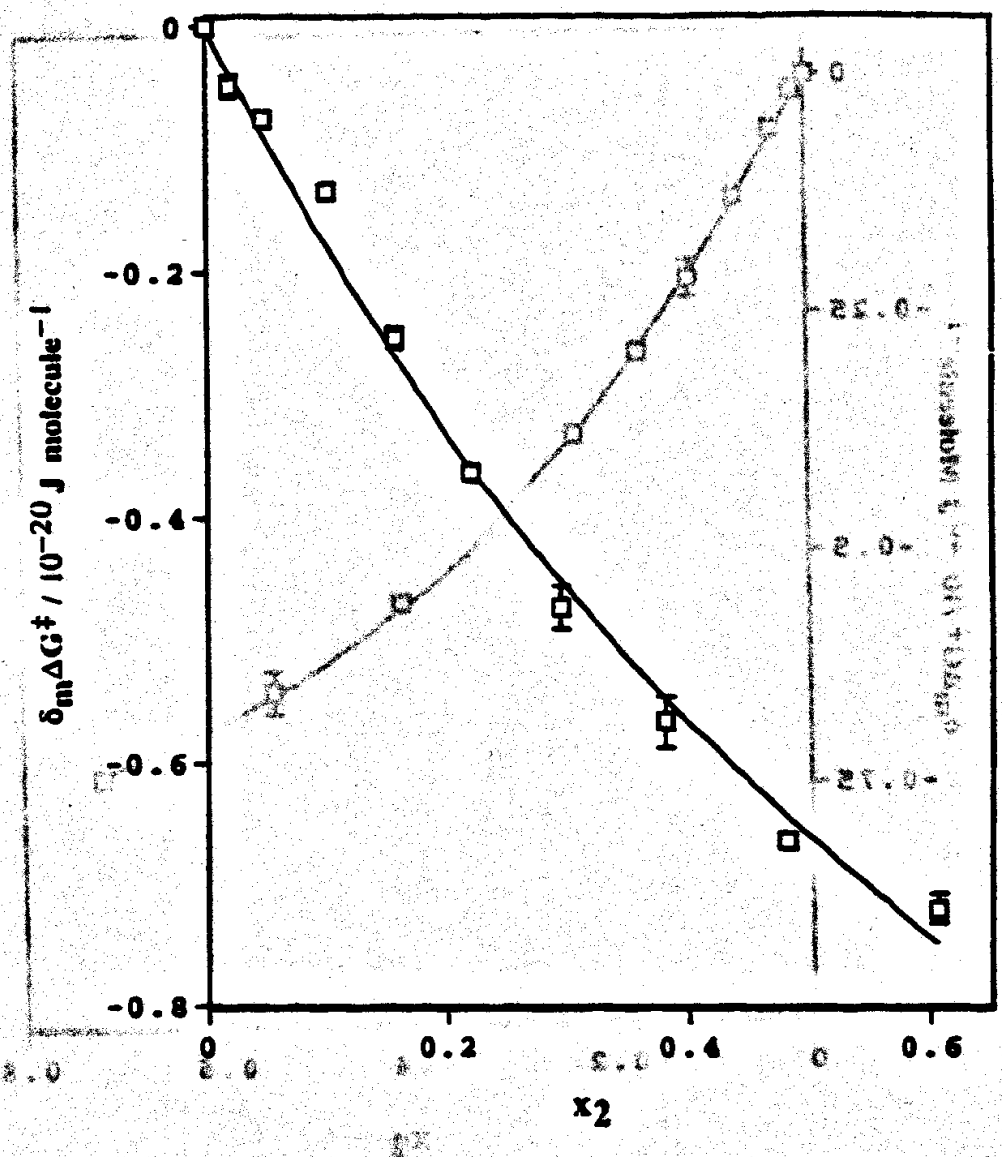

Figure 5.16 Solvent effect on the decomposition of N-chloroalanine in the methanol-water binary cosolvent system showing the experimental data points and the curve fit to the data with the one-step, cancellation approximation phenomenological model (equation 1.64).

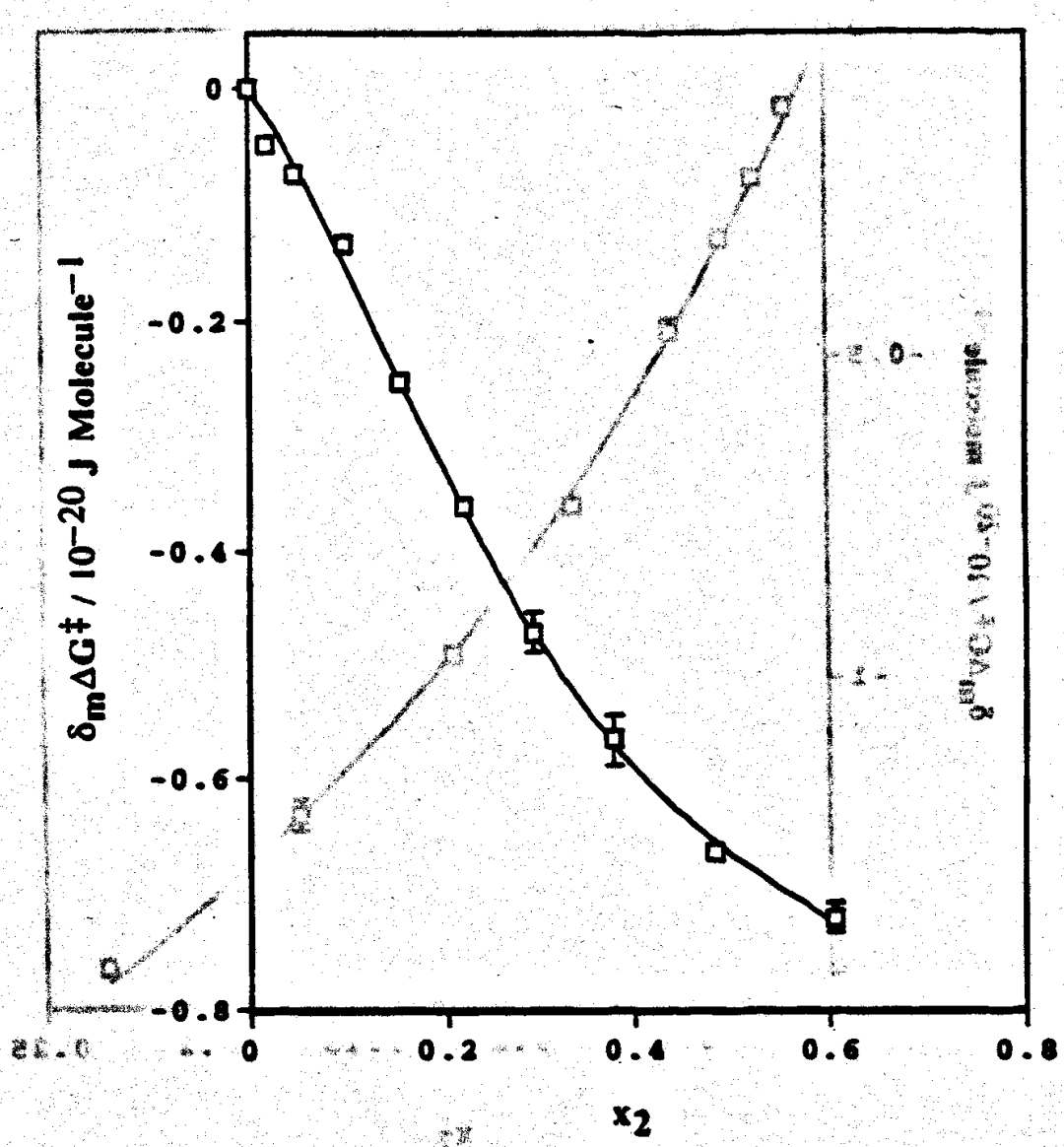

Figure 5.17 Solvent effect on the decomposition of N-chloroalanine in the methanol-water binary cosolvent system showing the experimental data points and the curve fit to the data with the two-step, cancellation approximation phenomenological model (equation 1.63).

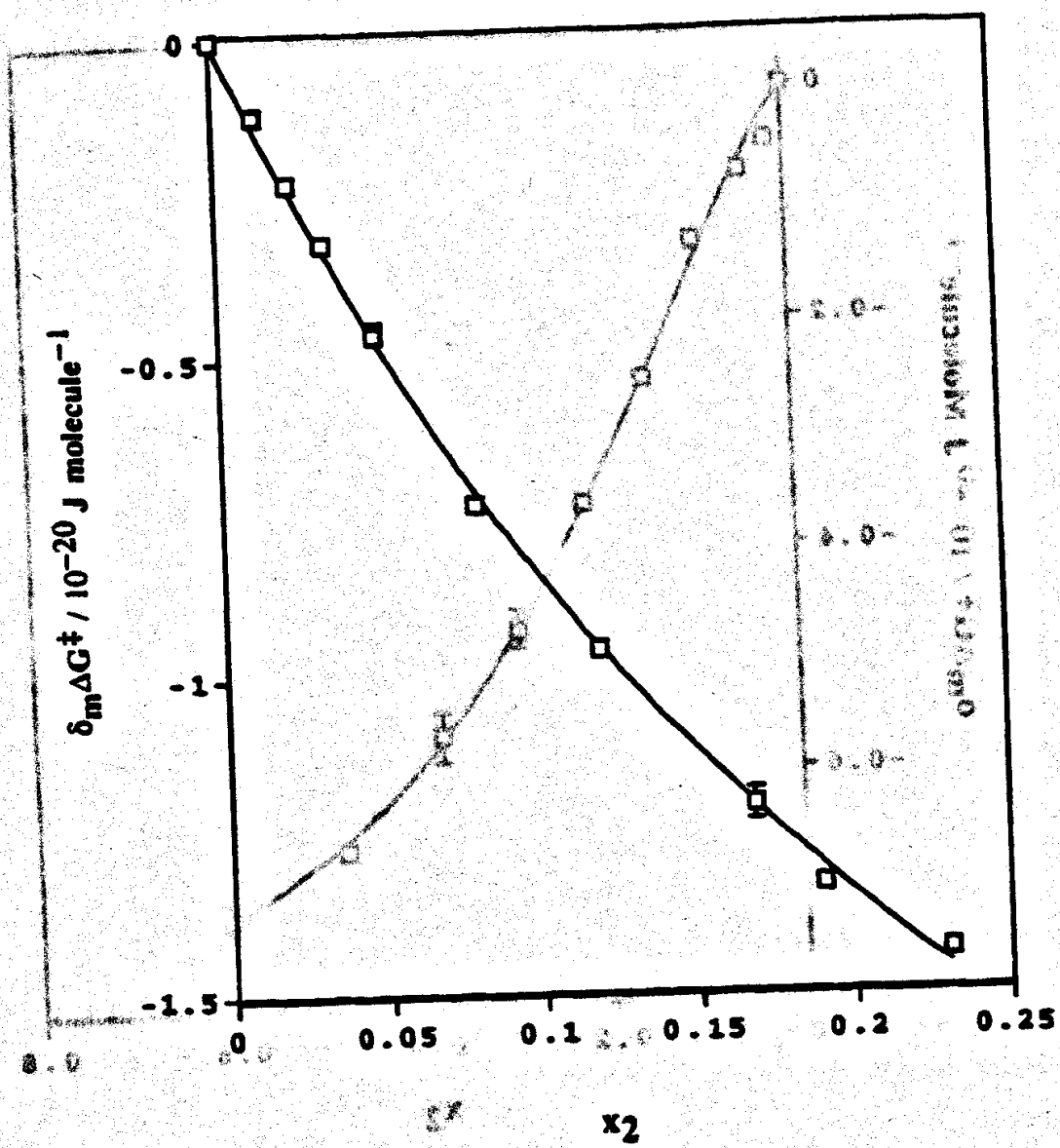

Figure 5.18 Solvent effect on the decomposition of N-chloroalanine in the dioxane-water binary cosolvent system showing the experimental data points and the curve fit to the data with the one-step, cancellation approximation phenomenological model (equation 1.64).

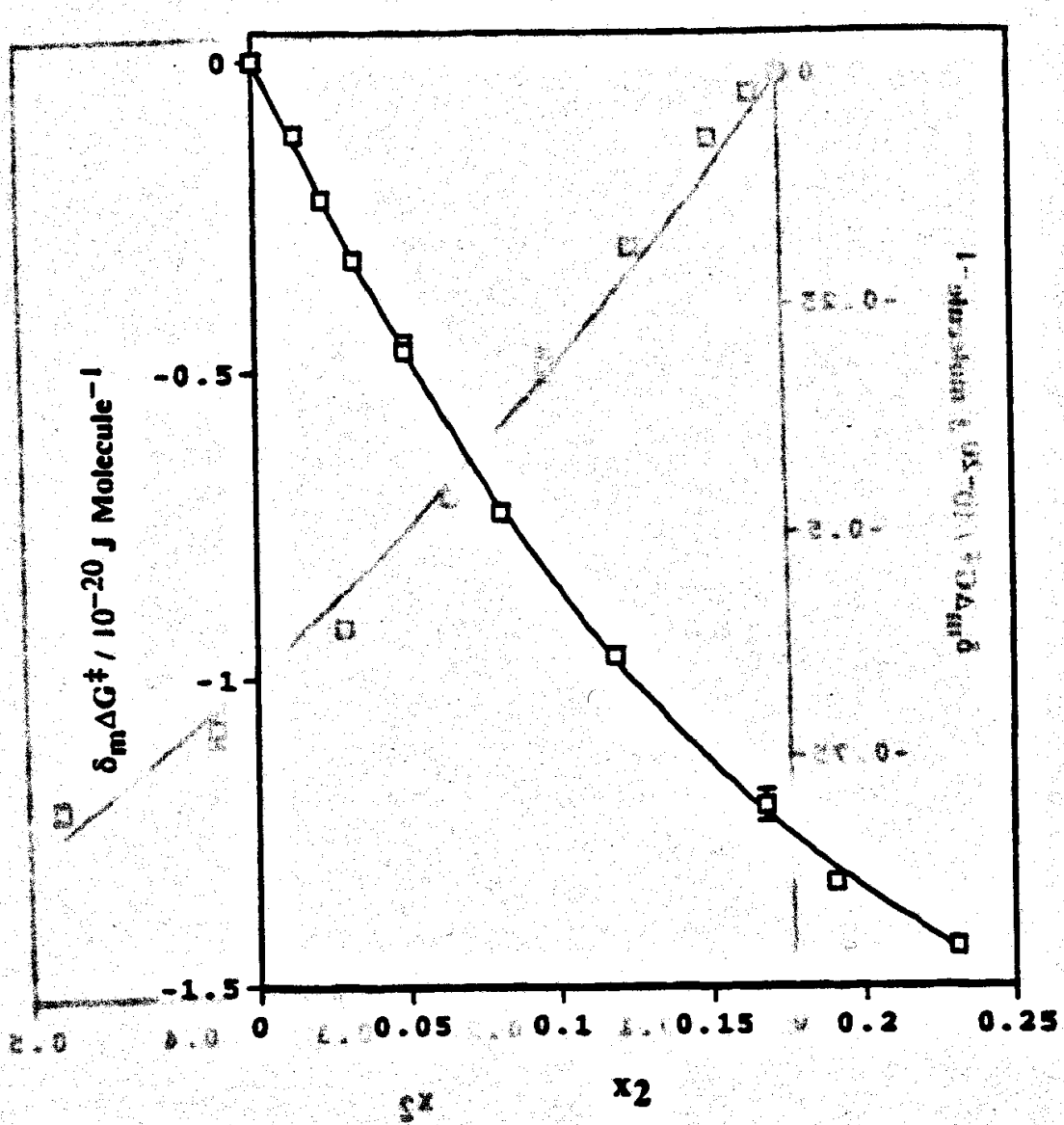

Figure 5.19 Solvent effect on the decomposition of N-chloroalanine in the dioxane-water binary cosolvent system showing the experimental data points and the curve fit to the data with the two-step, cancellation approximation phenomenological model (equation 1.63).

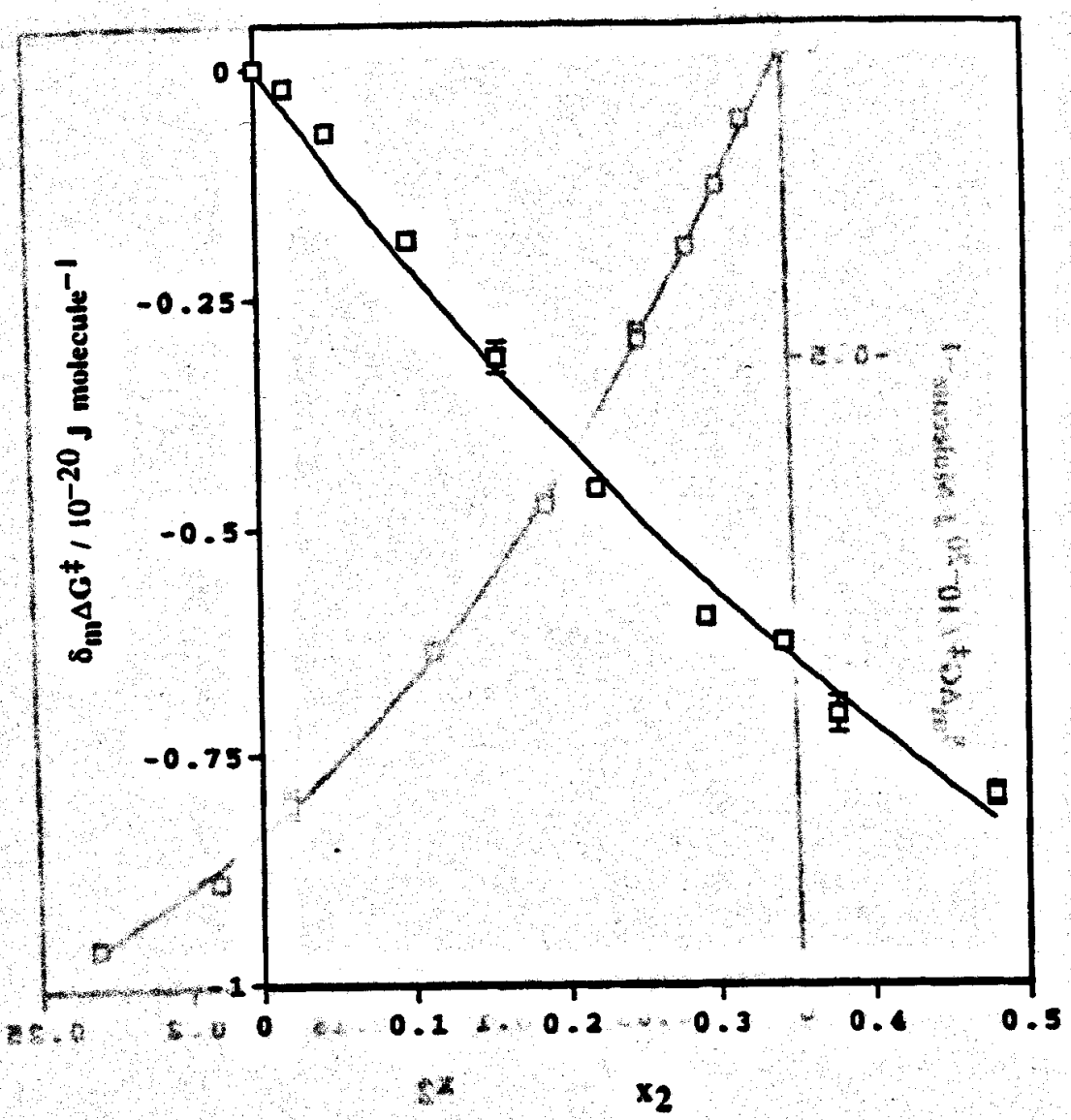

Figure 5.20 Solvent effect on the decomposition of N-chloroleucine in the methanol-water binary cosolvent system showing the experimental data points and the curve fit to the data with the one-step, cancellation approximation phenomenological model (equation 1.64).

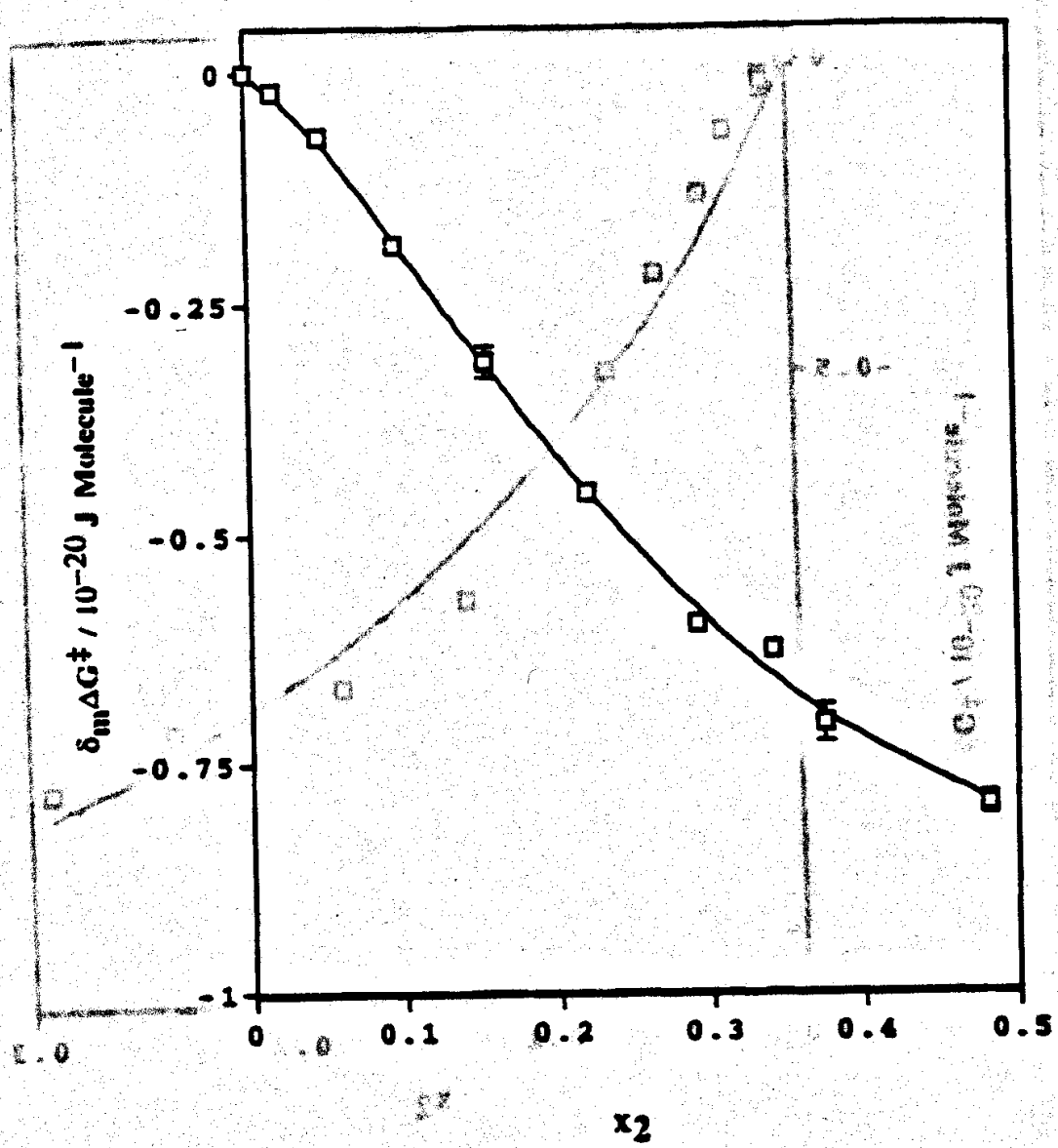

Figure 5.21 Solvent effect on the decomposition of N-chloroleucine in the methanol-water binary cosolvent system showing the experimental data points and the curve fit to the data with the two-step, cancellation approximation phenomenological model (equation 1.63).

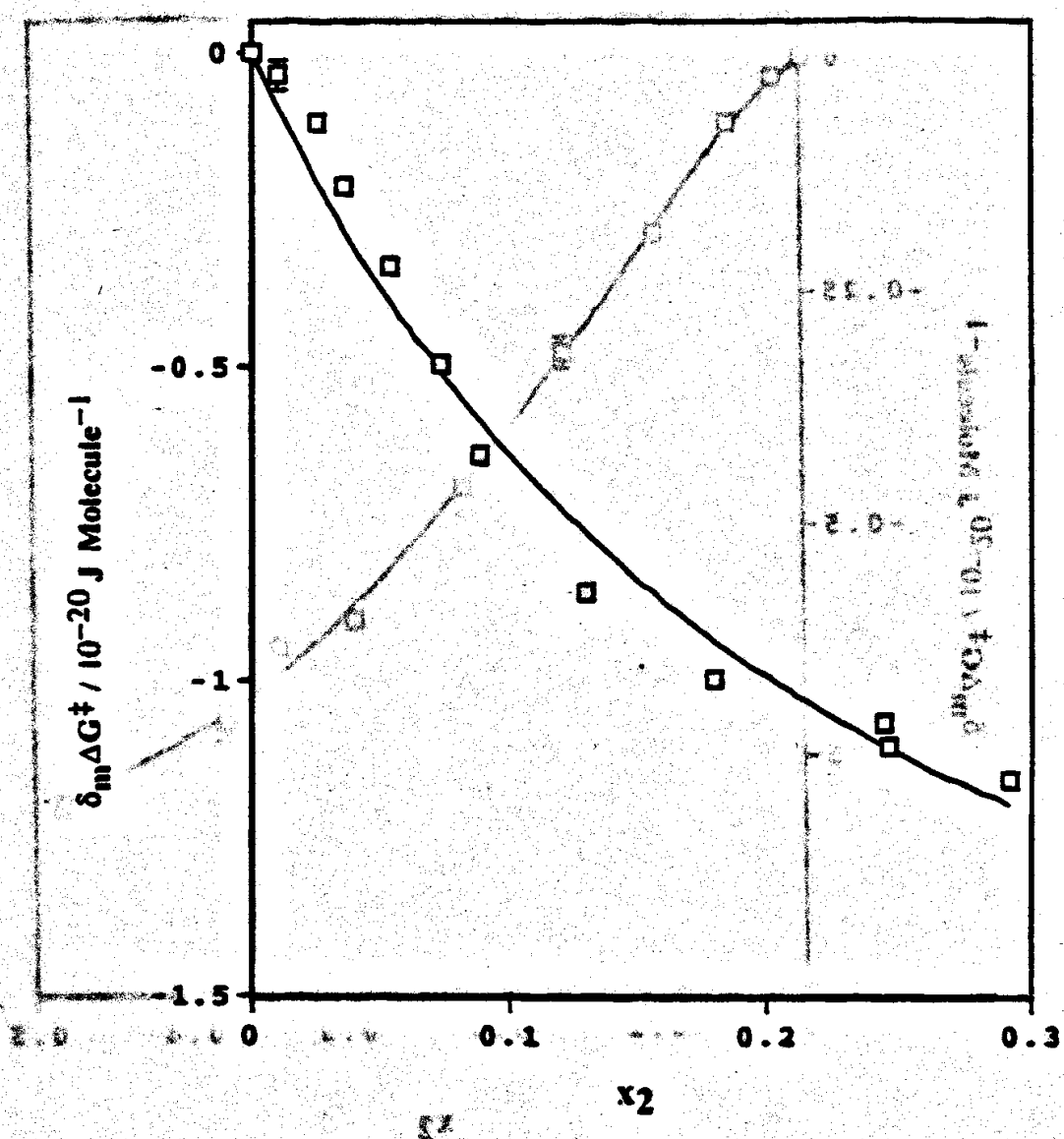

Figure 5.22 Solvent effect on the decomposition of N-chloroleucine in the 2-propanol-water binary cosolvent system showing the experimental data points and the curve fit to the data with the one-step, cancellation approximation phenomenological model (equation 1.64).

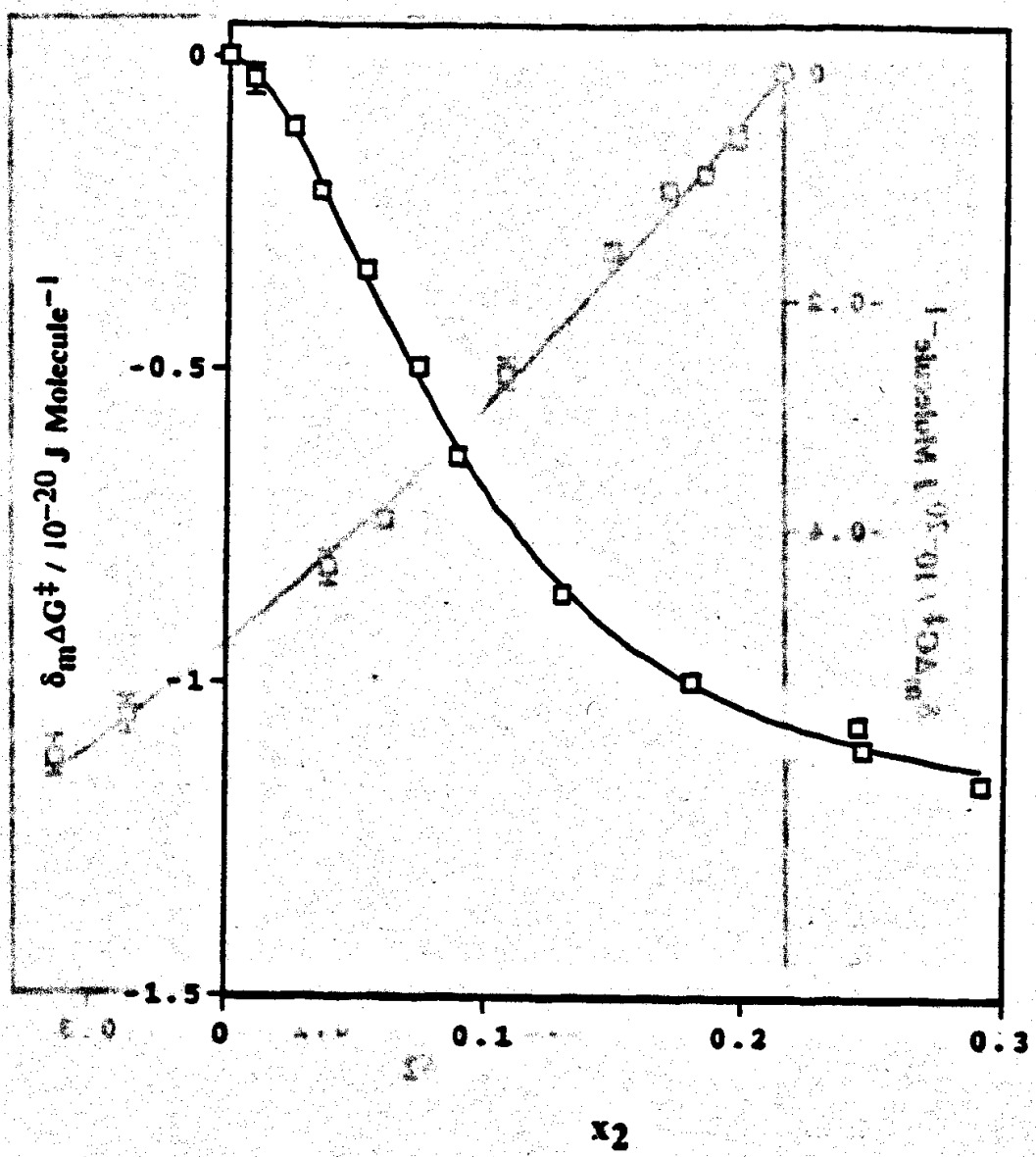

Figure 5.23 Solvent effect on the decomposition of N-chloroleucine in the 2-propanol-water binary cosolvent system showing the experimental data points and the curve fit to the data with the two-step, cancellation approximation phenomenological model (equation 1.63).

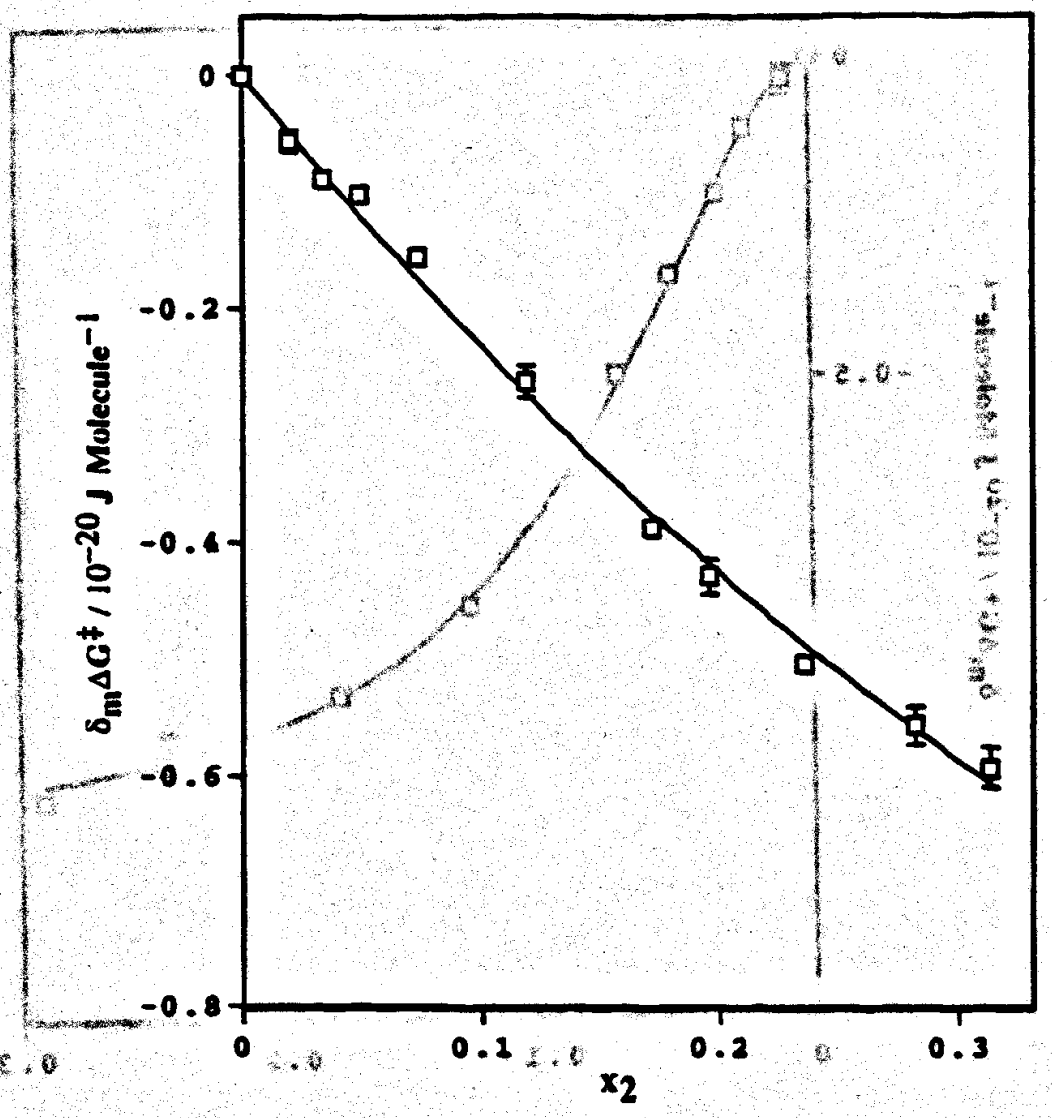

Figure 5.24 Solvent effect on the decomposition of N-chloroleucine in the ethylene glycol-water binary cosolvent system showing the experimental data points and the curve fit to the data with the one-step, cancellation approximation phenomenological model (equation 1.64).

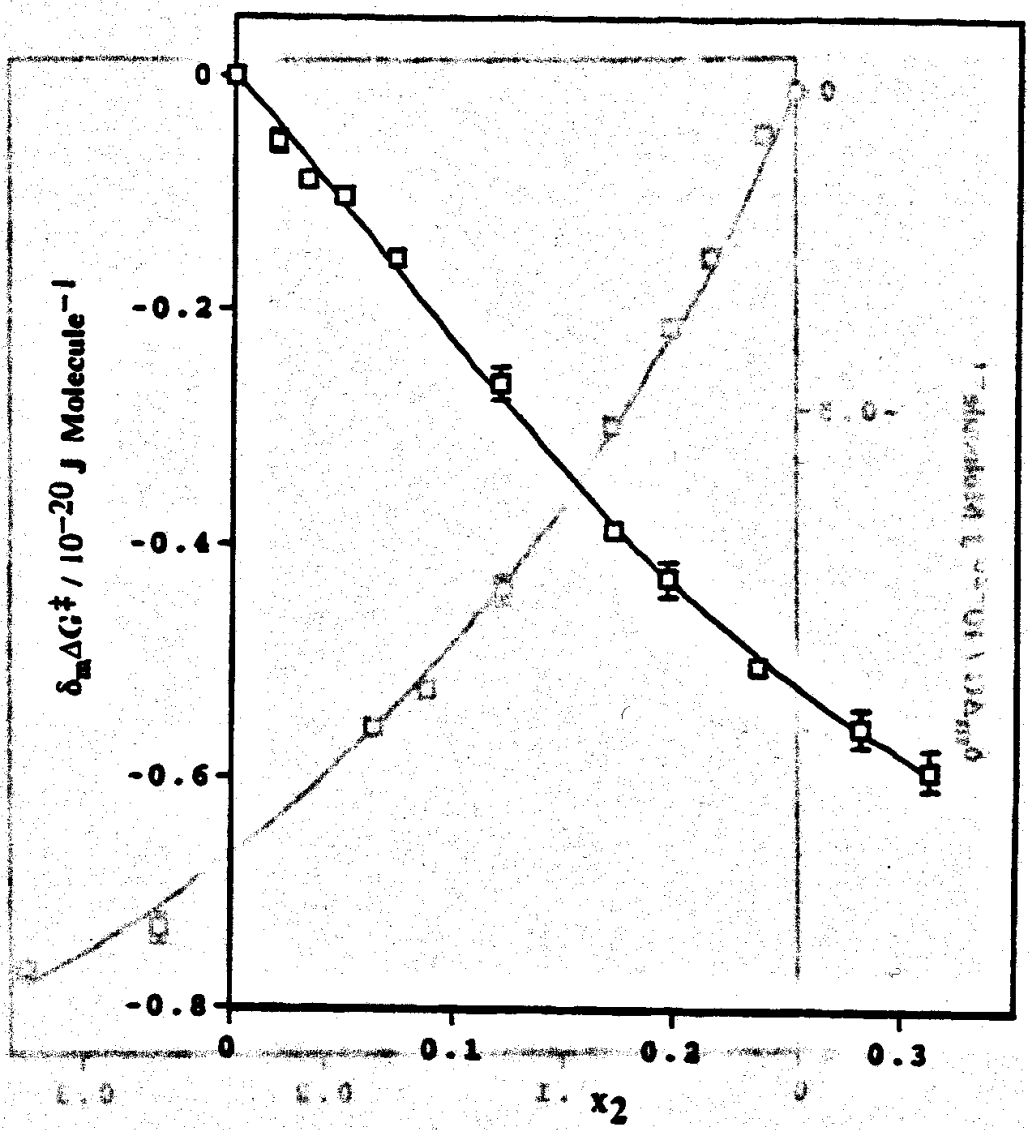

Figure 5.25 Solvent effect on the decomposition of N-chloroleucine in the ethylene glycol-water binary cosolvent system showing the experimental data points and the curve fit to the data with the two-step, cancellation approximation phenomenological model (equation 1.63).

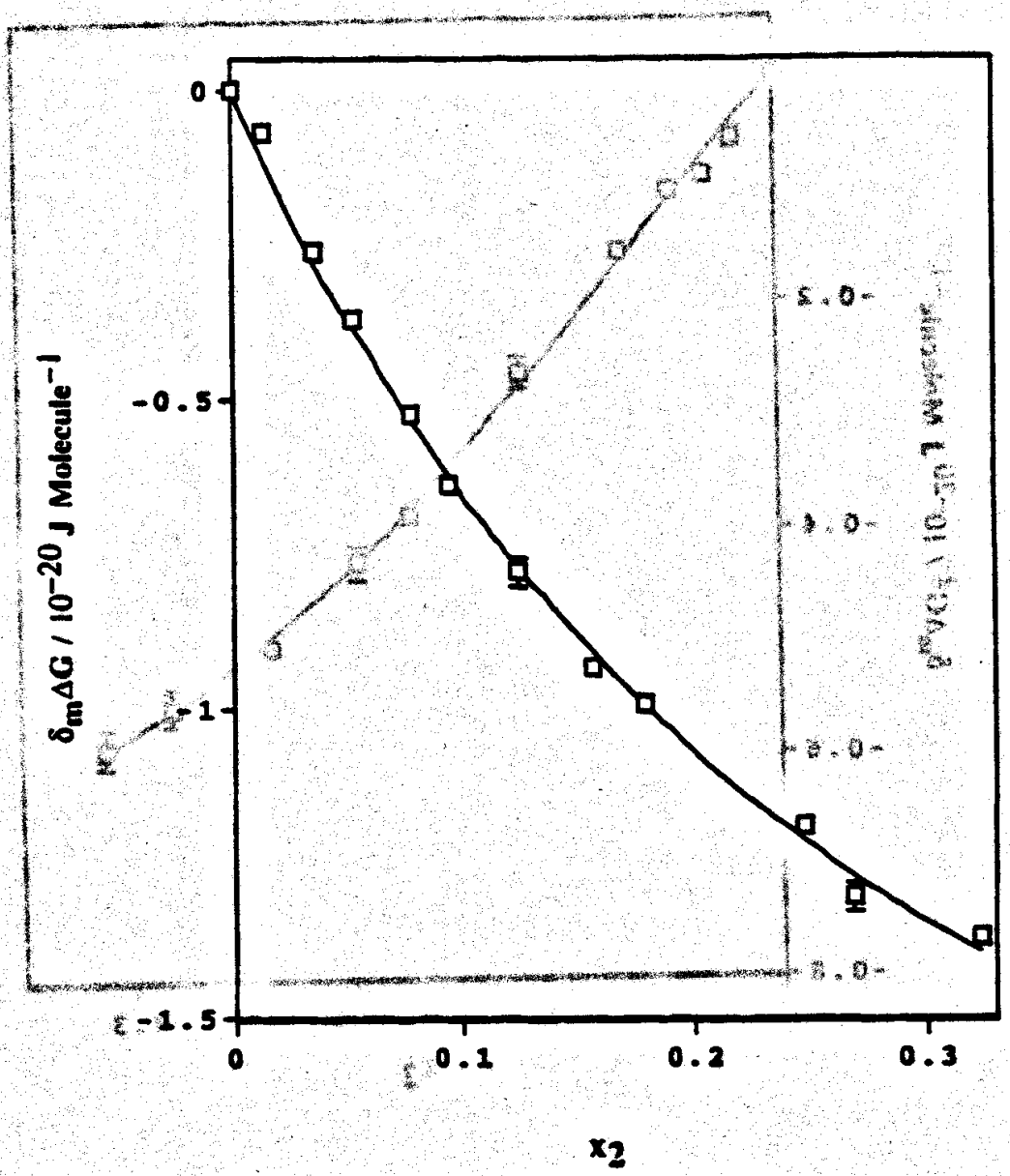

Figure 5.26 Solvent effect on the decomposition of N-chloroleucine in the acetonitrile-water binary cosolvent system showing the experimental data points and the curve fit to the data with the one-step, cancellation approximation phenomenological model (equation 1.64).

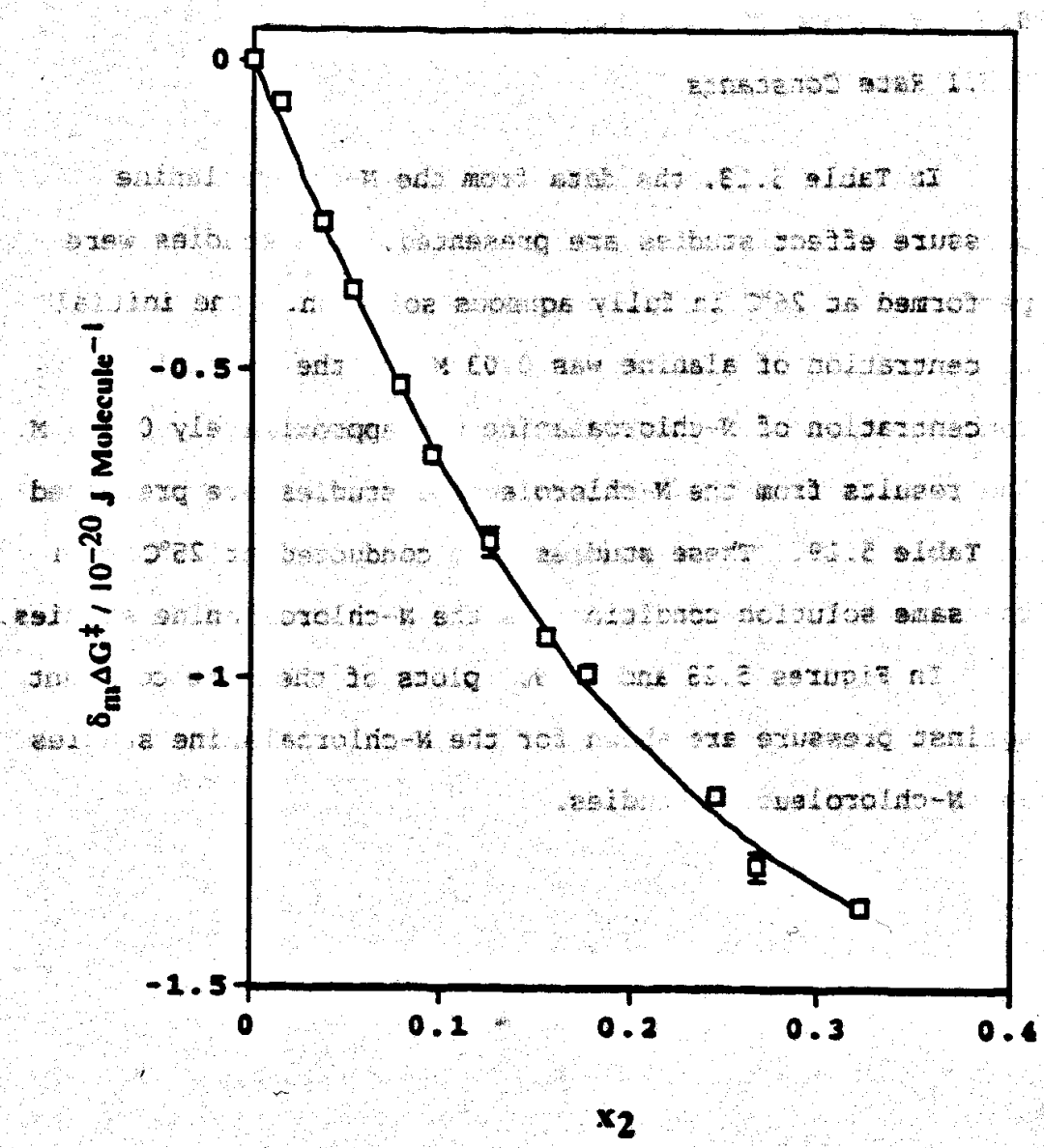

Figure 5.27 Solvent effect on the decomposition of N-chloroleucine in the acetonitrile-water binary cosolvent system showing the experimental data points and the curve fit to the data with the two-step, cancellation approximation phenomenological model (equation 1.63).

5.5 Pressure Effect Studies

5.5.1 Rate Constants

In Table 5.18, the data from the N-chloroalanine pressure effect studies are presented. All studies were performed at 25°C in fully aqueous solution. The initial concentration of alanine was 0.03 M and the initial concentration of N-chloroalanine was approximately 0.003 M. The results from the N-chloroleucine studies are presented in Table 5.19. These studies were conducted at 25°C with the same solution conditions as the N-chloroalanine studies.

In Figures 5.28 and 5.29, plots of the rate constant against pressure are shown for the N-chloroalanine studies and N-chloroleucine studies.

Table 5.18. Pressure effect on the decomposition of N-chloroalanine. The studies were performed at 26°C in fully aqueous solution.

Pressure/bar	k/min^{-1}
1	0.0185
1	0.0142
1	0.0164
1	0.0176
1	0.018
15	0.015
15	0.018
15	0.017
30	0.014
30	0.014
30	0.016
45	0.0132
45	0.017
100	0.0122
100	0.015
200	0.012
200	0.011
200	0.012
200	0.0091
300	0.01
300	0.009
500	0.0096
500	0.0106
1000	0.0093
1500	0.011
2000	0.0105
2482	0.009
2482	0.0102

Table 5.19 Pressure effects on the decomposition of N-chloroleucine. Studies were conducted in fully aqueous systems at 25°C. Only one rate determination was performe at each pressure.

Pressure/bar	k / min^{-1}
1	0.0201 (0.0002)[a]
100	0.015 (0.0012)
250	0.0141 (0.00023)
500	0.01390 (0.00070)
1000	0.01300 (0.00088)
1500	0.01243 (0.00048)

[a]Numbers in parentheses are standard deviations that were calculated by propagation of errors

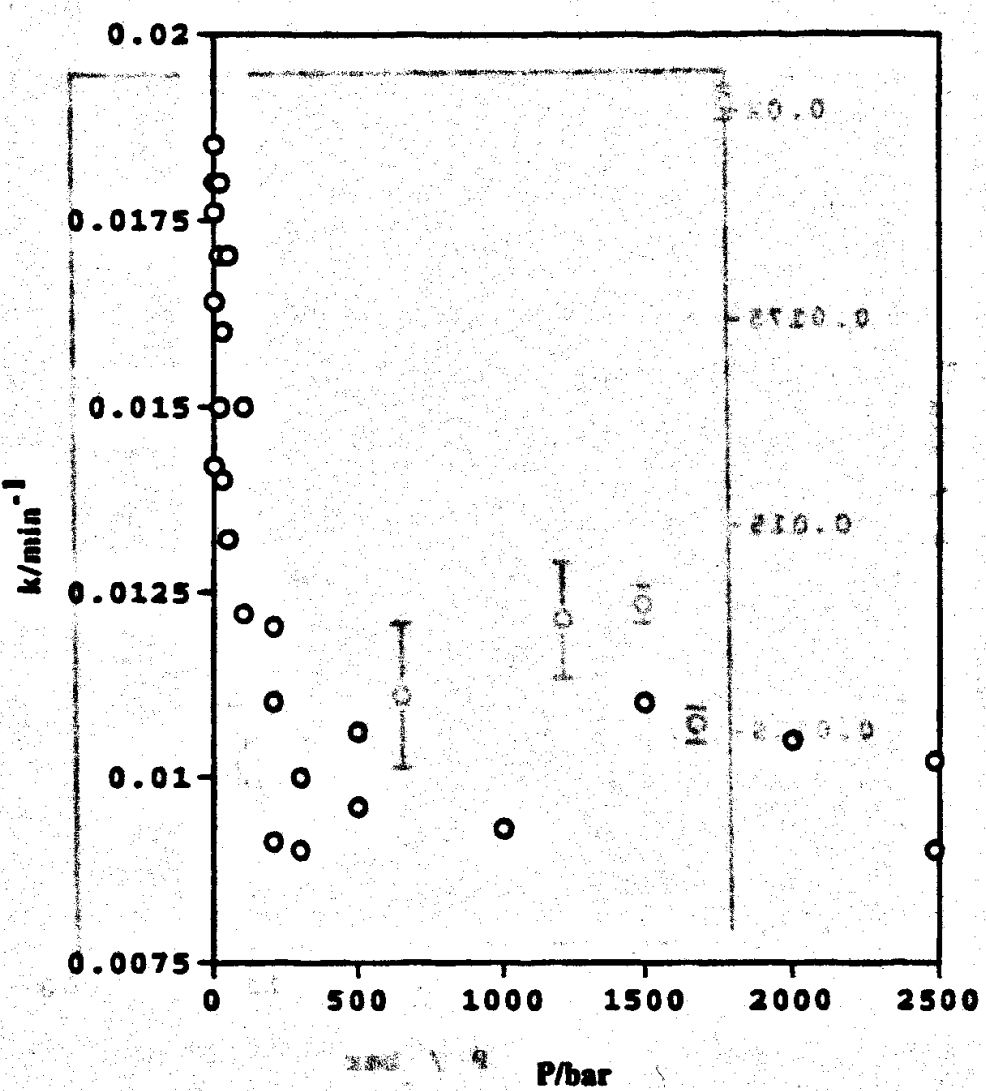

Figure 5.28 Pressure effects on the decarboxylative-dechlorination of N-chloroalanine. Studies were conducted in fully aqueous solution at 26°C. The data exhibit considerable scatter, but the direction of the effect is unquestionable; the rate constant decreases at higher pressures, indicating a positive volume of activation.

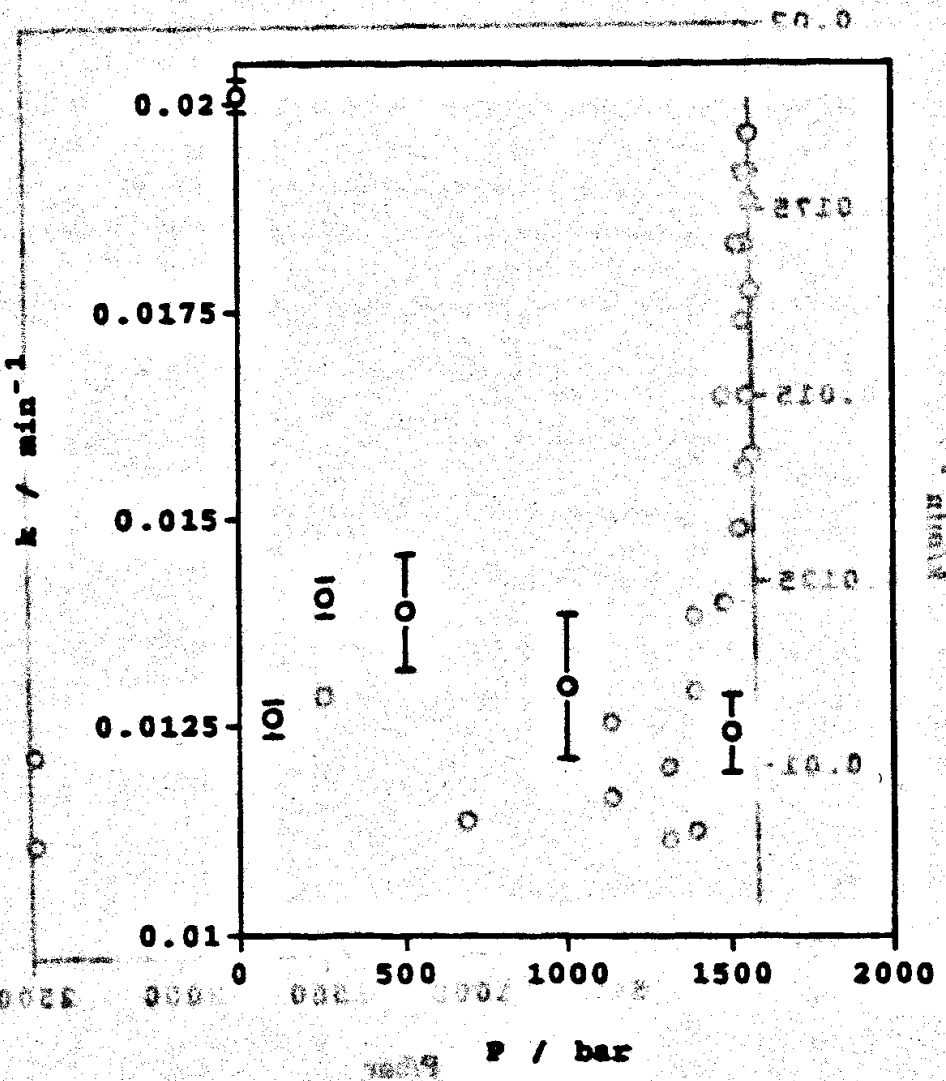

Figure 5.29 The pressure effect on the decarboxylative-dechlorination of N-chloroleucine. All studies were conducted in fully aqueous solutions at 25°C. The data are scattered, but the direction of the effect is unquestionable; the rate constant decreases at higher pressures, indicating a positive volume of activation.

5.5.2 Volume of Activation

Sufficient data were available (in the pressure range of 1 to 500 bar) to calculate the volume of activation for the decarboxylative-dechlorination of N-chloroalanine. As was discussed in Chapter 4, the data were fit to the quadratic equation (4.4) and the volume of activation was calculated from equation (4.5).

$$\ln\frac{k}{k_{1\ bar}} = aP + bP^2 \qquad (4.4)$$

$$\Delta V^{\ddagger} = -RTa \qquad (4.5)$$

The estimate for parameter a is $-0.0030 \pm 0.00033\ bar^{-1}$, and the estimate for parameter b is $0.000004 \pm 0.000001\ bar^{-2}$. The volume of activation is estimated to be 70 ± 8.2 cm^3/mole.

A plot of the fit to the data is shown in Figure 5.30. The data could not be successfully fit to the three-parameter models given by equations (4.6) and (4.7), as the parameter estimates were highly correlated and sensitive to initial estimates.

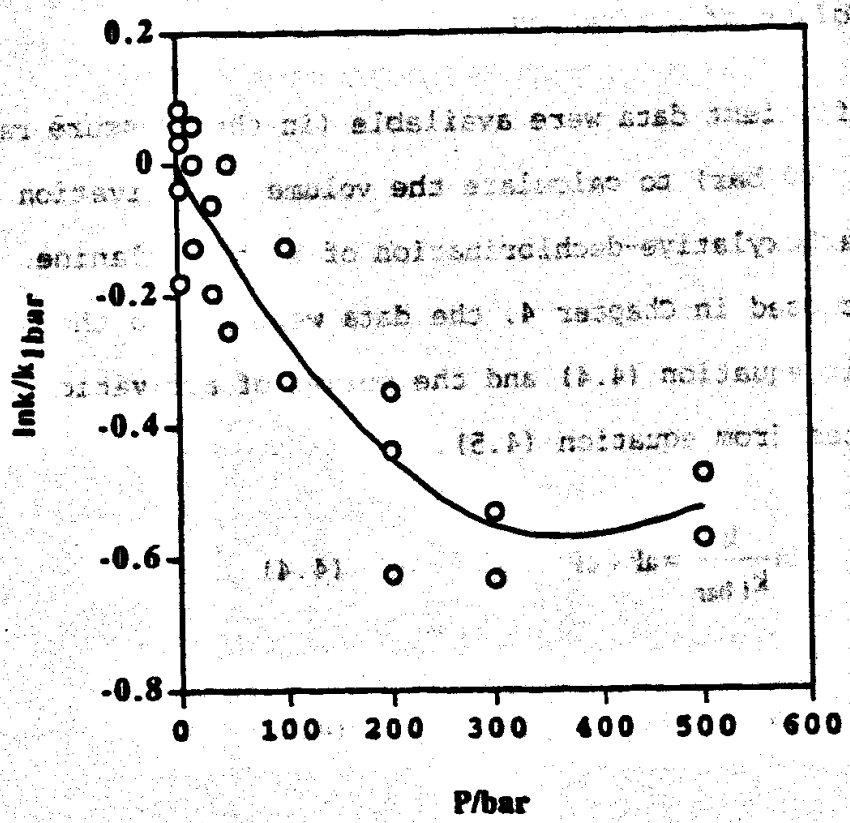

Figure 5.30 The fit of the N-chloroalanine data to equation (4.4). The volume of activation is estimated to be 70 ± 8.2 cm^3/mole.

5.6 Chapter 5 References

(1) Hand, V.C.; Synder, M.P.; Margerum, D.W. *J. Am. Chem. Soc.* (1983), **105**, 4022.

(2) Awad, R.; Hussain, A.; Crooks, P.A. *J. Chem. Perkin Trans 2* (1990), 1233.

(3) Kezdy, F.J.; Jaz, J.; Bruylants, A. *Bull. Chem. Soc. Belg.* (1958), **67**, 687.

(4) Metcalf, W.S. *J. Chem. Soc. B* (1942), **64**, 148.

Chapter 6. Discussion

6.1 Other Approaches to the Description of Solvent Effects on Chemical Reaction Kinetics

Prior to discussing the results of this investigation, a brief mention of some other common solvent effect models is appropriate. This description is not intended to be extensive but only to show the uniqueness of the phenomenological model compared to other works in the literature. For extensive discourses concerning these models, the interested reader is referred to literature reviews (1-9). I have placed these theories into two categories, namely those based on physical principles, and those based on empiricism. This classification scheme is not absolute, but can serve as a guide to the reader.

6.1.1 Models Based on Physical Theory

Hildebrand's regular solution theory (10-13) can be extended to chemical reaction kinetics to give a quantitative description of solvent effects on chemical reaction rates [equation (6.1).] (The reader is referred to Connors' recent review (6) for the derivation of this equation.)

$$\ln k = \text{constant} + \sum V_i(\delta_i - \delta_s)^2 - V_{\ddagger}(\delta_{\ddagger} - \delta_s)^2 \qquad (6.1)$$

Here, V is a molar volume, and δ is the solubility parameter, which is equal to the square root of the molar energy of vaporization of a solvent per unit volume, and the subscripts ‡ and s refer to the transition state and the solvent, respectively. The subscript i refers to any given reactant in the reaction system.

The $(\delta_i - \delta_s)^2$ and $(\delta_{\ddagger} - \delta_s)^2$ terms account for solute-solute interaction, solvent-solute interaction, and solvent-solvent interaction energies. The solute-solute interaction energy is the energy required to abstract a solute molecule from a pure solute; the solvent-solvent interaction energy is the energy required to create a cavity within the solvent into which the solute will be inserted; the solvent-solute interaction energy results from insertion of the solute into the cavity. The phenomenological model accounts for all these events as well and is, in this sense, related to this model, yet the phenomenological describes these interactions with different theoretical considerations and mathematical formalisms. In addition, regular solution theory is limited by its approximations to systems in which dispersion interactions predominate.

Nagy and coworkers have developed the competitive preferential solvation (COPS) theory that can describe

solvent effects on chemical kinetics (14,15), U.V. and N.M.R. spectroscopic shift data (14, 16-18), and solubility (19) through solvent-solute interactions that are modeled by a competitive solvation exchange scheme. This is similar to the phenomenological model's solvation effect component, which uses a solvation exchange scheme to describe solvent-solute interactions; however, the derivation and the final expression for COPS theory's description of solvent-solute interactions is different from the phenomenological model (14,15). COPS theory can be further contrasted to the phenomenological model in that COPS does not account for solvent-solvent and solute-solute interactions. COPS theory is based on these five postulates.

Postulate #1 The solvent constituents compete to solvate the solute, and the solute interacts with the entire surrounding medium.

Postulate #2 The molecules in the solvation shell are incessantly alternating between solvating and complexing states. Complexation is a state of preferred orientation between a solute and solvent molecule, while solvation is a less ordered state.

Postulate #3 The solvation shell composition is controlled by affinity constants, $K_{i(j)}$, $K_{i(k)}$, $K_{i(l)}$...and the respective solvent constituent concentrations C_j, C_k, C_l...

Postulate #4 The solute is considered to be partitioned among all solvent components, hence the solvation shell is comprised of a weighted mixture of pure solvent components. Mathematically, we write

$$C_i = X_{i(j)} + X_{i(k)} + X_{i(l)} + \ldots \qquad (6.2)$$

where

$$X_{i(j)} = C_i \times \frac{K_{i(j)}}{K_{i(j)}C_j + K_{i(k)} + K_{i(l)}C_l + \ldots} = C_i P_{i(j)} \qquad (6.3)$$

Here, C_i represents the concentration of solute, and $K_{i(j)}$ and C_j represent the affinity constant and concentration of solvent component j. Their product is divided by the summation of all other solvent component concentrations and affinity constant products. $P_{i(j)}$ is a generalized partition factor.

Postulate #5 The solvent effects on any physicochemical property, T, are additive in the solvation shell so that

$$T = P_{i(j)}T_{i(j)} + P_{i(k)}T_{i(k)} + P_{i(l)}T_{i(l)} \ldots \qquad (6.4)$$

Equation (6.4) is the general form of the model; it is tailored to describe the specific kinetics problem at ha

(15).

The last two models to be discussed in this section not related to the phenomenological model as they rely solely on electrostatics to describe the solvent effect reaction rates; however, these models are well known and should be mentioned. The first model, which describes solvent effects on reaction rates for dipoles, is given equation (6.5),

$$\ln k_s = \ln k_0 + \frac{N}{RT}\left(\frac{\varepsilon-1}{2\varepsilon+1}\right)\left(\frac{\mu_\ddagger^2}{r_\ddagger^3} - \sum\frac{\mu_i^2}{r_i^3}\right) \qquad (6.5$$

where k_s is the reaction rate in a test medium, k_0 is th rate constant in a reference solvent, N is Avogadro's number, ε is the dielectric constant of the medium, RT i the product of the gas constant and the absolute temperature, μ is the dipole moment, and r is the radiu (20). Equation (6.5) was derived from the Kirkwood expression for the transfer free energy of a dipole from medium of $\varepsilon = 1$ to one of dielectric constant ε (21).

An equivalent expression (22) for solvent effects reaction rates between ions is given by equation (6.6)

$$\ln k_s = \ln k_0 + \frac{Ne^2}{2RT}\left(1-\frac{1}{\varepsilon}\right)\left(\frac{Z_\pm^2}{r_\pm^3}-\sum\frac{Z_i^2}{r_i^3}\right) \qquad (6.6)$$

where e is the electron charge and Z is the valence of the ions (subject to the condition that $Z_\pm = \sum Z_i$). All other terms have been previously defined. Equation (6.6) was derived from the Born equation (23) for the free energy of transfer of an ion from a medium with a dielectric constant of one to a medium with a dielectric constant equal to ε.

Equations (6.5) and (6.6) assume that the solvent is a continuous isotropic medium, and, as is evident, only consider electrostatics in their description of the solvent effects on chemical reaction rates. They cannot account for specific solute-solvent interactions.

Many workers have discussed this limitation of these models (5,6,7,24). For example, Skwierczynski and Connors (25) have shown that plots of ln k against $\frac{1}{\varepsilon}$ for the demethylation of aspartame in various binary aqueous-organic cosolvent systems do not give the predicted linear behavior of equation (6.6), but show minima and maxima, and even show disparity in the direction of the solvent effect.

Plots of some of the data from the present study, according to equation (6.6), are shown in Figures 6.1 and 6.2 (Dielectric data were taken from references (26-28)). According to equation (6.6), a plot of ln k against 1/ε for

a given reaction in any cosolvent system should be linear and have the same slope regardless of the cosolvent system. As is evident from these figures, this prediction is not realized. Clearly, other factors in addition to electrostatics must be considered when describing solvent effects on chemical reaction rates; the need for such considerations has spawned the many empirically based models for solvent effects. These are discussed in the next section.

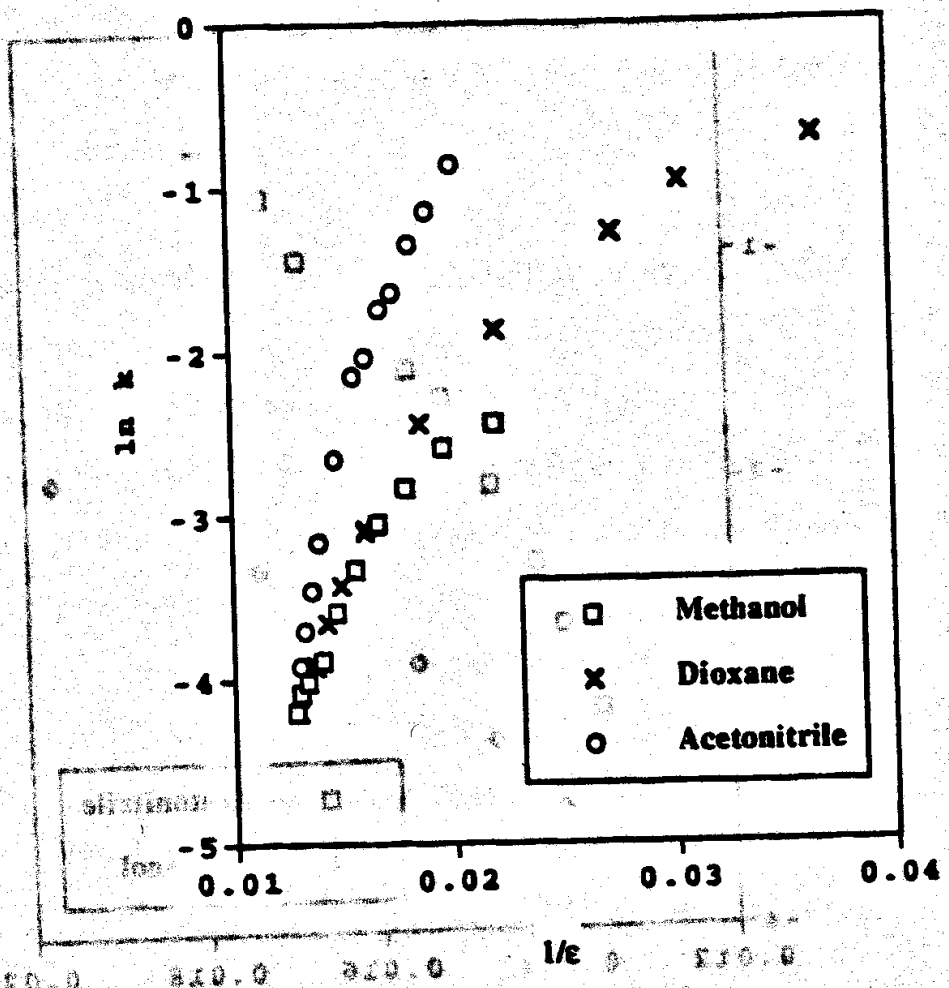

Figure 5.1 Solvent effect for the decarboxylative-dechlorination of N-chloroalanine. The dielectric data are from references (26-28).

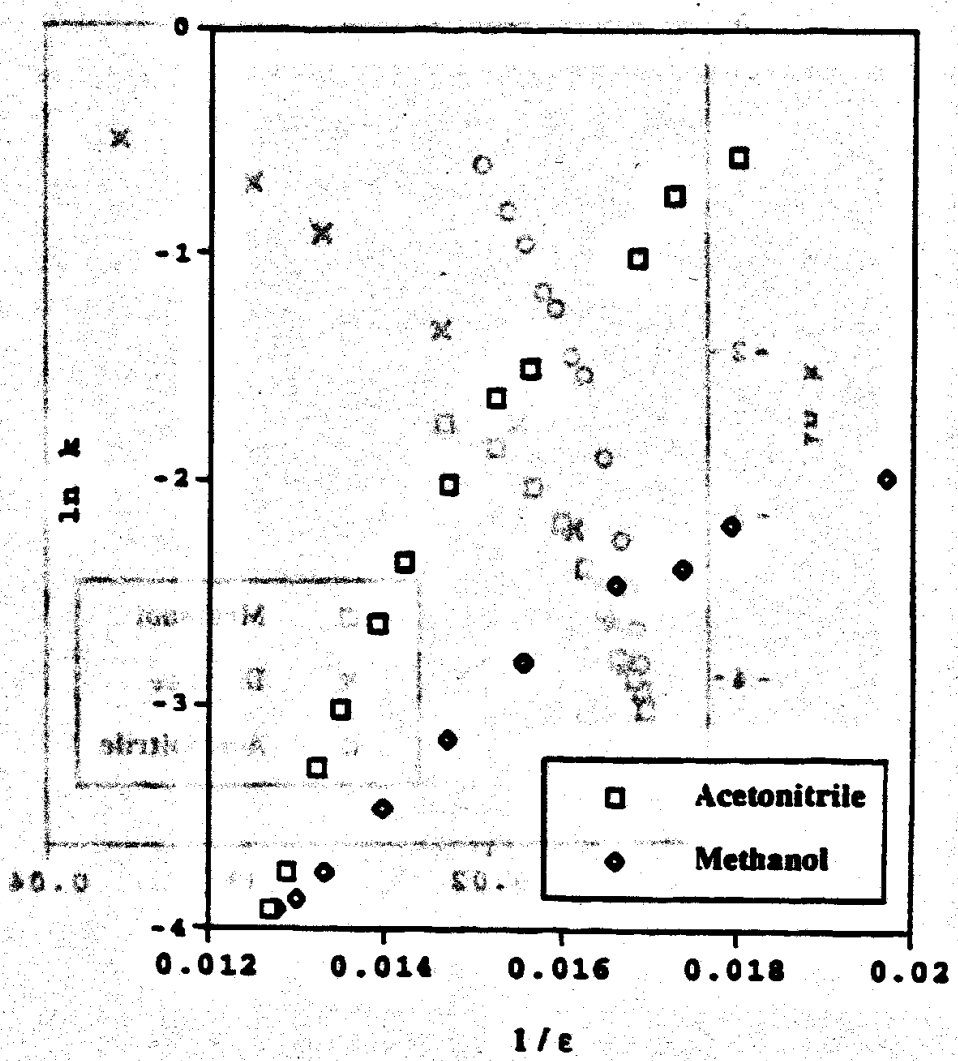

Figure 6.2 Solvent effect on the decarboxylative-dechlorination of N-chloroleucine. The dielectric data are from references (26,28).

6.1.2 Empirically Based Models

The empirically based models typically express the solvent effects on reaction rates as linear combinations of solvent polarity parameters. (Most of the polarity parameters are determined spectrophotometrically from solvatochromic frequency shifts in the spectrum of a specific probe molecule, or kinetically from solvent effects on the rate of a specific chemical reaction. The parameters, whether kinetically or spectrophotometrically determined, are claimed to give a quantitative measure of some physico-chemical property of the solvent, for example its polarizability, its hydrogen bond donating ability, or its hydrogen bond accepting ability.) If the solvent effect data for a test reaction are fitted to a linear combination of these parameters, then the influence a specific solvent property has on the reaction can be determined. In this manner the solvent effect is interpreted in terms of specific solvent properties. For example, if after fitting data to a linear combination of parameters which include a hydrogen bond donation parameter, it is found that the coefficient for the hydrogen bond donating parameter is small, then it is assumed that hydrogen bond donation to the reactant has only a minor effect on the reaction rate.

Because these linear solvent effect models are far removed from the phenomenological model, I will do little more than list some of the more prevalent ones found in the literature.

The Kamlet-Taft approach is popular (29-36). In this approach, the solvent effect for a reaction can be expressed as a linear combination of as many as six solvent parameters. The number of parameters can be reduced depending on the solvents and reaction that is being examined. The solvent parameters include a polarity/polarizability parameter π^*, a polarizability correction term δ, a solvent hydrogen bond donor (HBD) parameter α, a solvent hydrogen bond acceptor (HBA) parameter β, the Hildebrand solubility parameter δ_h^2, which accounts for solvent-solvent interactions and is an endoergic term accounting for the energy required to create a cavity in the solvent, and a coordinate covalency parameter, ξ. A collection of the parameter values for a variety of solvents is given in reference (34).

Koppel and Palmer (37) express the solvent effect on reaction rates as a linear function of the solvent polarity (measured by the Kirkwood dielectric function), the solvent polarizability, the solvent electrophilicity, and the solvent nucleophilicity. According to these authors, the first two solvent properties account for nonspecific

interactions, and the last two describe specific interactions.

A recent linear solvent effect model has been developed by Drago and coworkers (38); their model expresses the solvent effect on the rate constant for a reaction as a linear combination of the solvent's electrostatic bond-forming tendencies, covalent bond-forming tendencies and a solvent polarity parameter.

Grunwald and Winstein (39-42) have used a univariate linear model to describe the solvent effects for S_N1 solvolysis reactions. They describe the solvent effect as a function of the solvent ionizing power; this solvent property, the Y value, is defined by

$$Y = \log \frac{k^{t\text{-BuCl}}}{k_o^{t\text{-BuCl}}} \qquad (6.7)$$

where $k_o^{t\text{-BuCl}}$ is the solvolysis rate constant for t-butyl chloride in an 80% (V/V) ethanol-water solution (the reference solvent) and $k^{t\text{-BuCl}}$ is the rate constant in the test solvent.

As previously stated, this discussion of various solvent effect models is not intended to be exhaustive, but rather to inform the reader of some approaches taken by other workers in this field. Though some of the models

describe solvent effects on reaction rates by considering the solvent-solvent, solvent-solute, and/or solute-solute interactions, as does the phenomenological model, the mathematical forms used by these models to describe these interactions are quite different from that of the phenomenological model. In the next section, we will discuss the results obtained from application of the phenomenological model to the solvent effects on the decarboxylative-dechlorination of N-chloroalanine and N-chloroleucine.

6.2 Solvent and Pressure Effects on the Reaction Rate

Incorporation of organic cosolvent into the reaction solution caused an increase in the rate of reaction for both N-chloroalanine and N-chloroleucine. Protic cosolvents caused a 6 to 10-fold increase in the reaction rate, while nonprotic solvents caused about a 30-fold increase in the reaction rate. The organic cosolvent concentration was usually extended to 60 to 70% v/v.

The reaction rates for N-chloroalanine and N-choroleucine decomposition decreased as pressure was increased. This indicates the reactions possess a positive volume of activation which is consistent with the concerted fragmentation reaction mechanism shown in Scheme 2.7 in

Chapter 2; in this scheme, a charge dispersion is accompanied by simultaneous cleavage of the N-chloro bond and the carboxylate-α-carbon bond. (As discussed in Chapter 3, charge dispersions and bond cleavages usually lead to positive volume changes.)

6.3 The Curve-Fits

The data from these studies were fit to equations (1.63) and (1.64) using a nonlinear regression program, Systat® version 5.2.1.

$$\delta_m \Delta G^{\ddagger}_{rxn} = \left(\frac{\Delta g A^{\ddagger} \gamma' K_1 x_1 x_2 + 2\Delta g A^{\ddagger} \gamma' K_1 K_2 (x_2)^2}{(x_1)^2 + K_1 x_1 x_2 + K_1 K_2 (x_2)^2} \right) \quad (1.63)$$

$$\delta_m \Delta G^{\ddagger}_{rxn} = \frac{\Delta g A^{\ddagger} \gamma' K_1 x_2}{x_1 + K_1 x_2} \quad (1.64)$$

These are the resulting expressions for the two-step and one-step models, respectively, after application of full cancellation approximation, where for the two-step model $K_1^R = K_1^{\ddagger} = K_1$ and $K_2^R = K_2^{\ddagger} = K_2$ and for the one-step model $K_1^{\ddagger} = K_1^R = K_1$. The justification for using the full cancellation approximations will be discussed soon; however, I will first comment on the goodness of the fits to the data. For simplicity, I will refer to equations (1.63) and

(1.64) as the two-step and one-step models, where it is understood that the full cancellation approximation has been applied. The two-step model can quantitatively describe all the solvent effect data, whereas the one-step model can quantitatively fit most, but not all of them. The two-step model is especially useful when the solvent effect data show a sigmoidal pattern. Of course when the data reveal a hyperbolic pattern, then the one-step model, which is the equation of a rectangular hyperbola, can be used to quantitatively describe the data. We can conclude that the full cancellation approximation phenomenological model can quantitatively describe the kinetics data generated in this study. The justification for applying this approximation will now be presented.

When the data were fit to the one-step, 4 parameter, phenomenological model given by equation (1.62),

$$\delta_m \Delta G^{\ddagger}_{rxn} = \frac{(gA^{\ddagger}\gamma' - k_B T \ln K_1^{\ddagger}) K_1^{\ddagger} x_2}{x_1 + K_1^{\ddagger} x_2} - \frac{(gA^{R}\gamma' - k_B T \ln K_1^{R}) K_1^{R} x_2}{x_1 + K_1^{R} x_2} \qquad (1.62)$$

the parameter estimates were observed to be highly intercorrelated, (an indication that a model has too many parameters and should be simplified) and thus their values

are not highly reliable; yet, the estimates provided some information about the solvation exchange constants and the gA parameters, namely that $K_1^{\ddagger} \equiv K_1^R$, and $gA^{\ddagger} > gA^R$. In Table 6.1, the parameter estimates from some of these analyses, are presented along with their initial starting values. (Because final estimates are highly intercorrelated, the parameters are sensitive to initial starting values, which have therefore also been included in the table.) This trend of the data in Table 6.1 led me to apply the cancellation approximation to the phenomenological model.

Table 6.1 Initial and final parameter estimates for equation (1.62).

	$K_1^{\ddagger}$	K_1^R	$gA^{\ddagger}$	gA^R
	i-propanol-water system			
Initial Estimate	15	10	0.01	0.01
Final Estimate	8.4	10.1	0.028	0.0062
Initial Estimate	10	9	0.03	0.03
Final Estimate	8.5	9.62	0.044	0.022
	Acetonitrile-Water			
Initial Estimate	5	3	0.03	0.03
Final Estimate	5	7	0.0473	0.0009
Initial Estimate	3	5	0.03	0.03
Final Estimate	5	7	0.0465	5.5×10^{-7}

Though these data seem to indicate that $K_1^{\ddagger} \equiv K_1^R$, the question remains- is it justifiable to assume that $K_1^{\ddagger} \equiv K_1^R$? I use the reasoning that Khossravi and Connors (43) and Mulski and Connors (44) used when these workers applied the cancellation approximation to complexation data; their argument is now presented. This laboratory's analysis of solubility data, consisting of 62 systems comprised of combinations of 40 solutes in 12 different organic solvents (45-49), has shown that $K_1 = 4 \pm 2.9$ (range 0.3 to 15) and $K_2 = 5 \pm 4$ (range 0.7 to 21.5); Considering that these solutes ranged greatly in polarity and chemical structure, (for example the solutes included 2,2',4,4',6,6'-hexachlorobiphenyl and sucrose), the variations in K_1 and K_2 are small, which indicates that the exchange constants are rather insensitive to chemical structure and polarity. This insensitivity becomes further apparent upon inspection of the results in Table 6.2 for a variety of solutes in methanol-water cosolvents systems; the variation in these exchange constants is very small, namely $K_1 = 2.7 \pm 0.42$ and $K_2 = 1.44 \pm 0.31$. These data suggest that most of the variation in the exchange constants is solvent rather than solute dependent. Now, extending the results of this analysis to the kinetics work, we realize that the structures of the N-chloroamino acid and its proposed transition state are similar (see Scheme 2.7); and it seems

reasonable to postulate that the solvation exchange constants for the reactant and transition state are similar and that the cancellation approximation is properly applied to the analysis of kinetic data for this reaction.

Table 6.2 Exchange constants for a variety of solutes obtained from analysis of solubility data in a methanol-water system.

Solute	K_1	K_2	Reference
Naphthalene	2.52 (0.071)	1.19 (0.085)	46
Biphenyl	2.45 (0.07)	1.28 (0.07)	45
4-Hydroxy-biphenyl	2.33 (0.04)	1.61 (0.05)	45
4,4'-Dihydroxy-biphenyl	2.62 (0.08)	2.2 (0.11)	45
4-Bromobiphenyl	2.6 (0.13)	1.4 (0.16)	45
4-Nitroaniline	2.7 (0.35)	1.5 (0.49)	46
4-Chlorobiphenyl	2.49	1.30	48
2,2',4,4'6,6'-Hexachloro-biphenyl	3.76	1.21	48
2,4,6-Trichloro-biphenyl	2.78	1.27	48

As a means of exploring this assumption further, simulated solvent effect data were generated with the two-step, 6-parameter model [equation (1.51)]

$$\delta_m \Delta G^{\ddagger}_{rxn} =$$

$$\left(\frac{(-k_B T \ln (K_1^{\ddagger}) + gA^{\ddagger}\gamma')\, K_1^{\ddagger} x_1 x_2 + (-k_B T \ln (K_1^{\ddagger} K_2^{\ddagger}) + 2gA^{\ddagger}\gamma')\, K_1^{\ddagger} K_2^{\ddagger} (x_2)^2}{(x_1)^2 + K_1^{\ddagger} x_1 x_2 + K_1^{\ddagger} K_2^{\ddagger} (x_2)^2}\right)$$

$$-\left(\frac{(-k_B T \ln (K_1^{R}) + gA^{R}\gamma')\, K_1^{R} x_1 x_2 + (-k_B T \ln (K_1^{R} K_2^{R}) + 2gA^{R}\gamma')\, K_1^{R} K_2^{R} (x_2)^2}{(x_1)^2 + K_1^{R} x_1 x_2 + K_1^{R} K_2^{R} (x_2)^2}\right) \quad (1.61)$$

and then these data were analyzed with equation (1.63). To generate the data, the $gA^{\ddagger}$ and gA^{R} terms were set equal to 0.05 and 0.007 respectively; ($\Delta gA^{\ddagger}$ is then equal to 0.043.) The values for the exchange constants $K_1^{\ddagger}$, $K_2^{\ddagger}$, K_1^{R}, and K_2^{R} used to generate the data are given in Table 6.3, along with the estimates of $\Delta gA^{\ddagger}$, K_1, K_2 obtained by fitting the simulated data to equation (1.53). Reasonable values for the exchange constants were chosen and varied as shown in Table 6.3.

Table 6.3. The values for $K_1^{\ddagger}$, $K_2^{\ddagger}$, K_1^R, and K_2^R used to generate simulated solvent effect data with equation (1.61), and the parameter estimates obtained by fitting the data to equation (1.63). $gA^{\ddagger}$ and gA^R were set equal to 0.05 and 0.007 respectively. The numbers in parentheses are standard deviations.

Initial values $K_1^{\ddagger}$, $K_2^{\ddagger}$, K_1^R, and K_2^R used to generate simulated data with equation (1.61)				Parameter estimates obtained by fitting simulated data to equation (1.63)		
$K_1^{\ddagger}$	$K_2^{\ddagger}$	K_1^R	K_2^R	K_1	K_2	$\Delta gA^{\ddagger}$
5.5	2	5.5	2	5.5 (0)	2 (0)	0.043 (0)
8.25	3	5.5	2	10.23	3.91	0.0506 (0.000018)
11	4	5.5	2	13.9 (0.12)	6.49 (0.07)	0.05620 (0.000048)
22	8	5.5	2	22 (1.6)	21 (1.7)	0.0706 (0.00035)
33	12	5.5	2	35.4 (0.06)	13 (0.02)	0.1068 (0.00013)
55	20	5.5	2	20 (9)	120 (50)	0.089 (0.00072)
110	40	5.5	2	Did not converge		

Table 6.3 continued

Initial values $K_1^{\ddagger}$, $K_2^{\ddagger}$, K_1^R, and K_2^R used to generate simulated data with equation (1.61)				Parameter estimates obtained by fitting simulated data to equation (1.63)		
$K_1^{\ddagger}$	$K_2^{\ddagger}$	K_1^R	K_2^R	K_1	K_2	$\Delta gA^{\ddagger}$
2	5.5	2	5.5	2 (0)	5.5 (0)	0.043 (0)
3	8.25	2	5.5	2.6 (0.11)	14.9 (0.69)	0.05080 (0.000086)
4	11	2	5.5	2.2 (0.40)	37 (6.9)	0.0566 (0.00023)
8	22	2	5.5	Did not converge		
5.5	2	8.25	3	2.62 (0.085)	1.97 (0.085)	0.035 (0.00014)
5.5	2	11	4	0.03 (0.014)	900 (470)	0.027 (0.00066)
5.5	2	22	8	Did not converge		
2	5.5	3	8.25	0.61 (0.068)	8.3 (0.99)	0.0349 (0.99)
2	5.5	4	11	5×10^{-6}	4.7×10^{6}	0.025[b]

[b]Standard deviations were not computable.

The results from this analysis can be partitioned into 4 cases.

Case 1. $K_1^{\ddagger} > K_2^{\ddagger}$ and $K_1^{\ddagger}$, $K_2^{\ddagger}$ were varied in 1, 1.5, 2, 4, 6, 10, and 20-fold multiples of K_1^R, K_2^R. When $K_1^{\ddagger} = 22$, $K_2^{\ddagger} = 8$ and $K_1^R = 5.5$, $K_2^R = 2$, a 4-fold difference between $K_1^{\ddagger}$, $K_2^{\ddagger}$, and K_1^R, K_2^R, the estimated exchange constant values are much larger than commonly observed. The magnitude of the exchange constant estimates increases as $K_1^{\ddagger}$, $K_2^{\ddagger}$ are set to increasing larger multiples of K_1^R, K_2^R. The anomalous exchange constant estimates could therefore act to signal that the cancellation approximation is not valid. In this case, a four-fold difference in the values would be detectable.

Case 2. $K_2^{\ddagger} > K_1^{\ddagger}$, and $K_1^{\ddagger}$, $K_2^{\ddagger}$ were varied in 1, 1.5, 2, and 4-fold multiples of K_1^R, K_2^R. Here unusually large exchange constant estimates are observed when $K_1^{\ddagger}$, $K_2^{\ddagger}$ are only twice the values of K_1^R, K_2^R.

Case 3. $K_1^{\ddagger} > K_2^{\ddagger}$ and K_1^R, K_2^R were varied in 1.5, 2, and 4-fold multiples of $K_1^{\ddagger}$, $K_2^{\ddagger}$. Here a two-fold difference caused anomalies in the exchange constant estimates.

Case 4. $K_2^{\ddagger} > K_1^{\ddagger}$, and K_1^R, K_2^R were varied in 1.5, and 2-fold multiples of $K_1^{\ddagger}$, $K_2^{\ddagger}$. Here, a two-fold difference caused anomalies in the exchange constant estimates.

Though this analysis has investigated simulated data generated from variation of only a few of the many possible combinations of variables, it is still useful in showing that equation (1.63) cannot be used to describe data where 4-fold and larger differences between $K_1^{\ddagger}$, $K_2^{\ddagger}$ and K_1^R, K_2^R exist. Consequently our success in using equation (1.63) to fit kinetic data is consistent with the validity of the full cancellation approximation.

6.4 The Solvation Exchange Constants

An inspection of Tables 5.14 to 5.17 reveals that the exchange constant parameters seem reasonable (compared to estimates from other data we have previously modeled), though the K_2 value of 40 for the decomposition of N-chloroleucine in the 2-propanol-water cosolvent system is large relative to these values.

As this was the first time the phenomenological model has been applied to chemical kinetics data, I was uncertain how the exchange constants would vary with the different solvent systems and reactants that were used in these studies. I did notice that the solvation exchange constants displayed a solvent dependence as they had in the earlier solubility work. To explore this dependence, I plotted log K_1, (obtained from fits of the data to the one-step, cancellation approximation model), against log P (the logarithm of the 1-octanol-water partition coefficient) of the organic cosolvent used in each study (see Figure 6.3). A similar plot of log K_1K_2, (obtained from fits of the data to the two-step, cancellation approximation model) against log P was also made (see Figure 6.4). Such plots were previously used to investigate the solvent dependence of the exchange constants obtained by fitting solubility (47,49) and surface tension (50) data to the phenomenological model.

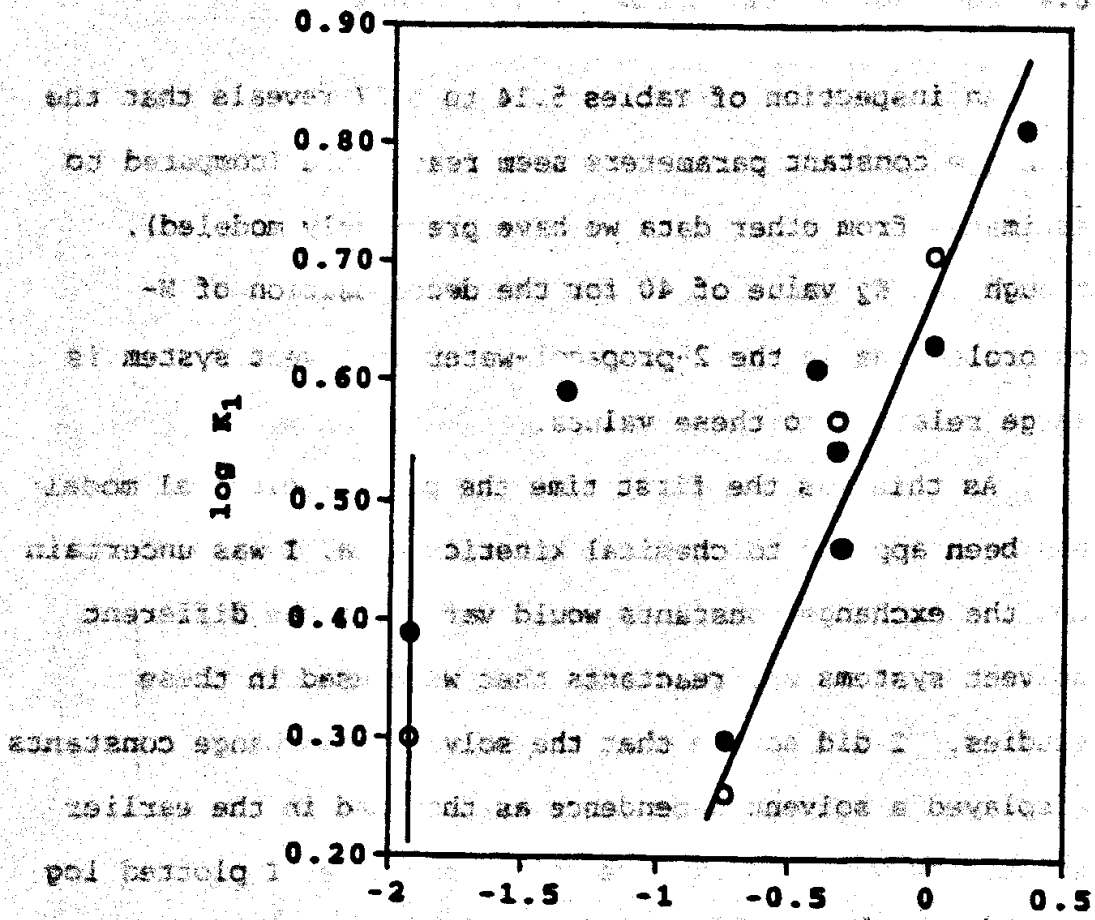

Figure 6.3 Plot of log K_I against log P of the organic cosolvent used in kinetics studies. The K_I values were obtained by fitting the kinetic data to the one-step, cancellation approximation model. The filled circles are from the N-chloroalanine studies, and the empty circles are from the N-chloroleucine studies. The lines have no theoretical significance.

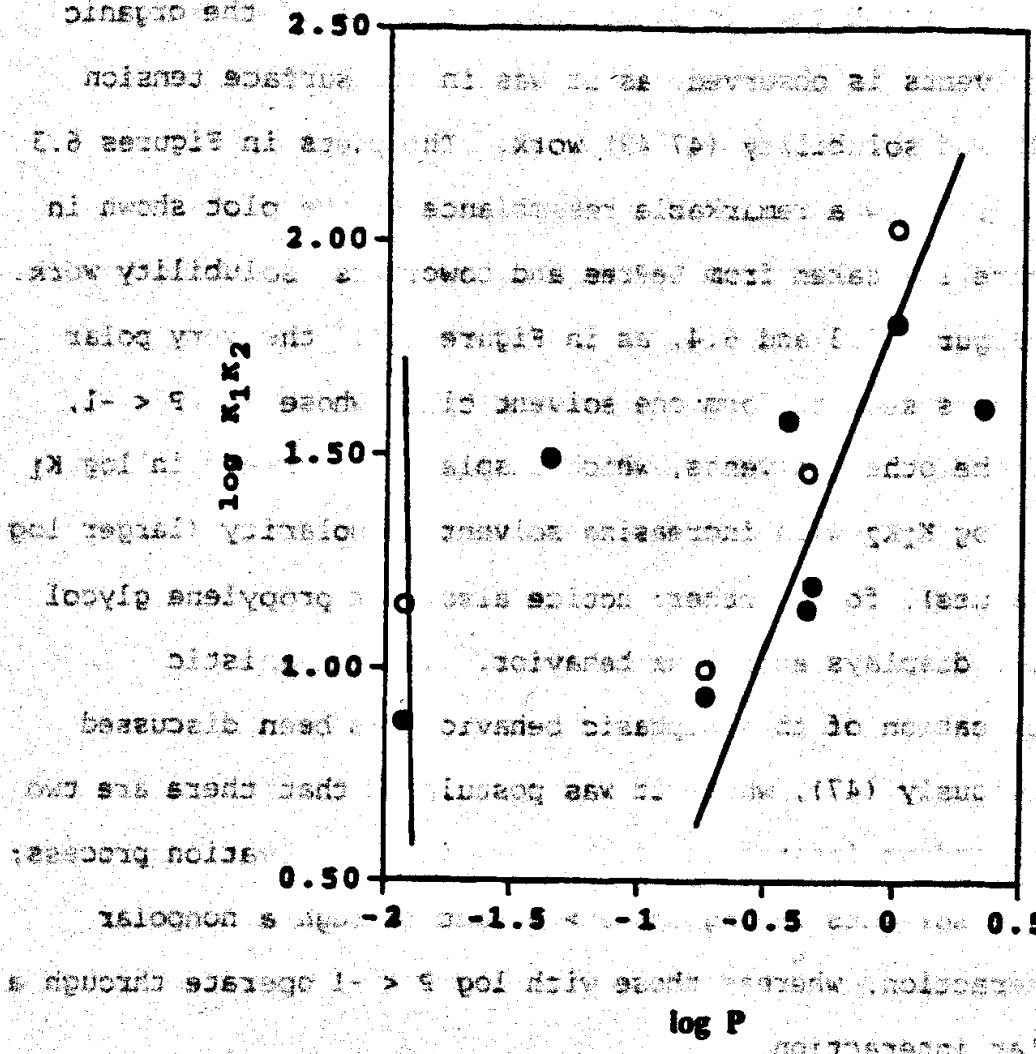

Figure 6.4 Plot of log K_1K_2 against log P of the organic cosolvent used in kinetics studies. The K_1K_2 values were obtained by fitting the kinetic data to the two-step, cancellation approximation model. The filled circles are from the N-chloroalanine studies, and the empty circles are from the N-chloroleucine studies. The lines have no theoretical significance.

In these two plots, biphasic behavior of the organic cosolvents is observed, as it was in the surface tension (50) and solubility (47,49) work. The plots in Figures 6.3 and 6.4 show a remarkable resemblance to the plot shown in Figure 1.4 taken from LePree and coworkers' solubility work. In Figures 6.3 and 6.4, as in Figure 1.4, the very polar solvents seem to form one solvent class whose log P < -1, and the other solvents, which display an increase in log K_1 and log K_1K_2 with increasing solvent nonpolarity (larger log P values), form another; notice also that propylene glycol still displays anomalous behavior. The mechanistic implication of this biphasic behavior has been discussed previously (47), where it was postulated that there are two independent interaction mechanisms in the solvation process; those solvents having log P > +1 act through a nonpolar interaction, whereas those with log P < -1 operate through a polar interaction.

The plots presented in Figures 6.3 and 6.4 are important for several reasons; the correlations between the log K_1 and the log P values, and the log K_1K_2 values and the log P values, suggest a means to approximately predict K_1 and K_2 values. The correlations also grant some physical meaning to the exchange constant values in the sense that they correspond to a specific solvent property. Owing to the similarity of Figures 6.3 and 6.4 to Figure 1.4, it can

be inferred that the phenomenological model describes equally well the solvation processes involved in equilibrium solubility studies and in non-equilibrium kinetics studies. This does not seem unreasonable, for if solvation is considered to be a weak interaction between a molecule in solution and the solvent, the process bywhich the molecule entered the solution should not affect this interaction. Moreover, the time scale of the solvation process will be much different (faster) than that of the chemical reaction.

6.5 The $\Delta gA^{\ddagger}$ Parameter

6.5.1 Average $\Delta gA^{\ddagger}$ Values and Their Implications for the Curvature Correction Factor.

The $\Delta gA^{\ddagger}$ parameter estimates in these studies showed an organic cosolvent-dependent variation. The average, standard deviation, and range of these values from the various solvent studies are presented in Table 6.4.

Table 6.4 The average, standard deviation and range of the $\Delta gA^{\ddagger}$ parameter estimates.

Model	Average value (Standard Deviation) / $Å^2$ molecule^{-1}	Range / $Å^2$ molecule^{-1}
N-Chloroalanine		
One-step, cancellation approximation	40 (15)	20.1 to 68
Two-step, cancellation approximation	30 (13)	16.8 to 55
N-Chloroleucine		
One-step, cancellation approximation	40 (13)	27 to 54
Two-step, cancellation approximation	30 (11)	19.8 to 43

All combinations of the average $\Delta gA^{\ddagger}$ values in the Table 6.4 are not significantly different from each other within 90% confidence limits ($P = 0.1$). Therefore, we can set the average $\Delta gA^{\ddagger}$ estimate for N-chloroalanine, $\Delta gA^{\ddagger}_{ala}$ equal to the average $\Delta gA^{\ddagger}$ estimate for N-chloroleucine, $\Delta gA^{\ddagger}_{leu}$. It will be shown that this equality implies that g, the curvature correction factor, is constant for N-chloroalanine, N-chloroleucine and both their transition states, but first we will chemically justify the equality

$$\Delta A^{\ddagger}_{ala} = \Delta A^{\ddagger}_{leu} \qquad (6.8)$$

where $\Delta A^{\ddagger}_{ala} = A^{\ddagger}_{ala} - A_{ala}$ and $\Delta A^{\ddagger}_{leu} = A^{\ddagger}_{leu} - A_{leu}$, and these quantities represent the changes in the cavity surface area due to the decomposition of N-chloroalanine and N-chloroleucine respectively. I use the following argument to support the equality shown in equation (6.8).

The structures of N-chloroalanine (*1*), and its proposed transition state (*2*), and N-chloroleucine (*3*) and its proposed transition state (*4*) are shown below: notice that the structures of N-chloroalanine and N-chloroleucine differ only in their α-carbon alkyl substituents. Notice also that the alkyl substituents of N-chloroalanine and N-chloroleucine are unaffected by the

transformation of these reactants into the transition state species.

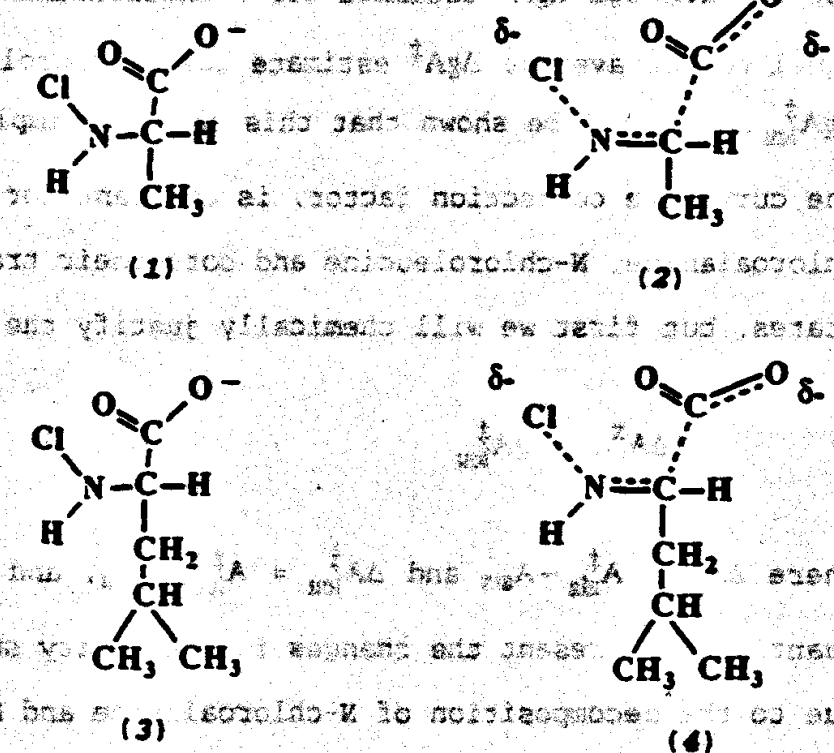

(1) (2)

(3) (4)

Because the proposed reaction mechanism (shown in Scheme 2.7) does not involve any changes to the alkyl substituent in going from initial to transition state, the contributions of the alkyl substituents to the surface areas of the reactant and transition state remain approximately constant, and are thus subtracted off when the difference in the reactant and transition state areas is taken. Therefore, even though the surface areas of N-chloroleucine

and its transition state are larger than the respective surface areas for N-chloroalanine, the *difference* between the areas of N-chloroleucine and its transition state is approximately equal to the area difference between N-chloroalanine and its transition state. Based on these considerations, the equality shown by equation (6.8) seems reasonable. (Actually, $\Delta A^{\ddagger}$ refers to the change in the cavity surface area; however, to a first approximation, the change in the cavity surface area can be equated to the change in the area of solute which is enclosed by the cavity.)

Now the constancy of g will be discussed. From the experimental data shown in Table 5.4, the $\Delta gA^{\ddagger}$ estimates for N-chloroalanine and N-chloroleucine are equated as shown in equations (6.9) and (6.10).

$$\Delta gA^{\ddagger}_{ala} = \Delta gA^{\ddagger}_{leu} \qquad (6.9)$$

$$gA^{\ddagger}_{ala} - gA_{ala} = gA^{\ddagger}_{leu} - gA_{leu} \qquad (6.10)$$

For the purpose of this proof, I will depart from the conventional symbolism used throughout this thesis and rewrite equation (6.10) to give equation (6.11).

$$aA^{\ddagger}_{ala} - bA_{ala} = cA^{\ddagger}_{leu} - dA_{leu} \qquad (6.11)$$

It can be shown that a=b=c=d by performing the following operations. Equation (6.8) is rearranged to give equation (6.12),

$$A^{\ddagger}_{ala} = A^{\ddagger}_{leu} + A_{ala} - A_{leu} \qquad (6.12)$$

which is substituted into equation (6.11) and rearranged to give equation (6.13).

$$aA^{\ddagger}_{leu} + aA_{ala} - aA_{leu} - bA_{ala} - cA^{\ddagger}_{leu} + dA_{leu} = 0 \qquad (6.13)$$

Collecting terms, we write equation (6.14).

$$(a-c)A^{\ddagger}_{leu} + (a-b)A_{ala} + (d-a)A_{leu} = 0 \qquad (6.14)$$

If it is assumed that the area terms are not equal to zero, then for equation (6.14) to be valid, a=b=c=d, which implies that g in equation (6.10) is a constant. We will use this fact in an impending calculation.

6.5.2 *The $\Delta gA^{\ddagger}$ Parameter Sign, Magnitude, and Variation*

The $\Delta gA^{\ddagger}$ estimate is proportional to the difference in the surface areas of the solvation shells that encompass the reactant and transition states; the estimate is proportional

to the molecular surface area of activation. In these studies, $\Delta gA^{\ddagger}$ is always greater than zero. As a means to investigate the correctness of the sign, pressure effect studies were performed to determine the sign of the activation volumes for decarboxylative-dechlorination of N-chloroalanine and N-chloroleucine. As shown in Figures 5.28 and 5.29, the reaction rate decreased at elevated pressures and, as discussed in Chapter 3, this behavior indicates that the volumes of activation for these reactions are positive, in agreement with the sign of the $\Delta gA^{\ddagger}$ estimates. Such agreement shows that the $\Delta gA^{\ddagger}$ parameter values derived from our treatment are consistent in direction with a classical quantity, $\Delta V^{\ddagger}$, evaluated by a completely independent method.

The sign of $\Delta gA^{\ddagger}$ is consistent with the sign of $\Delta V^{\ddagger}$, but what about the magnitude? To answer this question, the following calculations were performed with N-chloroalanine data and equation (6.15),

$$\Delta V^{\ddagger} = \sqrt{\left(\frac{A}{16\pi}\right)}\Delta A^{\ddagger} \qquad (6.15)$$

where the N-chloroalanine molecule is assumed to be a sphere; A is the surface area of an N-chloroalanine molecule (158 ± 5.0 $Å^2$). (This was estimated by using the

foil wrapping technique of Khossravi and Connors (45), which has been discussed in Chapter 1.) $\Delta A^{\ddagger}$ was calculated by dividing $\Delta gA^{\ddagger}$ by 0.4, a typical value for g; here we use the assumption that g is constant for both N-chloroalanine and its transition state.

I have calculated $\Delta V^{\ddagger}$ values using equation (6.15) and the average $\Delta gA^{\ddagger}$ value presented in Table 6.4 (for the two-step model, cancellation approximation); I have also done the calculation using the minimum and the maximum $\Delta gA^{\ddagger}$ values for the range given in Table 6.4 (for the two-step model, cancellation approximation). The results of all the calculations are presented in Table 6.5, and can be compared to the experimentally determined volume of activation for N-chloroalanine decomposition, 70 ± 8.2 cm^3/mole or 120 ± 14 $Å^3$ $molecule^{-1}$. The disparity between the calculated $\Delta V^{\ddagger}$ values and the experimental $\Delta V^{\ddagger}$ value is 2-fold or less. These calculations suggest that the magnitudes of the $\Delta gA^{\ddagger}$ estimates are physically significant; however, this inference was made by comparison to an experimentally determined volume of activation whose value may be inaccurate because it was estimated from the scattered data shown in Figure 5.30; and we do not insist on the quantitative validity of the calculation.

Table 6.5 $\Delta gA^{\ddagger}$ estimates (average value and minimum and maximum of the range presented in Table 6.4) and calculated $\Delta V^{\ddagger}$ values for N-chloroalanine. The experimentally determined value for $\Delta V^{\ddagger}$ is 120 ± 14 $Å^3$ molecule^{-1}.

$\Delta gA^{\ddagger}/Å^2$ molecule^{-1}	Calculated[a] $\Delta V^{\ddagger}/ Å^3$ molecule^{-1}
30	130
16.8	70
55	240

[a]Compare to experimentally determined value of 120 ± 14 $Å^3$molecule^{-1}

The $\Delta gA^{\ddagger}$ estimates for N-chloroalanine show about a 3.3-fold solvent-to-solvent variation, and those for N-chloroleucine show about a 2-fold solvent-to-solvent variation. Clearly the $\Delta gA^{\ddagger}$ values are not constant, but the solvent-to-solvent variation is much less than is usually seen with the solubility data. A possible explanation for the solvent-to-solvent variation may be drawn from data presented in Table 3.4 of Section 3.4. The data in this table demonstrated the existence of a solvent effect on the activation volume for a Menshutkin reaction; specifically the magnitude of the volume was observed to increase with the nonpolarity of the solvent because the electric field around an ion decreases less rapidly with distance in a solvent of lower dielectric constant;

therefore, electrostriction is greater in solvents of low dielectric constant than in solvents of higher dielectric constant.

As discussed in Chapter 2, the decarboxylative-dechlorination of N-chloro-α-amino acids occurs through a charge dispersion, which would create an opposite but related effect to electrostriction, and thus a solvent effect on the $\Delta V^{\ddagger}$ of this reaction would also be expected. The previous analysis suggested that $\Delta gA^{\ddagger}$ was related to $\Delta V^{\ddagger}$, and thus $\Delta gA^{\ddagger}$ should be expected to display a solvent effect as well. This may explain why dioxane, which has a small dielectric constant relative to the other organic cosolvents used in this study, gives a large $\Delta gA^{\ddagger}$ value.

6.6 Conclusions

The phenomenological model was used to quantitatively describe the solvent effects on the decarboxylative-dechorination of N-chloroalanine in 8 aqueous-organic cosolvent systems, and of N-chloroleucine in 4 aqueous-organic cosolvent systems. The two-step cancellation approximation was able quantitatively fit all the data, while the one-step cancellation approximation model can quantitatively fit most, but not all, the data. The logarithm of the solvation exchange constants was correlated with the log P (P is the 1-octanol-water partition

coefficient) of the organic cosolvents used in each study. The plots indicated that the organic cosolvents used in this study fell into two classes; this trend has been observed from previcus analysis of surface tension and solubility data. The $\Delta gA^{\ddagger}$ values, which are proportional to the molecular surface area of activation, were positive for every system that was studied. Volumes of activation for the reactions, which were determined by pressure effect experiments, were also positive, showing that the $\Delta gA^{\ddagger}$ parameter values derived from our treatment are consistent in direction with the classical quantity, $\Delta V^{\ddagger}$, evaluated by a completely different method. In addition, the magnitude of the $\Delta gA^{\ddagger}$ values for N-chloroalanine agreed reasonably well with the $\Delta V^{\ddagger}$ value determined in this study.

6.7 Chapter 6 References

(1) Amis, E.S. "Solvent Effects on Reactions Rates and Mechanisms"; Academic Press: New York, 1966.

(2) Kosower, E.M. "An Introduction to Physical Organic Chemistry"; Wiley: New York, 1968; Part 2.

(3) Dack, M.R.J. "Solutions and Solubilities"; Dack, M.R.J., Ed., Wiley-Interscience: New York, 1975; Vol VIII, Part II, Chapter XI.

(4) Entelis, S.G.; Tiger, R.P. "Reaction Kinetics in the Liquid Phase"; Wiley (Halsted): New York, 1976.

(5) Reichardt, C."Solvents and Solvent Effects in Organic Chemistry"; VCH: Weinheim, 1988; Chapters 5,7.

(6) Connors, K.A. "Chemical Reaction Kinetics: The Study of Reaction Rates in Solution"; VCH : New York, 1990.

(7) Reichardt, C. *Angew. Chem. Int. Ed. Eng.* (1965), **4**, 29.

(8) Blokzijl, W.; Engberts, J.B.F.N.; Blandamer, M.J. *Trends Org. Chem.* (1992), **3**, 295.

(9) Benson, S.W.; "The Foundation of Chemical Kinetics"; McGraw-Hill: New York, 1960, Chapter VX.

(10) Hildebrand, J.H.; Scott, R.L. "Solubility of Nonelectrolytes" 3rd ed.; Reinhold: New York, 1950.

(11) Hildebrand, J.H.; Scott, R.L. "Regular Solutions"; Prentice-Hall: Englewood Cliffs, 1962.

(12) Hildebrand, J.H.; Prausnitz, J.M. Scott, R.L. "Regular and Related Solutions" Van Nostrand Reinhold: New York, 1970.

(13) Grant, D.J.W.; Higuchi, T. "Solubility of Organic Compounds"; Saunders, W.H., Ed.; Techniques of Chemistry Volume XXI, Wiley: New York, 1990, Chapter 2.

(14) Muanda, W.M.; Nagy, B.J.; Nagy, O.B. *Tetrahedron Letters* (1974), **38**, 3421.

(15) Nagy, O.B.; Muanda, W.M.; Nagy, B.J. *J. Phys. Chem.* (1973), **83**, 1961.

(16) Nagy, O.B.; Muanda, W.M.; Nagy, B.J. *J. Chem. Soc. Faraday Trans. I* (1978), **74**, 2210.

(17) Parbhoo, B.; Nagy, O.B. *J. Chem. Soc. Faraday Trans. I* (1986), **82**, 1787.

(18) Szpakowska, M.; Nagy, O.B. *J. Phys. Chem.* (1989), **93**, 3851.

(19) Parbhoo, B.; Nagy, O.B. *J. Chem. Soc. Faraday Trans. I* (1989), **85**, 2891.

(20) Glasstone, S.; Laidler; K.J.; Eyring, H. "The Theory of Rate Processes"; McGraw-Hill: New York, 1941, 419.

(21) Kirkwood, J.G. *J. Phys. Chem.* (1934), **2**, 357.

(22) Glasstone, S.; Laidler; K.J.; Eyring, H. "The Theory of Rate Processes"; McGraw-Hill: New York, 1941, 427.

(23) Born, M. *Z. Physik*, (1920), **1**, 45.

(24) Schmid, R. *Rev. Inorg. Chem.* (1990), **11**, 255.

(25) Skwierczynski, R.D.; Connors, K.A. *J. Pharm. Sci.* (1994), **83**, 1690.

(26) Moreau, C.; Douheret, G.T. *J. Chem. Thermodynamics* (1976), **8**, 403.

(27) Critchfield, F.E.; Gibson, J.A.; Hall, J.L. *J. Am. Chem. Soc.* (1953), **75**, 1991.

(28) Albright, P.S.; Gosting, L.J. *J. Am. Chem. Soc.* (1946) **68**, 1061.

(29) Yokoy, T.; Taft, R.W.; Kamlet, M.J. *J. Am. Chem. Soc.* (1976), **98**, 3233.

(30) Kamlet, M.J.; Taft, R.W. *J. Am. Chem. Soc.* (1976), **98**, 377.

(31) Kamlet, M.J.; Abboud, J.L.; Taft, R.W. *J. Am. Chem. Soc.* (1977), **99**, 6027.

(32) Minesinger, R.R.; Jones, M.E.; Kamlet, M.J. *J. Org. Chem.* (1977), **42**, 1929.

(33) Kamlet, M.J.; Abboud, J.M.; Abraham, M.H.; Taft, R.W. *J. Org. Chem.* (1983), **48**, 2877.

(34) Taft, R.W.; Abboud, J.L.; Kamlet, M.J.; Abraham, M.H. *J. Soln. Chem.* (1985), **14**, 153.

(35) Abraham, M.H.; Doherty, R.M.; Kamlet, M.J.; Taft, R.W. *Chem. Ber.* (1986), **22**, 55.

(36) Abraham, M.H.; Doherty, R.M.; Kamlet, M.J.; Harris, J.M.; Taft, R.W. *J. Chem. Soc. Perkin Trans. 2* (1987) 913.

(37) Koppel, I.A.; Palm, A. "Advances in Linear Free Energy Relationships"; Chapman, N.B.; Shorter, J., Eds.; Plenum Press, London, 1972, Chapter 5.

(38) Ferris, D.C.; Drago, R.S. *J. Am. Chem. Soc.* (1994), **116**, 7509.

(39) Grunwald, E.; Winstein, S. *J. Am. Chem. Soc.* (1948), **70**, 846.

(40) Winstein, S.; Grunwald, E.; Jones, H.W. *J. Am. Chem. Soc.* (1951), **73**, 2700.

(41) Winstein, S.; Fainberg, A.H.; Grunwald, E.; *J. Am. Chem. Soc.* (1957), **79**, 4146.

(42) Fainberg, A.H.; Winstein, S. *J. Am. Chem. Soc.* (1956), **78**, 2770.

(43) Khossravi, D.; Connors, K.A. *J. Soln. Chem.* (1993), **22**, 677.

(44) Mulski, M.J.; Connors, K.A. *Supramolecular Chemistry* (1995): in press.

(45) Khossravi, D.; Connors, K.A. *J. Pharm. Sci.* (1992), **81**, 371.

(46) Khossravi, D.; Connors, K.A. *J. Pharm. Sci.* (1993), **82**, 817.

(47) LePree, J.M.; Mulski, M.J.; Connors, K.A. *J. Chem. Soc. Perkins Trans. 2* (1994), 1491.